

Bijjective enumeration of planar bipartite maps with three tight boundaries, or how to slice pairs of pants

J eremie Bouttier*[†] Emmanuel Guitter* Gr egory Miermont[‡]

November 28, 2022

We consider planar maps with three boundaries, colloquially called pairs of pants. In the case of bipartite maps with controlled face degrees, a simple expression for their generating function was found by Eynard and proved bijectively by Collet and Fusy. In this paper, we obtain an even simpler formula for *tight* pairs of pants, namely for maps whose boundaries have minimal length in their homotopy class. We follow a bijective approach based on the slice decomposition, which we extend by introducing new fundamental building blocks called bigeodesic triangles and diangles, and by working on the universal cover of the triply punctured sphere. We also discuss the statistics of the lengths of minimal separating loops in (non necessarily tight) pairs of pants and annuli, and their asymptotics in the large volume limit.

*Universit  Paris-Saclay, CNRS, CEA, Institut de physique th orique, 91191, Gif-sur-Yvette, France

[†]Univ Lyon, Ens de Lyon, Univ Claude Bernard, CNRS, Laboratoire de Physique, F-69342 Lyon

[‡]ENS de Lyon, UMPA, CNRS UMR 5669, 46 all e d'Italie, 69364 Lyon Cedex 07, France

Contents

1. Introduction	3
2. Basic building blocks	8
2.1. Preliminaries: geodesics and related concepts	8
2.2. Tight slices	10
2.3. Bigeodesic diangles	11
2.4. Bigeodesic triangles	14
3. Assembling the building blocks	15
3.1. Description of the assembling procedures I and II	16
3.2. Properties of the assembling procedures	18
3.3. Enumerative consequences	20
3.4. Disassembling a triply pointed map	20
4. The universal cover of a map with three boundaries	22
4.1. Construction and properties of the universal cover	22
4.2. Visualizing the assembling procedures on the universal cover	26
4.3. Tightness of the boundaries resulting from the assembling procedures	32
5. Decomposing a map with three tight boundaries	34
5.1. Graph-theoretical properties of the universal cover	35
5.2. Infinite geodesics and Busemann functions	37
5.3. Busemann functions associated with tight boundaries	38
5.4. Leftmost bigeodesics and the diangle lemma	39
5.5. Equilibrium vertices and the triangle lemma	43
5.6. Decomposing a map of type I	45
5.7. Decomposing a map of type II	49
6. Equivalence with the Eynard-Collet-Fusy formula, and limiting statistics in random maps with boundaries	50
6.1. The structure of outermost minimal separating cycles	51
6.2. A re-derivation of the ECF formula for pairs of pants	55
6.3. Scaling limits of separating loop statistics	57
7. Conclusion	62
A. A slice-theoretic enumeration of triply pointed maps	64
B. Connection with well-labeled maps	66
References	73

1. Introduction

Context and motivations. The study of maps (graphs embedded into surfaces) is an active field of research, at the crossroads between combinatorics, theoretical physics and probability theory. The combinatorial theory of maps started with the pioneering work of Tutte in the 1960's [Tut68], and we refer to the recent review by Schaeffer [Sch15] for an account of its many developments ever since. In theoretical physics, maps are intimately connected with matrix models and two-dimensional quantum gravity: see for instance the review by Di Francesco, Ginsparg and Zinn-Justin [DFGZJ95], the book by Ambjørn, Durhuus and Jonsson [ADJ97], and the book by Eynard [Eyn16] for more recent mathematical advances including the theory of topological recursion. Probability theory aims at understanding the geometric properties of large random maps and their limits: this topic is covered in several sets of lecture notes [LGM12, Mie14, Bud17, Cur19], and we also mention the review by Miller [Mil18] which discusses the connection with Liouville quantum gravity, a rigorous approach to two-dimensional quantum gravity.

A key tool in the study of maps is the *bijective approach*, which consists in finding correspondences between different families of maps, or with other combinatorial objects such as trees or lattice walks. Bijections often yield elementary derivations of enumerative results, but are also useful to understand properties of maps such as distances (see the aforementioned references). There exists by now several general bijective frameworks, and in this paper we focus on a specific one, called the slice decomposition.

Colloquially speaking, the *slice decomposition* consists in performing a canonical decomposition of maps, by cutting them along leftmost geodesics. It was first mentioned in the papers [BG09b, BG12, AB12], mostly as a reformulation of the decomposition of mobiles [BDFG04]. Its real significance was highlighted in the paper [BG14]—see also [Bou19, Chapter 2] for a recent exposition—which considers so-called irreducible maps for which bijections were not known before. The slice decomposition also passes naturally to the scaling limit [LG13, BM17]. However, it has so far been understood only in the case of *disks* and *annuli*, namely planar maps with one or two boundaries. Our purpose is to understand the case of maps with other topologies, with the long-term goal of developing a bijective approach to topological recursion.

In this paper, we make a first step in this direction, by considering *pairs of pants*, namely planar maps with three boundaries. For simplicity, we restrict to the case of bipartite maps with controlled face degrees (also known as Boltzmann maps), though we believe that our treatment can be extended to the non bipartite or to the irreducible settings as considered in [BG12, BG14]. A simple explicit expression of the generating function of bipartite pairs of pants was given by Eynard [Eyn16, Proposition 3.3.1] and derived bijectively by Collet and Fusy [CF12]. We note that equivalent formulas appeared previously in the physics literature, see for instance [AJM90, Equation (45)] or [ADJ97, Equation (4.94)]. Here, we obtain an even simpler formula for *tight* pairs of pants, namely for maps whose boundaries have minimal length in their homotopy class. As we shall see, our formula is equivalent to the Eynard-Collet-Fusy formula, but our derivation is fundamentally different.

Our approach, whose general idea is displayed in Figure 1.1, consists in decomposing

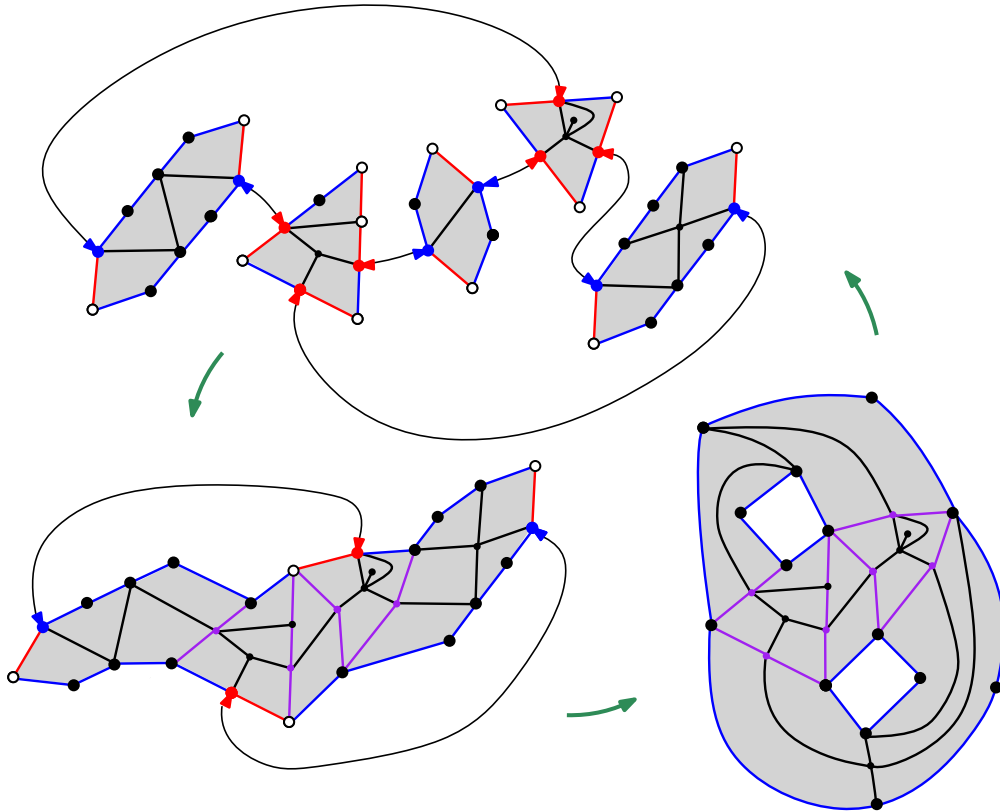


Figure 1.1: Illustration of the main bijective construction discussed in this paper. Starting from elementary pieces, namely two bigeodesic triangles and three bigeodesic diangles (top), one builds a pair of pants with three tight boundaries (bottom right). To better visualize the construction, we pass through an intermediate partial assembling (bottom left). Conversely, the building blocks can be recovered by cutting along appropriately defined bigeodesics, here displayed in purple.

tight pairs of pants into geometric pieces which we call (bigeodesic) diangles and triangles. While the former are, in a sense, generalizations of the existing notion of slices, the second are new objects (although they appear implicitly in earlier work [BG08], see the discussion in Appendix B). As was pointed to us by Bram Petri, the way in which the elementary pieces are assembled is very much reminiscent of classical constructions of pairs of pants in hyperbolic geometry from ideal hyperbolic triangles, see for instance [Thu97, Section 3.4]. In particular, some notions of importance in this paper, which we refer to as “equilibrium vertices” in triangles and “exceedances” in diangles, have natural analogs in hyperbolic geometry: the equilibrium vertices correspond to tangency points of the inner circles of the ideal triangles, and the exceedances correspond to the invariants $d(v)$ in [Thu97].

We believe that many other connections exist between these classical concepts and

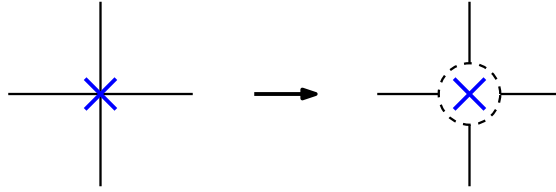


Figure 1.2: An intuitive way to think of a boundary-vertex: we remove a small disk around it, and keep all incident edges connected along a circle made of special (dashed) edges, which are considered as having length zero. Note that a path passing through a boundary-vertex may “circumvent” it in two ways, which will correspond to different homotopy classes when there are other boundaries.

our work. In particular, in the context of the classification of Riemann and hyperbolic surfaces [IT92], pants decompositions play a fundamental role. It is therefore natural to expect that similar decompositions should exist in the context of maps. In particular, the tightness constraint which we introduce should be an important ingredient: indeed, it should translate the natural idea of cutting surfaces along closed geodesics, in order to obtain canonical decompositions. Such pants decompositions will be explored in future research, but provide one of our main motivations for the present paper.

Overview. A *planar map* is a connected multigraph embedded into the sphere without edge crossings, and considered up to homeomorphism. It consists of *vertices*, *edges*, *faces* and *corners*, see [Sch15] for precise definitions. Until further notice, we only consider finite maps, i.e. maps with a finite number of edges (hence of vertices, faces and corners). A *path* on a map is a sequence of consecutive edges, and the *length* of a path is its number of edges. Given a face, its *contour* is the closed path formed by its incident edges, and its *degree* is the length of the contour. A planar map is *bipartite* if all its faces have even degree.

A *boundary* is either a marked face or a marked vertex on the map. We will use the denominations *boundary-face* and *boundary-vertex* when we wish to specify the nature of a boundary. We define the *length* of a boundary as being equal to its degree in the case of a boundary-face, and to zero in the case of a boundary-vertex. Faces which are not boundaries are called *inner faces*. A map is said *essentially bipartite* if all its inner faces have even degree. The sum of the lengths of the boundaries of an essentially bipartite map is necessarily even.

We intuitively think of boundaries as representing punctures on the sphere. This is rather natural in the case of a boundary-face (we just remove its interior from the surface), but slightly less in the case of boundary-vertex: see Figure 1.2. A path on the map, together with a choice of circumventing direction when passing through a boundary-vertex, corresponds to a path on the punctured sphere. Two closed paths are said to be in the same *homotopy class*, or *freely homotopic*, if they can be continuously deformed into one another on the punctured sphere. A boundary-face is said *tight* if its contour has minimal length in its homotopy class (if the boundary-face is incident to a boundary-

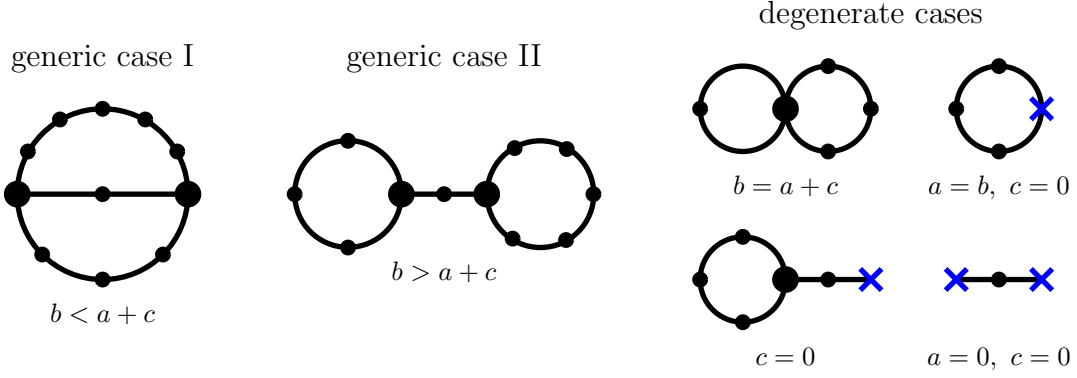


Figure 1.3: The possible types of maps with three tight boundaries and no inner face. Tightness implies that there are no vertices of degree one, except possibly boundary-vertices, indicated here by blue crosses. To identify the different types, assume without loss of generality that the boundary lengths are $b \geq a \geq c$. There exists two generic situations, denoted I and II, corresponding to the cases $b < a + c$ and $b > a + c$ respectively. The degenerate cases correspond to having $b = a + c$ or/and some lengths equal to zero. We may check that there are $a + b + c - 1$ vertices different from boundary-vertices in all cases.

vertex, the contour should be considered as the contour of the corresponding face in the map modified as in Figure 1.2). A boundary-vertex is by convention always tight.

We are interested in essentially bipartite planar maps with three distinct boundaries which are labeled (distinguishable). Such maps cannot have symmetries, and therefore we do not root (i.e., mark a corner on) the boundaries. Two situations may occur: either all the boundary lengths are even, and the planar map is truly bipartite, or two lengths are odd and the third is even, and following [CF12] we say that the map is *quasi-bipartite*. We may now state our main enumerative result:

Theorem 1.1. *Let a, b and c be integers or half-integers such that $a + b + c$ is an integer. Then, the generating function $T_{a,b,c}$ of essentially bipartite planar maps with three labeled distinct tight boundaries of lengths $2a, 2b, 2c$, counted with a weight t per vertex different from a boundary-vertex and, for all $k \geq 1$, a weight g_{2k} per inner face of degree $2k$, is equal to*

$$T_{a,b,c} = R^{a+b+c} \frac{d \ln R}{dt} - t^{-1} \mathbf{1}_{a=b=c=0} \quad (1.1)$$

where R is the formal power series in t, g_2, g_4, \dots determined by

$$R = t + \sum_{k \geq 1} \binom{2k-1}{k} g_{2k} R^k \quad (1.2)$$

and where $\mathbf{1}_P$ is equal to 1 if P is true, and to 0 otherwise.

It is not difficult to check that the right-hand side of (1.1) is indeed a well-defined power series in t, g_2, g_4, \dots . It is useful to look first at the case where g_2, g_4, \dots all vanish. This corresponds to maps without inner faces. In this case, $T_{0,0,0}$ vanishes while, for a, b, c not all zero, $T_{a,b,c}$ is equal to $t^{a+b+c-1}$: this means that there should exist exactly one such map, with $a+b+c-1$ vertices different from boundary-vertices. This is indeed true, as illustrated on Figure 1.3.

Our expression for $T_{a,b,c}$ is very similar to the aforementioned Eynard-Collet-Fusy (ECF) formula for maps with three boundaries that are not necessarily tight. In fact, the ECF formula simply differs by some binomial factors. As we will see in Section 6, the two formulas are equivalent, by a canonical decomposition which consists in cutting a map with three arbitrary boundaries along outermost minimal separating loops, resulting in three annular maps and one tight pair of pants. However, our expression for $T_{a,b,c}$ being even simpler than the ECF formula, it is desirable to have a direct bijective proof of it, and this is the main objective of the present paper.

Our results have interesting consequences for the statistics of large random planar maps, which are explored in Section 6.3. There, for simplicity, we restrict our attention to the case of quadrangulations. The aforementioned canonical decomposition of a map with three boundaries into three annular maps and a tight pair of pants allows one to define the exterior areas, corresponding to the number of faces in the annular maps, the interior area, corresponding to the number of faces in the tight pair of pants, and the minimal separating cycle lengths, corresponding to the lengths of the three boundaries of the tight pair of pants. In Theorem 6.9, we give a detailed limit theorem for the joint law of these quantities in large quadrangulations with three boundaries. We also provide an analogous statement for random annular quadrangulations in Theorem 6.7, which relies on the results obtained in [BG14].

Our strategy to prove Theorem 1.1 is the following. For $a = b = c = 0$, the right-hand side of (1.1) can be rewritten as $d \ln(R/t)/dt$ which, by results from [BDFG04], is already known to be equal to the generating function $T_{0,0,0}$ of triply pointed bipartite maps (for completeness, we provide a slice-theoretic rederivation of this fact in Appendix A). Then, we will exhibit a bijection implying, as Corollary 3.2 below, that we have for any a, b, c

$$T_{a,b,c} + t^{-1} \mathbf{1}_{a=b=c=0} = R^{a+b+c} \frac{X^3 Y^2}{t^6} \quad (1.3)$$

where R, X and Y are the generating functions of combinatorial objects called respectively elementary slices, bigeodesic diangles, and bigeodesic triangles (all these series are equal to t when g_2, g_4, \dots all vanish). These combinatorial objects will be defined in Section 2. The notations are chosen to be consistent with those of [BG08, BG09a]: as we discuss in Appendix B, bigeodesic diangles and triangles are the slice-theoretic equivalents of objects appearing in the decomposition of well-labeled maps (the slice interpretation of R being already known). This makes a connection with the bijective approach developed in [Mie09, AB13, BFG14]. Comparing (1.3) with the known expression for $T_{0,0,0}$, we get $X^3 Y^2 / t^6 = d \ln R / dt$ and Theorem 1.1 follows.

Outline. Section 2 introduces the basic building blocks of our approach, namely tight slices, bigeodesic diangles and bigeodesic triangles, and derives some elementary enumeration results for those pieces. Section 3 explains how these pieces can be assembled to produce a map with three tight boundaries. This allows us to state our main bijective result, Theorem 3.1. To prove this theorem, the difficult part is to decompose a map with three tight boundaries back into basic building blocks. This decomposition takes place on the universal cover of the map, which is a periodic infinite map which we describe in Section 4. Section 5 then presents the decomposition of a map with three tight boundaries, by first introducing the important geometric tool of Busemann functions associated with infinite geodesics, and finishes the proof of Theorem 3.1 by showing that this decomposition is indeed the inverse of the assembling procedure. Section 6 discusses how to recover the ECF formula from our results and a decomposition of pairs of pants into annular maps and tight pairs of pants, and then states and proves our probabilistic applications on the statistics of minimal separating cycles and areas in large random quadrangulations with three boundaries. Concluding remarks and discussion on future directions are gathered in Section 7. Finally, we recall in Appendix A how to obtain the classical recursion relation (1.2) for slices, as well as the reason why $d \ln(R/t)/dt$ is the generating function of triply pointed maps, and in Appendix B we present another approach to bigeodesic diangles and triangles in the case of quadrangulations, based on a bijection with labeled trees.

Acknowledgements. We thank Marie Albenque, Timothy Budd, Vincent Delecroix, Marco Mazzucchelli and Bram Petri for valuable discussions. We also thank the two anonymous referees for suggesting useful improvements to the paper. This project results from an institutional collaboration between CEA and ENS de Lyon, and was initiated at the occasion of the *Séminaire de combinatoire de Lyon à l'ENS* which is funded by the Labex Milyon (ANR-10-LABX-0070). The work of JB is partly supported by the Agence Nationale de la Recherche via the grants ANR-18-CE40-0033 “Dimers” and ANR-19-CE48-0011 “Combiné”.

2. Basic building blocks

In this section we introduce the fundamental building blocks of our approach. We start with some preliminary definitions.

2.1. Preliminaries: geodesics and related concepts

In a map, a *geodesic* between two vertices v_1 and v_2 is a path of minimal length connecting them. This minimal length is by definition the (graph) *distance* $d(v_1, v_2)$ between the vertices v_1 and v_2 . Maps are assumed to be connected, so geodesics between any two given vertices always exist and $d(v_1, v_2)$ is a finite integer.

A *geodesic vertex* between v_1 and v_2 is a vertex v belonging to a geodesic between

them. Clearly, v is a geodesic vertex if and only if

$$d(v, v_1) + d(v, v_2) = d(v_1, v_2). \quad (2.1)$$

Bigeodesics. In general, there may exist many geodesics between v_1 and v_2 . But, using the (local) planar structure of a map, it is often possible to single out a canonical one. The previous works on slice decomposition were using the notion of leftmost geodesic determined by the choice of an initial direction at v_1 . Here, we will need a related but slightly different notion, which is that of leftmost bigeodesic determined by the choice of a geodesic vertex between v_1 and v_2 .

A *bigeodesic* between two vertices v_1 and v_2 is a triple made of a geodesic vertex v between them and of two geodesics, one between v and v_1 and one between v and v_2 . Clearly the concatenation of these two geodesics is a geodesic between v_1 and v_2 , so that a bigeodesic between v_1 and v_2 is entirely specified by the data of a geodesic between v_1 and v_2 and of a vertex v along this geodesic.

Viewing the bigeodesic as “launched” from the geodesic vertex v towards v_1 and v_2 respectively, we may introduce the notion of *leftmost bigeodesic* as follows. Assume that $d(v_1, v_2) \geq 2$ and that v is distinct from v_1 and v_2 . We may partition the set of edges incident to v into three types:

- (i) those leading to a vertex strictly closer to v_1 ,
- (ii) those leading to a vertex strictly closer to v_2 ,
- (iii) those leading to a vertex that is neither strictly closer to v_1 nor to v_2 .

Ignoring the edges of type (iii), it is easily seen that, by planarity, there exists an edge e_1 of type (i) and an edge e_2 of type (ii) such that, when turning clockwise around v , all edges of type (i) appear between e_1 and e_2 and all edges of type (ii) appear between e_2 and e_1 . We then consider the leftmost geodesic from v to v_1 starting with e_1 , i.e. the geodesic whose first step goes along e_1 from v to its neighbor at distance $d(v, v_1) - 1$ from v_1 , and at each step, goes along the leftmost edge (as viewed from the previous edge) among all those going from the currently attained vertex to a vertex closer to v_1 , until v_1 is eventually reached. We similarly pick the leftmost geodesic from v to v_2 starting with e_2 . Concatenating these two geodesics, we obtain a bigeodesic between v_1 and v_2 launched from v , which is by definition the leftmost bigeodesic we are looking for. Observe that the leftmost bigeodesic is not well-defined if $v = v_1$ or $v = v_2$, and in particular if $d(v_1, v_2) < 2$.

Geodesic boundary intervals. Consider a planar map with one boundary-face, which we denote f_0 and which we choose as the external face in the planar representation of the map. Let c and c' be two corners incident to f_0 . These corners split the contour of f_0 in two portions, which we call *boundary intervals*. When turning counterclockwise around the map (i.e., when walking along the contour with f_0 on the right), the portion that starts at c and ends at c' is denoted $[c, c']$. It forms a path on the map, which may not be simple in general. In the particular case where it forms a geodesic between the vertices

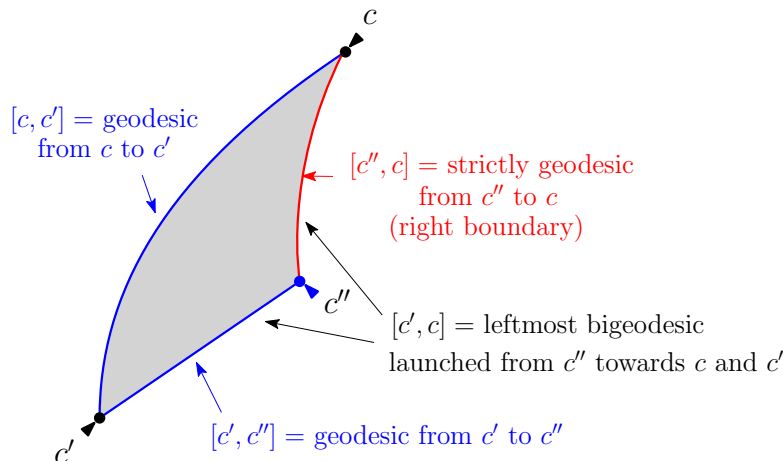


Figure 2.1: Generic structure of a tight slice (the boundary-face is the outer face). In this figure and the following, we represent geodesic boundary intervals in blue and strictly geodesic ones in red. The corner c'' is shown in blue since it is an intermediate corner on the geodesic boundary interval $[c', c]$. The width of the slice is the length of $[c', c'']$.

incident to c and c' , then we say that the boundary interval $[c, c']$ is *geodesic* (the path is necessarily simple in this case). Furthermore, if there exists no other geodesic in the map with the same endpoints, then $[c, c']$ is said *strictly geodesic*. In the figures, we will often use the graphical convention of representing geodesic boundary intervals in blue, and strictly geodesic boundary intervals in red.

2.2. Tight slices

Our first building block is what we call a *tight slice*, defined as a planar bipartite map with one boundary-face having three distinguished (not necessarily distinct) incident corners c , c' and c'' appearing counterclockwise around the map such that:

- the boundary intervals $[c, c']$ and $[c', c]$ are geodesic,
- the boundary interval $[c'', c]$, called the *right boundary*, is strictly geodesic,
- the intervals $[c'', c]$ and $[c, c']$ share only a common vertex at c .

See Figure 2.1 for an illustration. Note that the constraints imply that $[c', c'']$ is also geodesic, and the length of this interval is called the *width* of the slice. The only tight slice of width zero is equal to the *vertex-map*, reduced to a single vertex and a single face both of degree zero. Note that, if $c \neq c''$ (hence $c' \neq c''$), then $[c', c]$ is nothing but the leftmost bigeodesic launched from the vertex incident to c'' towards those incident to c and c' respectively. A tight slice of width 1 is called an *elementary slice*.

Proposition 2.1. *The generating function of tight slices of width ℓ , counted with a weight t per vertex not incident to the right boundary and a weight g_{2k} per inner face of degree $2k$ for all $k \geq 1$, is equal to R^ℓ , with R defined as in Theorem 1.1.*

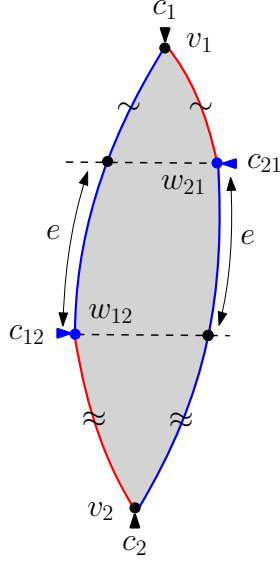


Figure 2.2: Schematic picture of a bigeodesic diangle of nonnegative exceedance e . The boundary intervals with the \sim label have the same length and meet only at v_1 , and similarly for the \approx label. The remaining two other boundary intervals, of length e , may however share common vertices as soon as $e > 0$.

Proof. It is known that R counts elementary slices (for completeness, we provide a proof in Appendix A). Given a tight slice of arbitrary width, let us consider all the vertices incident to the boundary interval $]c', c''[$ (with endpoints excluded), and the leftmost bigeodesics launched from them towards the vertices incident to c' and c . These bigeodesics necessarily follow the boundary towards c' , but may enter inside the map towards c . Cutting also these bigeodesics splits the map into a ℓ -tuple of elementary slices, and it is straightforward to check that the decomposition is bijective. \square

2.3. Bigeodesic diangles

Our second building block is what we call a *bigeodesic diangle*, or a *diangle* for short, which is again a planar bipartite map with one boundary-face, with now four distinguished (not necessarily distinct) incident corners c_1, c_{12}, c_2, c_{21} appearing counterclockwise around the map, and having the following properties:

- the boundary intervals $[c_1, c_2]$ and $[c_2, c_1]$ are geodesic,
- the boundary intervals $[c_{12}, c_2]$ and $[c_{21}, c_1]$ are strictly geodesic,
- $[c_{21}, c_1]$ and $[c_1, c_2]$ share only a common vertex at the vertex v_1 incident to c_1 and similarly, $[c_{12}, c_2]$ and $[c_2, c_1]$ share only a common vertex at the vertex v_2 incident to c_2 .

See Figure 2.2 for an illustration. Note that the boundary intervals $[c_1, c_{12}]$ and $[c_2, c_{21}]$ are necessarily geodesic. Let us denote by w_{12} and w_{21} the vertices incident to c_{12} and

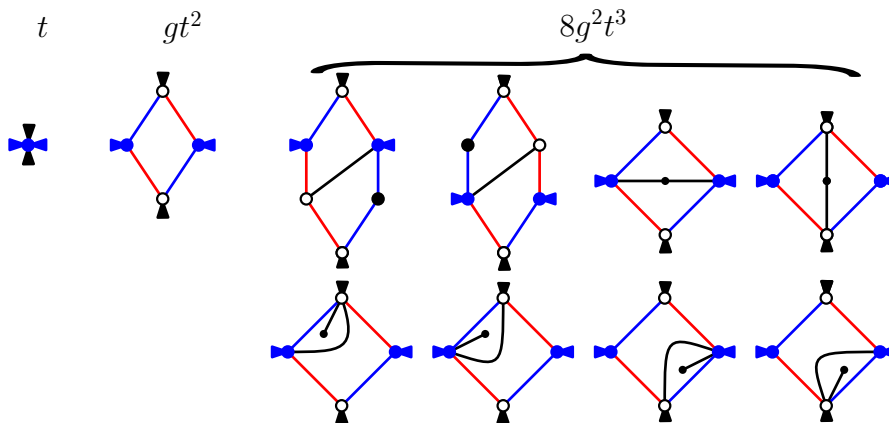


Figure 2.3: The first terms in the expansion of X for quadrangulations ($g_{2k} = g \delta_{k,2}$). The unfilled vertices (circles) receive no weight.

c_{21} . If w_{12} is different from v_1 and v_2 , then $[c_1, c_2]$ is the leftmost bigeodesic launched from w_{12} towards v_1 and v_2 . Similarly, if w_{21} is different from v_1 and v_2 , then $[c_2, c_1]$ is the leftmost bigeodesic launched from w_{21} . The corners c_{12} and c_{21} (or the vertices w_{12} and w_{21} depending on the context) will be referred to as the *attachment points* of the diangle, for reasons which will become clear in the next section.

The *exceedance* e of the diangle is defined as

$$e = d(w_{12}, v_1) - d(w_{21}, v_1) = d(w_{21}, v_2) - d(w_{12}, v_2). \quad (2.2)$$

A diangle is said *balanced* if its exceedance e is 0, that is if w_{12} and w_{21} are at the same distance from v_1 , say. Note that the vertex-map again satisfies all the required criteria for a balanced diangle. Apart from this trivial case, any other balanced diangle has $d(v_1, v_2) \geq 2$, with w_{12} and w_{21} different from v_1 and v_2 and from each other, with $[c_1, c_2]$ and $[c_2, c_1]$ meeting only at v_1 and v_2 . This latter property is not necessarily true for unbalanced diangles, as indicated in the caption of Figure 2.2.

We denote by X the generating function of balanced bigeodesic diangles, where the boundary-face and the vertices incident to the strictly geodesic intervals $[c_{12}, c_2]$ and $[c_{21}, c_1]$ other than w_{12} and w_{21} receive no weight. Note that the vertex-map contributes a weight t to X .

Even though we shall not need any precise expression for X , let us mention that, by the results of [BG08], a very explicit formula can be given in the case of quadrangulations ($g_{2k} = g \delta_{k,2}$), see equation (B.3) in Appendix B. It yields the expansion $X = t + gt^2 + 8g^2t^3 + 73g^3t^4 + 711g^4t^5 + \dots$, and the maps corresponding to the first terms of this expansion are displayed in Figure 2.3.

With the same weighting convention as for balanced diangles, we have the following property:

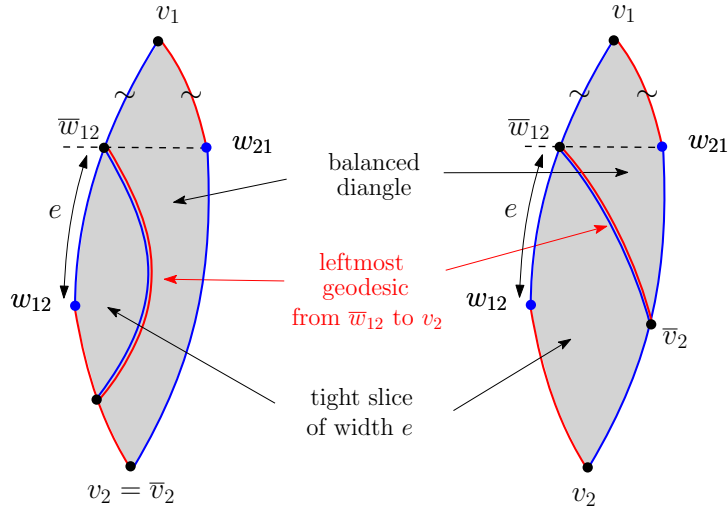


Figure 2.4: Decomposition of a bigeodesic diangle of exceedance e into a pair made of a balanced bigeodesic diangle and a tight slice of width e . Different situations occur according to which boundary is first hit by the leftmost geodesic from \bar{w}_{12} to v_2 .

Proposition 2.2. *The generating function of bigeodesic diangles with nonnegative exceedance e is equal to $R^e X$.*

Proof. The property is obvious for $e = 0$, so we may assume $e > 0$. Let \bar{w}_{12} denote the vertex along $[c_1, c_2]$ which is at the same distance from v_1 as w_{21} . We have $d(w_{12}, \bar{w}_{12}) = e$. Consider the leftmost bigeodesic launched from \bar{w}_{12} towards v_1 and v_2 : its part towards v_1 follows the boundary, while its part towards v_2 may enter inside the diangle. We denote by \bar{v}_2 the first vertex common to this part and $[c_2, c_1]$. Then, as illustrated in Figure 2.4, the bigeodesic splits the map into two pieces. One of them is a balanced diangle with distinguished corners incident to $v_1, \bar{w}_{12}, \bar{v}_2$ and w_{21} , and the other is a tight slice of width $e > 0$. The decomposition is clearly a bijection and implies the wanted expression, by Proposition 2.1 (note that the weight t for w_{12} must be transferred to \bar{w}_{12} in the tight slice). \square

When all face weights are set to zero, $R^e X$ is equal to t^{e+1} , which accounts for the diangle made of a chain of $e + 1$ vertices and e edges, with $v_1 = w_{21}$ at one extremity and $v_2 = w_{12}$ at the other.

It is interesting to note that a tight slice of (positive) width e is nothing but a diangle of exceedance e for which $c_{12} = c_2$ (with the correspondance $c = c_1, c' = c_{12} = c_2, c'' = c_{21}$). Note however that the weighting conventions differ slightly (there is an extra weight t for diangles).

We will not consider diangles with negative exceedance in this paper, since their enumeration is more subtle.

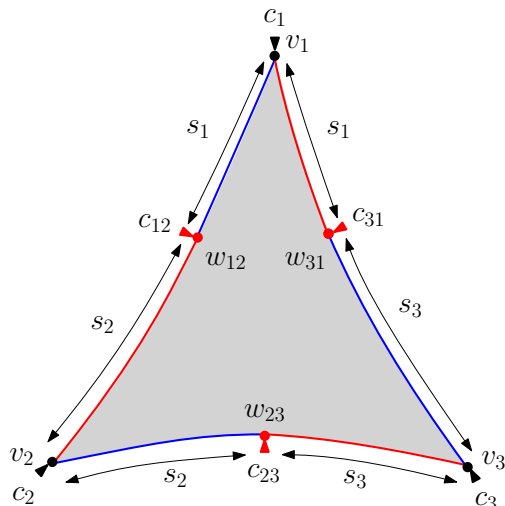


Figure 2.5: Schematic picture of a bigeodesic triangle. The vertices w_{12} , w_{23} and w_{31} are colored in red to indicate that any geodesic from v_1 to v_2 (respectively from v_2 to v_3 , from v_3 to v_1) must pass via w_{12} (respectively w_{23} , w_{31}).

2.4. Bigeodesic triangles

Our third and final building block is what we call a *bigeodesic triangle*, or *triangle* for short, which is again a planar bipartite map with one boundary-face. It now has six distinguished incident corners $c_1, c_{12}, c_2, c_{23}, c_3, c_{31}$ appearing counterclockwise around the map, and having the following properties:

- the boundary intervals $[c_1, c_2]$, $[c_2, c_3]$ and $[c_3, c_1]$ are geodesic, with no common vertex except at their endpoints v_1, v_2 , and v_3 (incident to c_1, c_2 and c_3 , respectively),
- the boundary intervals $[c_{12}, c_2]$, $[c_{23}, c_3]$ and $[c_{31}, c_1]$ are strictly geodesic,
- the boundary intervals $[c_1, c_{12}]$ and $[c_{31}, c_1]$ (respectively $[c_2, c_{23}]$ and $[c_{12}, c_2]$, $[c_3, c_{31}]$ and $[c_{23}, c_3]$) have the same length s_1 (respectively s_2, s_3).
- any geodesic from v_1 to v_2 (respectively from v_2 to v_3 , from v_3 to v_1) passes via w_{12} (respectively w_{23}, w_{31}), the vertex incident to c_{12} (respectively c_{23}, c_{31}).

See Figure 2.5 for an illustration. Note that, if two corners among $c_1, c_{12}, c_2, c_{23}, c_3, c_{31}$ are equal, then the above properties imply that the triangle is reduced to the vertex-map. Note also that the boundary intervals $[c_1, c_{12}]$, $[c_2, c_{23}]$ and $[c_3, c_{31}]$ are necessarily geodesic and that $d(v_1, v_2) = s_1 + s_2$, $d(v_2, v_3) = s_2 + s_3$ and $d(v_3, v_1) = s_3 + s_1$. As in the case of diangles, the interval $[c_1, c_2]$ is the leftmost bigeodesic launched from w_{12} towards v_1 and v_2 . Note also that a geodesic from v_1 to v_2 , which has to pass via w_{12} , necessarily sticks to $[c_{12}, c_2]$ between w_{12} and v_2 since $[c_{12}, c_2]$ is strictly geodesic. Similar properties hold under cyclic permutations of the indices 1, 2, 3. The corners c_{12}, c_{23}, c_{31} (or the

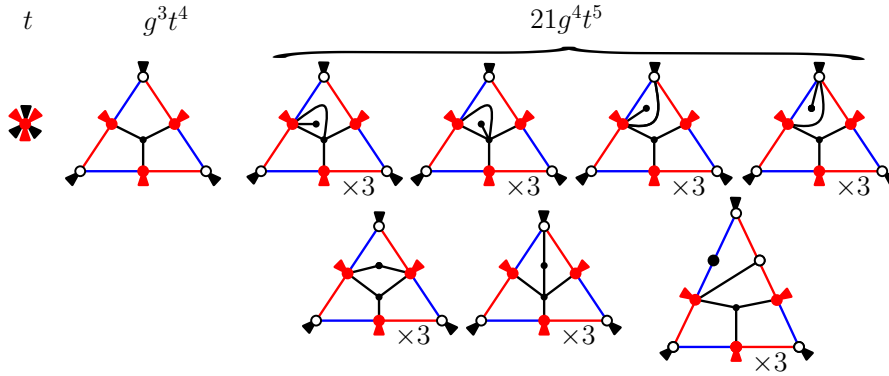


Figure 2.6: The first terms in the expansion of Y for quadrangulations ($g_{2k} = g \delta_{k,2}$). The unfilled vertices (circles) receive no weight.

vertices w_{12}, w_{23}, w_{31} depending on the context) will be referred to as the *attachment points* of the triangle.

We call Y the generating function of bigeodesic triangles, where the boundary-face and the vertices incident to the strictly geodesic intervals $[c_{12}, c_2]$, $[c_{23}, c_3]$ and $[c_{31}, c_1]$ other than w_{12} , w_{23} and w_{31} receive no weight. The vertex-map contributes a term t to Y .

As was the case for the generating function X of diangles, we shall not need any precise expression for Y , even though the results of [BG08] provide an explicit formula in the case of quadrangulations ($g_{2k} = g \delta_{k,2}$), see again equation (B.3) in Appendix B. It yields the expansion $Y = t + g^3 t^4 + 21 g^4 t^5 + 324 g^5 t^6 + \dots$, and the maps corresponding to the first terms of this expansion are displayed in Figure 2.6.

3. Assembling the building blocks

We now explain how to assemble a map with three tight boundaries from the basic building blocks introduced in the previous section. We start from a quintuple consisting of the following pieces:

- three bigeodesic diangles of nonnegative exceedances denoted by e_1 , e_2 and e_3 ,
- two bigeodesic triangles.

Recall that the boundaries of bigeodesic diangles and triangles are conventionally colored in red and blue: a boundary edge is colored red if it belongs to a boundary interval that is constrained to be strictly geodesic, and is colored blue otherwise (i.e. it belongs to a geodesic boundary interval which is not necessarily strictly geodesic). Generally speaking, the assembling procedure consists in gluing the boundaries of the different pieces together, a red edge being always glued to a blue edge. Some blue edges will possibly remain unmatched and form the boundaries of the assembled map.

We shall discuss in fact two alternative assembling procedures, hereafter numbered I and II, which are complementary in the sense that each of them generates only a strict

subset of the set of maps with three tight boundaries but, taken together, they generate the full set.

3.1. Description of the assembling procedures I and II

In a nutshell, the assembling procedures consist of two operations, which we call *attachment* and *red-to-blue gluing*. We start by describing these operations in detail in the case of procedure I, referring again to Figure 1.1 for an illustration, then turn to procedure II which only differs at the level of the attachment operation.

Procedure I. Recall from Sections 2.3 and 2.4 that the attachment points of diangles and triangles are the vertices from which their bigeodesic boundaries are launched. The *attachment* operation consists in identifying the attachment points as shown on Figure 3.1(a). The resulting object is a planar map which, in addition to the inner faces of the initial triangles and diangles, has three extra *special* faces, hereafter denoted F_A , F_B and F_C . Each special face is incident to four attachment points (after identification) and its contour is made of alternating blue and red intervals, four of each color, with an excess of blue edges ($e_1 + e_2$ for F_A , $e_2 + e_3$ for F_B , $e_3 + e_1$ for F_C).

The second operation is performed independently on each special face, and consists in gluing all its incident red edges to blue edges so as to form a face of smaller degree with only blue incident edges (thus the term *red-to-blue gluing*). More precisely, consider a special face, say F_A , and follow its contour keeping the face on the left (i.e. we turn counterclockwise around F_A , when it is represented as a bounded face in the plane): each red edge immediately followed by a blue edge is glued to it, and we repeat the process until no red edge is left. A convenient global description of this operation can be given as follows: number the edges along the contour of F_A by integers, starting at an arbitrary position and in the same direction as before. We set $\epsilon_n = 1$ if the edge numbered n is blue, and $\epsilon_n = -1$ if it is red. The sequence $(\epsilon_n)_n$ is naturally defined for all $n \in \mathbb{Z}$ by periodicity, with a period δ_A equal to the degree of F_A . Then, a red edge at position k will be matched and glued to the blue edge at position ℓ , where ℓ is the smallest integer larger than k such that $\sum_{n=k}^{\ell} \epsilon_n = 0$. Such ℓ necessarily exists since $\epsilon_k = -1$ and $\sum_{n=k}^{k+\delta_A-1} \epsilon_n = e_1 + e_2 \geq 0$. See Figure 3.1 for an illustration. After the gluing step, a number $e_1 + e_2$ of blue edges remain unmatched. If $e_1 + e_2 > 0$, these edges form the contour of a boundary-face. If $e_1 + e_2 = 0$, we instead obtain a boundary-vertex, which corresponds to the vertex preceding any edge k such that $\sum_{n=k}^{\ell} \epsilon_n \leq 0$ for all $\ell \geq k$. Indeed, such vertices corresponds to the maxima of the lattice path of Figure 3.1(c)—which is periodic when $e_1 + e_2 = 0$ —and all of them are identified by gluing. All in all, F_A becomes a boundary of length $e_1 + e_2$, and performing the same operation on F_B and F_C , these become boundaries of lengths $e_2 + e_3$ and $e_3 + e_1$ respectively.

The assembling procedure is trivially adapted to the case where a triangle is reduced to the vertex-map, by equipping its unique vertex with three attachment points (dividing the surrounding corner in three sectors). Similarly, when one of the exceedances is 0 and the corresponding (balanced) diangle is reduced to the vertex-map, we equip its unique vertex with two attachment points. If $e_1 = e_2 = e_3 = 0$ and all the triangles/diangles

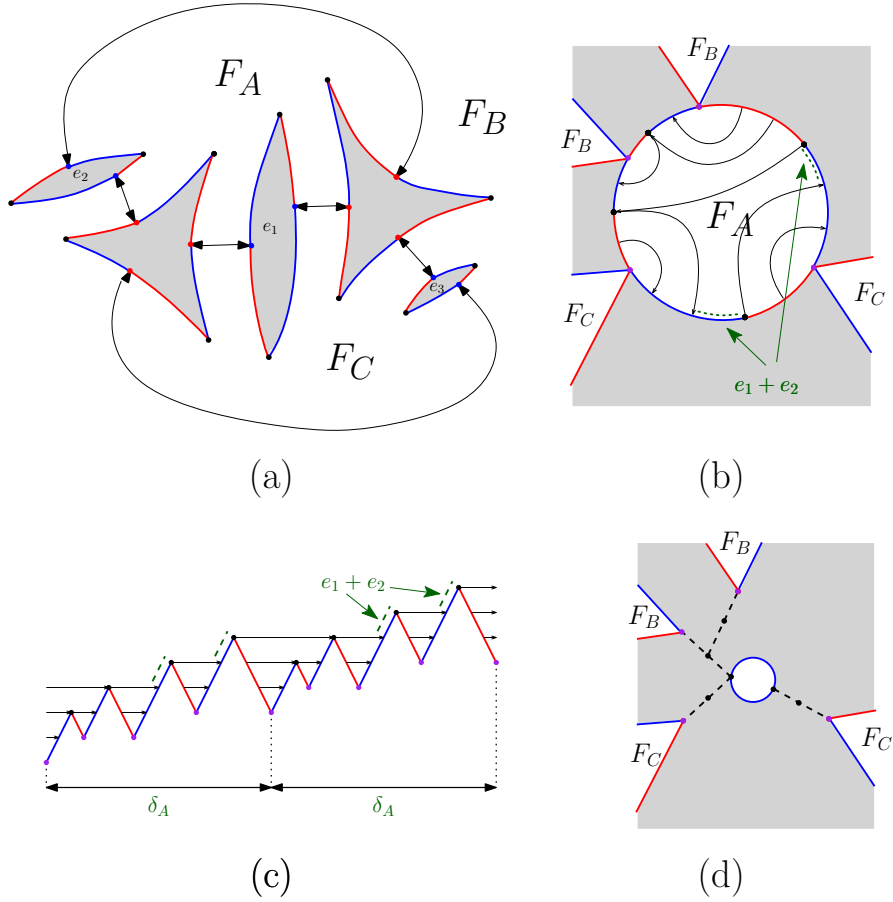


Figure 3.1: The assembling procedure of type I. (a) We first identify the attachment points of the two triangles and the three diangles as shown so as to create a planar map with three special faces F_A , F_B and F_C . (b) The red-to-blue gluing around the special face F_A : the arrows indicate the resulting identification between vertices (the identified attachment points are shown in purple). Here, $e_1 + e_2 = 2$ blue edges remain unmatched. (c) Alternate representation of the gluing process: the cyclic sequence of edges counterclockwise around F_A may be coded by the quasi-periodic lattice path with a unit up (respectively down) step for each blue (respectively red) edge (the increments of the path are denoted ϵ_n in the text). Each down (red) step is then matched to the next up (blue) step on its right which returns to the same height. A number $e_1 + e_2$ of blue edges remain unmatched for each period $\delta_A = \deg(F_A)$. (d) Result of the gluing of F_A : we obtain a boundary of length $e_1 + e_2$ (the glued edges are represented by dashed lines). The red-to-blue gluing of F_B and F_C is performed similarly.

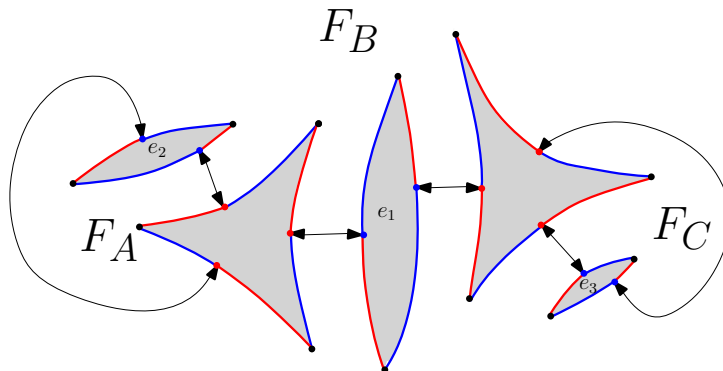


Figure 3.2: The first step of the assembling procedure of type II, creating a planar map with three special faces F_A , F_B and F_C .

are reduced to the vertex-map, the object resulting from the assembling procedure is the vertex-map itself. Besides this pathological case, we always obtain a map in which the three boundaries are distinct elements of the map.

Procedure II. It differs from the previous one only by the identification between attachment points, following now the prescription of Figure 3.2. The resulting object is still a planar map with three special faces: two of them (F_A and F_C) are now incident to two attachment points (after identification) and the third one (F_B) to eight attachment points. They all have a boundary made of alternating blue and red intervals. We then repeat the red-to-blue gluing operation described in the case I, creating three boundaries of respective lengths e_2 (from F_A), e_3 (from F_C) and $2e_1 + e_2 + e_3$ (from F_B). Again, the assembling procedure is trivially extended to the case where some of the triangles/diangles are reduced to the vertex-map, and the three boundaries are distinct as soon as at least one of the building blocks is non trivial.

3.2. Properties of the assembling procedures

Let us first observe that, for both assembling procedures, the resulting map is essentially bipartite: indeed its inner faces are those of the initial triangles and diangles, with no modification of the degrees. The boundary lengths are given by:

$$\text{procedure I: } \begin{cases} 2a = e_1 + e_2 \\ 2b = e_2 + e_3 \\ 2c = e_3 + e_1 \end{cases} \quad \text{procedure II: } \begin{cases} 2a = e_2 \\ 2b = 2e_1 + e_2 + e_3 \\ 2c = e_3 \end{cases} \quad (3.1)$$

Here, a , b and c may either be integers or half-integers. They are all integers (i.e., the map is bipartite) if e_1 , e_2 and e_3 have the same parity in case I, or if e_2 and e_3 are even in case II. Otherwise, two of them are half-integers and the third is an integer, and the map is quasi-bipartite.

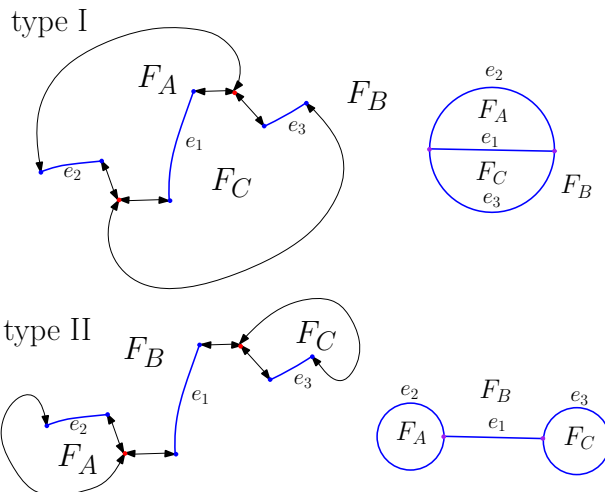


Figure 3.3: When the triangles and diangles have no inner faces, the assembling procedures I and II generate maps corresponding to the generic cases I and II of Figure 1.3.

We also see that, since e_1 , e_2 and e_3 are assumed nonnegative, we have the “triangle inequality” $b \leq c + a$ in case I, while we have $b \geq c + a$ in case II (in both cases, we have $a \leq b + c$ and $c \leq a + b$). Upon permuting a , b and c in case II, it is possible to obtain any possible triple of boundary lengths in a bipartite or quasi-bipartite map with three boundaries.

This suggests to introduce the following definition: a map with three boundaries is said of *type I* (respectively *II*) if the largest of the three boundary lengths is smaller than or equal to (respectively larger than or equal to) the sum of the two other boundary lengths. Clearly a map with three boundaries is either of type I or type II, and may be both in the equality case. We may now state the main bijective result of this paper, illustrated by Figure 1.1 in the case of procedure I.

Theorem 3.1. *For e_1 , e_2 and e_3 fixed nonnegative integers, the assembling procedure I (respectively II) is a bijection between the set of quintuples made of two bigeodesic triangles and three bigeodesic diangles of nonnegative exceedances e_1 , e_2 and e_3 , where at least one element differs from the vertex-map, and the set of essentially bipartite planar maps with three tight boundaries of type I (respectively II), where the lengths of the boundaries are given by (3.1).*

It is instructive to examine the case where the triangles and diangles have no inner faces: the triangles are then reduced to the vertex-map, while the diangles are segments of lengths e_1 , e_2 and e_3 (see Figure 3.3). When these lengths are all positive, we recover precisely from the assembling procedures I and II the two generic maps I and II displayed in Figure 1.3. The degenerate cases correspond to having one or two lengths vanish, and the case $e_1 = e_2 = e_3 = 0$ (all diangles reduced to the vertex-map) is pathological when there are no inner faces.

To establish Theorem 3.1, two statements remain to be proved. First, we need to show that the boundaries of the maps resulting from the assembling procedures are indeed tight: this will be done in Section 4, see Proposition 4.4. Second, we must check that both procedures are bijections: for this, we will exhibit the inverse bijections in Section 5, see Propositions 5.14 and 5.16. Both proofs are most conveniently performed by considering the universal cover of a map with three boundaries, which we introduce in the next section. Before this, let us explain why Theorem 3.1 implies Theorem 1.1, and also sketch the inverse of procedure I in the simpler case of maps with three boundary-vertices ($e_1 = e_2 = e_3 = 0$).

3.3. Enumerative consequences

Recall that $T_{a,b,c}$ denotes the generating function of essentially bipartite planar maps with three tight boundaries of lengths $2a$, $2b$, $2c$, with the weighting convention of Theorem 1.1. As discussed in Section 1, this theorem is implied by the following corollary of Theorem 3.1.

Corollary 3.2. *We have*

$$T_{a,b,c} = R^{a+b+c} \frac{X^3 Y^2}{t^6} - t^{-1} \mathbf{1}_{a=b=c=0} \quad (3.2)$$

where X and Y are the generating functions of bigeodesic balanced diangles and triangles, respectively, as defined in Section 2.

Proof. By Proposition 2.2, the generating function of quintuples made of two bigeodesic triangles and three bigeodesic diangles of nonnegative exceedances e_1 , e_2 and e_3 , is equal to $R^{e_1+e_2+e_3} X^3 Y^2$. We exclude the quintuple with all elements reduced to the vertex-map by subtracting a term $t^5 \mathbf{1}_{e_1=e_2=e_3=0}$.

We then apply Theorem 3.1 and note that, by (3.1), we have $e_1 + e_2 + e_3 = a + b + c$ and $\mathbf{1}_{e_1=e_2=e_3=0} = \mathbf{1}_{a=b=c=0}$ both in procedures I and II. The claim then follows from the fact that the weight of a quintuple, defined according to the conventions of Section 2, is equal to t^6 times that of the corresponding map, defined as in Theorem 1.1. This is clear for face weights since the inner faces are not modified by the bijection. For vertex weights, the corrective factor t^6 comes from the identifications between attachment points, see again Figures 3.1(a) and 3.2: there are generically twelve attachment points in a quintuple, and they are identified in pairs so lead to six vertices in the assembled map. We still obtain a difference of six in the situations where some diangles or triangles are reduced to the vertex-map. Note that the gluing between blue and red edges does not require corrective factors, since by convention the vertices which are incident to red edges and which are not attachment points receive no weight. In particular, potential boundary-vertices are obtained from such unweighted vertices, as wanted. \square

3.4. Disassembling a triply pointed map

We now sketch the proof of Theorem 3.1 in the case of procedure I with $e_1 = e_2 = e_3 = 0$, which generates a triply pointed map (three boundary-vertices). Boundary-vertices are

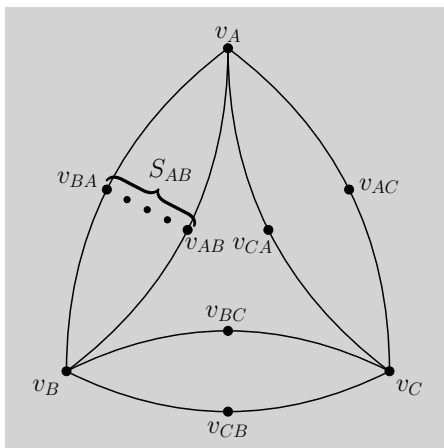


Figure 3.4: Sketch of the decomposition of a triply pointed map, with marked vertices v_A , v_B and v_C . The set S_{AB} consists of geodesic vertices between v_A and v_B at distance r_A from v_A . We pick its extremal elements v_{AB} and v_{BA} , from which the two leftmost bigeodesics launched towards v_A and v_B delimit a maximal diangle containing all other elements of S_{AB} , but not v_C . Similarly, we construct two other disjoint diangles, formed by leftmost bigeodesics launched from vertices v_{BC} and v_{CB} , v_{CA} and v_{AC} respectively. The complementary region consists of two geodesics triangles (one inside and one outside).

always considered tight, so we only have to exhibit the inverse bijection. The key point is to identify the attachment points: once we know them, the decomposition into diangles and triangles is done by cutting along leftmost bigeodesics.

Consider a planar bipartite map with three marked distinct vertices v_A , v_B and v_C (as there are no boundary-faces, being essentially bipartite is the same as being bipartite). Let us denote by d_{AB} , d_{BC} and d_{CA} their mutual distances. By the triangle inequalities and bipartiteness, there exists three nonnegative integers r_A , r_B and r_C , at most one of them vanishing, such that

$$d_{AB} = r_A + r_B, \quad d_{BC} = r_B + r_C, \quad d_{CA} = r_C + r_A. \quad (3.3)$$

We then consider the set S_{AB} of geodesic vertices between v_A and v_B which are at distance r_A from v_A (hence distance r_B from v_B). In the generic situation where r_A, r_B, r_C are all nonzero, we may single out canonically two “extremal” elements v_{AB} and v_{BA} of S_{AB} as follows. For v and v' in S_{AB} , consider the two leftmost bigeodesics towards v_A and v_B which are launched from v and v' : these bigeodesics delimit two regions, which turn out to be balanced bigeodesic diangles. Then, v_{AB} and v_{BA} are chosen in such a way that the diangle not containing v_C is the largest possible (and contains in particular all other elements of S_{AB}), and such that v_A, v_{AB}, v_B and v_{BA} appears in clockwise order around it. See Figure 3.4 for an illustration. We similarly define the vertices v_{BC}, v_{CB}, v_{CA} and v_{AC} . In this way, we obtain three balanced bigeodesic diangles (the specific choice of r_A, r_B, r_C ensures that these are disjoint), and the complementary region forms

two bigeodesic triangles, thereby giving the quintuple we are looking for. Note that some diangles or triangles may be reduced to the vertex-map, for instance it may happen that $v_{AB} = v_{BA}$ (resp. $v_{AB} = v_{BC} = v_{CA}$), in which case the corresponding diangle (resp. triangle) is equal to the vertex-map.

In the situation where, say, r_C vanishes, v_C is actually an element of S_{AB} : we simply cut the map along the leftmost bigeodesic launched from v_C towards v_A and v_B , which transforms the map into a single balanced bigeodesic diangle. This may be seen as a degeneration of the generic situation, upon taking $v_C = v_{AB} = v_{BA} = v_{BC} = v_{CB} = v_{CA} = v_{AC}$, all other elements of the quintuple being equal to the vertex-map.

This informal discussion overlooks some important details, such as the fact that, in general, the leftmost bigeodesics merge before reaching v_A , v_B or v_C . We shall be more precise below when discussing the general inverse bijection, which applies to both types of boundaries (vertices or faces). Still, the core idea will be the same: upon defining in a suitable way the distances d_{AB}, d_{BC}, d_{CA} between the three boundaries, we will define some parameters r_A, r_B, r_C via the *equilibrium conditions* (3.3), and we will then construct some *equilibrium vertices*, analogous to the vertices $v_{AB}, v_{BA}, v_{BC}, v_{CB}, v_{CA}, v_{AC}$ defined above. Once these equilibrium vertices are constructed, the decomposition is done by cutting along leftmost bigeodesics. The main change induced by the presence of boundary-faces is that all this construction must be performed on the universal cover of the map, which we will define now.

4. The universal cover of a map with three boundaries

In this section we introduce the universal cover of a map with three boundaries, which will be one of our main topological tools. Its construction and some of its properties are discussed in Section 4.1. We explain in Section 4.2 how to visualize the assembling procedures directly on the universal cover, before proving in Section 4.3 that the maps resulting from the assembling procedures have tight boundaries.

4.1. Construction and properties of the universal cover

Let M be a map with three boundaries $\partial_A, \partial_B, \partial_C$, that are either boundary-faces or boundary-vertices. We view M as a graph embedded in a topological sphere S' , and we let x_A, x_B, x_C be three distinguished points of S' , such that x_i belongs to the i -th boundary component, that is $x_i = \partial_i$ in the case of a boundary-vertex, or $x_i \in \partial_i$ in the case of a boundary-face. We let S be the triply punctured sphere $S' \setminus \{x_A, x_B, x_C\}$.

The universal cover of the triply punctured sphere. The universal cover of the surface S is the data of a simply connected topological space \tilde{S} and of a mapping $p : \tilde{S} \rightarrow S$ such that for every $x \in S$, there is a neighborhood U of x in S such that $p^{-1}(U)$ is a disjoint union of open sets U_i , with $p|_{U_i} : U_i \rightarrow U$ a homeomorphism. The pair (\tilde{S}, p) is unique up to the natural notion of isomorphism.

It will be useful to consider the following concrete construction. Let S_0 denote the unit square with its four corners removed, and with its four sides denoted by $s_a, s_{\bar{a}}, s_c, s_{\bar{c}}$ in

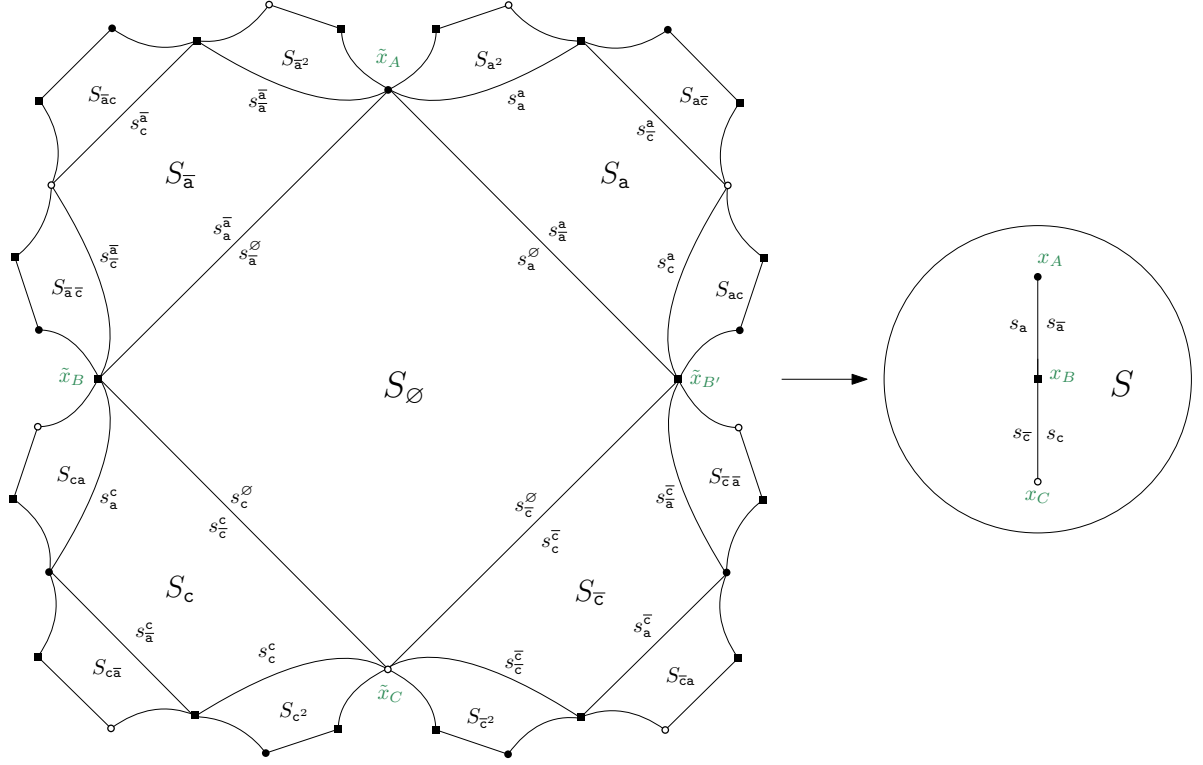


Figure 4.1: A part of the universal cover of the triply punctured sphere. The ideal corners $\tilde{x}_A, \tilde{x}_B, \tilde{x}_C, \tilde{x}_{B'}$ correspond respectively to the punctures x_A, x_B, x_C and x_B again.

counterclockwise direction. Note that the space obtained by gluing S_0 along its sides by identifying s_a with $s_{\bar{a}}$ and s_c with $s_{\bar{c}}$ (with a head to tail matching of their orientations so that the resulting surface is orientable) is homeomorphic to the triply punctured sphere S , and we let $p : S_0 \rightarrow S$ be the resulting projection.

Let $F = \langle \mathbf{a}, \mathbf{c} \rangle$ be the free group with two generators \mathbf{a}, \mathbf{c} , that is the set of reduced finite words \mathbf{w} made of the four letters $\mathbf{a}, \bar{\mathbf{a}}, \mathbf{c}, \bar{\mathbf{c}}$, where $\bar{\mathbf{a}} = \mathbf{a}^{-1}, \bar{\mathbf{c}} = \mathbf{c}^{-1}$ are the inverses of \mathbf{a}, \mathbf{c} (we thus let $\bar{\bar{\mathbf{a}}} = \mathbf{a}, \bar{\bar{\mathbf{c}}} = \mathbf{c}$). Here, we say that a word is reduced if it does not contain an occurrence of any letter followed immediately by its inverse. The group operation is defined by letting \mathbf{vw} be the reduced word obtained from the concatenation of \mathbf{v} and \mathbf{w} . The empty word \emptyset is the neutral element of F . We identify F with its Cayley graph with generators $\{\mathbf{a}, \bar{\mathbf{a}}, \mathbf{c}, \bar{\mathbf{c}}\}$, which is the infinite 4-regular tree with root \emptyset , and we let $|\mathbf{w}|$ be the length of the word \mathbf{w} , which is also its distance in the tree to the root.

For every $\mathbf{w} \in F$, we let $S_{\mathbf{w}}$ be a copy of S_0 , that we can view as $\{(x, \mathbf{w}) : x \in S_0\}$, with its four sides denoted by $s_{\mathbf{a}}^{\mathbf{w}}, s_{\bar{\mathbf{a}}}^{\mathbf{w}}, s_{\mathbf{c}}^{\mathbf{w}}, s_{\bar{\mathbf{c}}}^{\mathbf{w}}$, again oriented counterclockwise around $S_{\mathbf{w}}$. We consider the space \tilde{S} obtained by gluing the spaces $S_{\mathbf{w}}$ along their sides, in such a way that $s_{\mathbf{l}}^{\mathbf{w}}$ is glued with $s_{\bar{\mathbf{l}}}^{\mathbf{w}^{-1}}$ for every letter $\mathbf{l} \in \{\mathbf{a}, \bar{\mathbf{a}}, \mathbf{c}, \bar{\mathbf{c}}\}$ (with a head to tail matching of their orientations). See Figure 4.1. We then extend the projection p to a mapping

$p : \tilde{S} \rightarrow S$ by letting $p(x, \mathbf{w}) = p(x)$ for every $x \in S_0$ and $\mathbf{w} \in F$. This is easily seen to be the universal cover of S .

The universal cover comes with its group of automorphisms $\text{Aut}(p)$, that are the homeomorphisms $u : \tilde{S} \rightarrow \tilde{S}$ such that $p \circ u = p$. This group is isomorphic to the free group F via the natural action of F on \tilde{S} defined by $\mathbf{w} \cdot (x, \mathbf{v}) = (x, \mathbf{wv})$. Note that the element of $\text{Aut}(p)$ corresponding to \mathbf{w} sends $S_{\mathbf{v}}$ to $S_{\mathbf{wv}}$, which may be arbitrarily far apart. We denote by A and C the elements of $\text{Aut}(p)$ corresponding to the action of \mathbf{a} and \mathbf{c} respectively. It will be also convenient to introduce the automorphisms $B := A^{-1}C^{-1}$ and $B' := C^{-1}A^{-1}$ corresponding the respective actions of the elements $\mathbf{b} := \bar{\mathbf{a}}\bar{\mathbf{c}}$ and $\mathbf{b}' := \bar{\mathbf{c}}\bar{\mathbf{a}}$ of F .

Classically, \tilde{S} is a topological space homeomorphic to the open unit disk. In fact, the universal cover of the triply punctured sphere can also be constructed via hyperbolic geometry, see e.g. [Sti12, Section 5.3]. Figure 4.3 (left) displays the connection with our present construction: the gluing of the squares $(S_{\mathbf{w}})_{\mathbf{w} \in F}$ can be realized as a regular tiling in the hyperbolic plane made of ideal quadrangles.

For our purposes, it will be convenient to augment \tilde{S} by adding back the corners of the squares $S_{\mathbf{w}}$, and we denote the resulting space by \tilde{S}' . Note that, after gluing, a corner is common to infinitely many squares: for instance, the corner denoted \tilde{x}_A on Figure 4.1 is common to all the squares $S_{\mathbf{a}^n}$ for $n \in \mathbb{Z}$, similarly \tilde{x}_C is common to all the $S_{\mathbf{c}^n}$, while \tilde{x}_B (resp. $\tilde{x}_{B'}$) is common to all the $S_{\mathbf{b}^n}$ and $S_{\mathbf{b}^n \mathbf{c}}$ (resp. $S_{(\mathbf{b}')^n}$ and $S_{(\mathbf{b}')^n \mathbf{a}}$). The corners form a subset of the ‘ideal boundary’ of \tilde{S} (which corresponds to the boundary of the disk in Figure 4.3), and we therefore call them *ideal corners*. The projection $p : \tilde{S} \rightarrow S$ extends to a continuous mapping¹ from \tilde{S}' to the sphere S' , and the group of automorphisms $\text{Aut}(p)$ acts naturally on \tilde{S}' , each ideal corner being left invariant by an infinite cyclic subgroup.

Finally, we recall that for any continuous path $\gamma : [0, 1] \rightarrow S$ and any $\tilde{\gamma}(0) \in p^{-1}(\gamma(0))$, there is a unique continuous path $\tilde{\gamma} : [0, 1] \rightarrow \tilde{S}$ starting at $\tilde{\gamma}(0)$ and such that $p \circ \tilde{\gamma} = \gamma$. This path is called the *lift* of γ starting at $\tilde{\gamma}(0)$. The lift remains well-defined if the endpoint $\gamma(1)$ is one of the punctures x_A, x_B, x_C , in that case $\tilde{\gamma}(1)$ is an ideal corner. Lifting a path joining two punctures may be done by splitting the path at an intermediate point, and choosing a preimage for that point.

Lifting the map M on the universal cover. We now explain how the above considerations interact with the map M . By viewing the (oriented) edges of M as paths in S' parametrized by $[0, 1]$, we can consider the lifts of these edges in \tilde{S}' , which form an embedded graph \tilde{M} in \tilde{S}' .

The resulting embedded graph \tilde{M} is an infinite map in the non-compact surface \tilde{S}' , with some faces or vertices of infinite degrees (see Figure 4.2 and the right of Figure 4.3 for an example). More precisely, \tilde{M} has two possible types of vertices and faces: *regular*

¹Note however that, if we identify \tilde{S} with the open unit disk as in Figure 4.3, then p does not extend to a continuous function on the closed unit disk. It only admits non-tangential limits at the ideal corners, which form a dense countable subset of the unit circle. This is consistent with the topology of \tilde{S}' resulting from the gluing of squares: in the hyperbolic plane picture, given an ideal corner \tilde{x} , a neighborhood basis for \tilde{x} consists of the interiors of horocycles of center \tilde{x} .

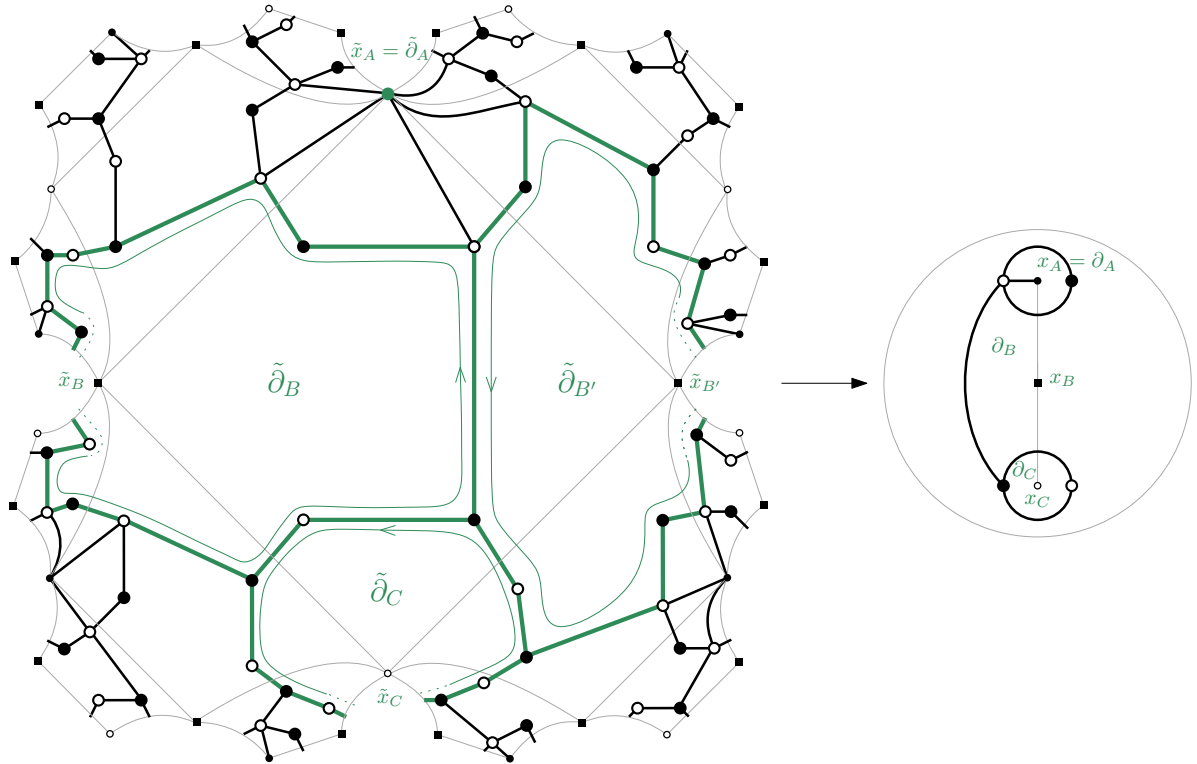


Figure 4.2: A part of the universal cover of a dumbbell-shaped map, having two boundary-faces ∂_B and ∂_C and one boundary-vertex $\partial_A = x_A$. We display in green the distinguished ideal vertex $\tilde{\partial}_A = \tilde{x}_A$, and the contours (oriented counterclockwise by convention) of the distinguished ideal faces $\tilde{\partial}_B$, $\tilde{\partial}_C$ and $\tilde{\partial}_{B'}$. The embedding is good, according to the definition given in Section 5.1.

vertices and faces, which are the preimages of the non-boundary vertices and faces of M (keeping the same finite degree), and *ideal* vertices and faces, which have infinite degree, project to the boundaries of M , and are in bijection with the ideal corners of \tilde{S}' .

Let us provide some elements of justification to this dichotomy. First, since $p : \tilde{S} \rightarrow S$ is a cover, it is immediate that a non-boundary vertex of M , being placed at a point of S , lifts to vertices of \tilde{M} with the same finite degree. Next, if f is a face of M which is not a boundary-face, then (at least when f is not incident to a boundary-vertex, otherwise we have to adapt slightly the argument) its contour ∂f is homotopic in S to a point, so that its lifts form closed paths in \tilde{S} bounding the preimages of f by p (which therefore keep the same finite degree). Now, if f is a boundary-face of M , then its contour ∂f is not homotopic to a point, so that its preimages in \tilde{S} are domains bounded by lifts of ∂f , which form infinite paths of edges, resulting in ideal faces with infinite degree. Finally, a boundary-vertex v of M , being placed at a puncture, lifts to an ideal corner \tilde{x} of \tilde{S}' , and has infinite degree since \tilde{x} is common to infinitely many squares S_w contributing at least one edge incident to \tilde{x} .

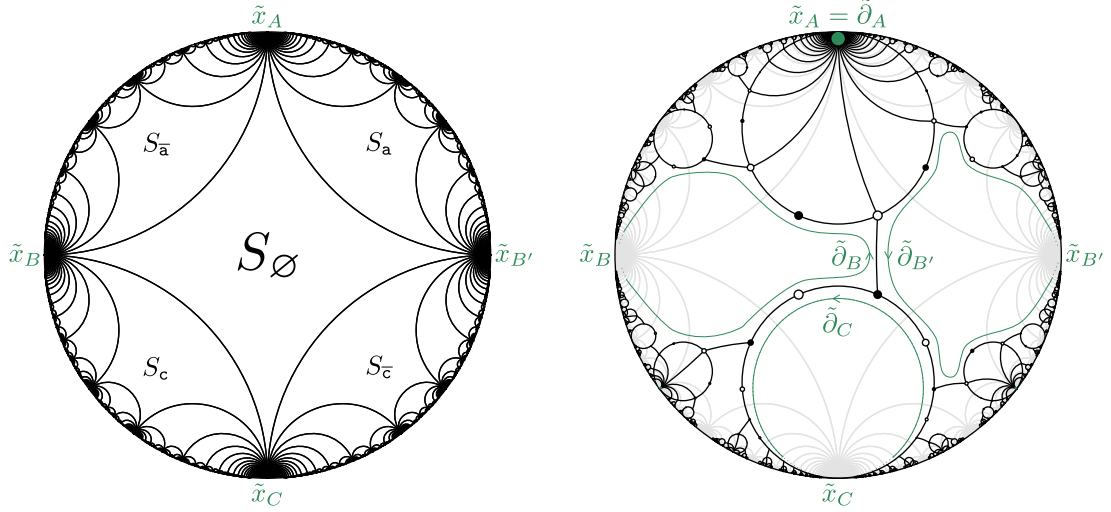


Figure 4.3: Left: the regular tiling of the hyperbolic plane (here represented in the Poincaré disk model) realizing the gluing of squares of Figure 4.1. Right: the corresponding representation of the universal cover of the dumbbell-shaped map of Figure 4.2. The green vertex at the ideal corner \tilde{x}_A has infinite degree. The contour of $\tilde{\partial}_C$ follows a horocycle with center the ideal corner \tilde{x}_C .

We call the infinite map \tilde{M} the *universal cover* of the map M . We endow the set of its vertices $V(\tilde{M})$ with the graph distance \tilde{d} , as for finite maps. The automorphism group of \tilde{M} is the same as that of \tilde{S} , $\text{Aut}(p)$. It acts freely on the regular vertices and faces, but each ideal vertex or face is left invariant by an infinite cyclic subgroup, precisely the same as that fixing the corresponding ideal corner of \tilde{S}' . We point out that, in the concrete construction of \tilde{S} done above, it comes endowed with a distinguished fundamental domain S_\emptyset , which in turn distinguishes four ideal corners $\tilde{x}_A, \tilde{x}_B, \tilde{x}_C$ and $\tilde{x}_{B'}$ (see again Figure 4.1), and therefore four ideal vertices or faces $\tilde{\partial}_A, \tilde{\partial}_B, \tilde{\partial}_C$ and $\tilde{\partial}_{B'}$ of \tilde{M} (see again Figure 4.2). We emphasize that this “rooting” results from our construction of \tilde{S} and *not* from any extra data on M other than its distinguished boundaries.

Note that there is an important flexibility in our construction. Indeed, we can choose in an arbitrary way the embedding of M in S or the projection $p : S_0 \rightarrow S$: the resulting \tilde{S} , \tilde{M} and extension of p to \tilde{S} will always be the same, up to isomorphisms. This observation will be useful in Section 5.

Finally, we record the important observation that, if M is essentially bipartite, then its universal cover \tilde{M} is bipartite. Indeed, every simple cycle in \tilde{M} is contractible and encloses a finite number of faces of finite even degree, thus has even length.

4.2. Visualizing the assembling procedures on the universal cover

We now explain how the assembling procedures I and II can be visualized on the universal cover of the triply punctured sphere. Let us start again from three (bigeodesic) diangles and two triangles, as at the beginning of Section 3. In the description given in Section 3.1,

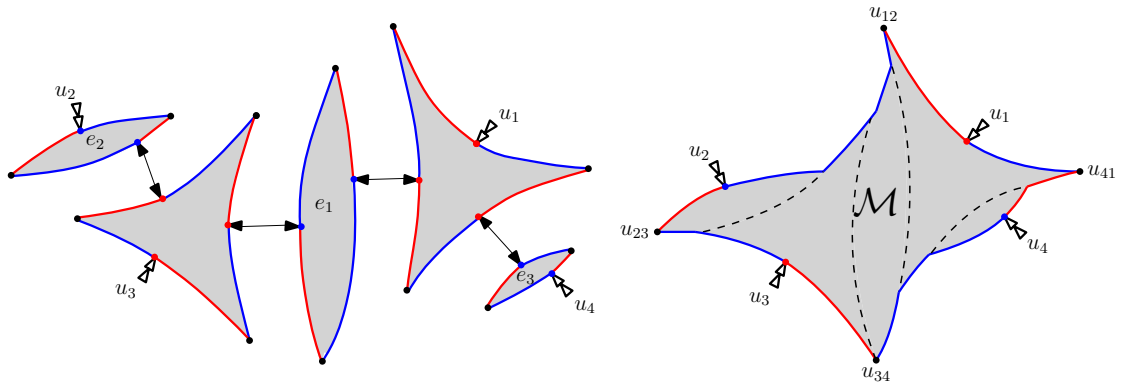


Figure 4.4: The partially assembled map \mathcal{M} obtained from three bigeodesic diangles and two bigeodesic triangles. See again Figure 1.1 for a concrete example.

the assembling was done in two successive operations, attachment then red-to-blue gluing. Here, it is convenient to give an alternative (but equivalent) description in which the assembling is done even more progressively, by doing first a partial attachment and a partial red-to-blue gluing, thereby giving a *partially assembled map*, and then completing the assembling by another round of attachment and red-to-blue gluing.

Precisely, the partially assembled map, which we denote by \mathcal{M} , is constructed as displayed on Figure 4.4. Namely, we identify some of the attachment points of the diangles and triangles together, but some of them, denoted u_1, u_2, u_3 and u_4 , remain unattached for now. Note that the attachments that we perform are exactly those which are common to procedures I and II, see again Figures 3.1(a) and 3.2. This results in a map with one unique special face. We then perform red-to-blue gluing counterclockwise around the special face (i.e. with this face on the left), with the important prescription that we do not perform gluings which would require passing over the attachment points u_1, \dots, u_4 . For instance, a red edge preceding the attachment point u_1 on the right triangle remains unglued, since it would be glued with a blue edge beyond u_1 . The partially assembled map \mathcal{M} is a planar bipartite map with one boundary-face and eight distinguished incident corners: the attachment points u_1, u_2, u_3, u_4 , at which we switch from blue to red when turning counterclockwise around \mathcal{M} , and the corners $u_{12}, u_{23}, u_{34}, u_{41}$ at which we switch back from red to blue. In the situation displayed on Figure 4.4, u_{12} corresponds to a corner of the right triangle, but it could also be, say, a corner of the middle diangle, if the latter were longer. It is straightforward to check that $[u_1, u_{12}]$ (resp. $[u_{41}, u_{12}]$) is a strictly geodesic (resp. geodesic) boundary interval of \mathcal{M} , as defined in Section 2.1, and similarly for the other intervals around \mathcal{M} . Furthermore, by the definition of exceedances, we see that

$$\begin{aligned}
 d(u_1, u_{12}) + e_1 + e_2 &= d(u_{12}, u_2), \\
 d(u_2, u_{23}) + e_2 &= d(u_{23}, u_3), \\
 d(u_3, u_{34}) + e_1 + e_3 &= d(u_{34}, u_4), \\
 d(u_4, u_{41}) + e_3 &= d(u_{41}, u_1),
 \end{aligned} \tag{4.1}$$

where d denotes the graph distance in \mathcal{M} and where, by a slight abuse, we identify corners with their incident vertices. Note that the boundary-face of \mathcal{M} is not necessarily simple, as there may be contacts between the different blue intervals (as said in the caption of Figure 2.2, such contacts may exist in a diangle of positive exceedance, and may subsist in the partial gluing, for instance if all the remaining pieces are equal to the vertex-map).

In order to complete the assembling procedures, we have to identify the remaining attachment points u_1, \dots, u_4 together: let \mathcal{M}_I (resp. \mathcal{M}_{II}) be the map obtained from \mathcal{M} by identifying u_1 with u_2 and u_3 with u_4 (resp. u_1 with u_4 and u_2 with u_3). Note that these identifications are exactly those which are specific to Figure 3.1(a) (resp. Figure 3.2). In the terminology of Section 3.1, the maps \mathcal{M}_I and \mathcal{M}_{II} have three “special” faces, and we complete the assembling procedures by performing red-to-blue gluing in each special face. It is straightforward to check that, for both procedure I and procedure II, we obtain the same final result as with the previous construction.

The interest of our alternative description is that it is now easier to visualize the universal cover of the resulting assembled maps. Precisely, we consider the square tiling $(S_w)_{w \in F}$ of Section 4.1, and inside each square S_w we place a *copy* \mathcal{M}_w of the partially assembled map \mathcal{M} . We then identify the attachment points of these copies together as follows. In the case of procedure I displayed on Figure 4.5, the attachment point u_1^w of \mathcal{M}_w is identified with the attachment point u_2^{wa} of \mathcal{M}_{wa} , and u_3^w is identified with u_4^{wc} , for all $w \in F$. Similarly, in the case of procedure II, looking again at Figure 3.2, we see that the attachment point u_2^w of \mathcal{M}_w is identified with the attachment point u_3^{wa} of \mathcal{M}_{wa} , and u_4^w is identified with u_1^{wc} . Of course, these identifications require to deform the copies, and we can place the identified attachment vertices on the sides of the squares if we want. At this stage, we obtain infinite maps denoted by $\tilde{\mathcal{M}}_I$ and $\tilde{\mathcal{M}}_{II}$, which are the respective universal covers of \mathcal{M}_I and \mathcal{M}_{II} , upon seeing their three special faces as the three boundaries.

To complete the assembling procedure in the universal cover, we have to perform a final round of red-to-blue gluing in each special (ideal) face. To better understand how this works, it is useful to set up some notations. We first introduce the shorthand notations

$$I_1 := [u_{41}, u_{12}], \quad I_2 := [u_{12}, u_{23}], \quad I_3 := [u_{23}, u_{34}], \quad I_4 := [u_{34}, u_{41}] \quad (4.2)$$

for the sides of \mathcal{M} (so that I_j is a bigeodesic launched from the assembling point u_j). We also introduce the unified notations

$$\text{procedure I: } \begin{cases} I_a := I_1 \\ I_{\bar{a}} := I_2 \\ I_c := I_3 \\ I_{\bar{c}} := I_4 \end{cases} \quad \text{procedure II: } \begin{cases} I_a := I_2 \\ I_{\bar{a}} := I_3 \\ I_c := I_4 \\ I_{\bar{c}} := I_1 \end{cases} \quad (4.3)$$

and, for $w \in F$ and $1 \in \{a, \bar{a}, c, \bar{c}\}$, we let I_1^w be the corresponding side of the copy \mathcal{M}_w . The interest of the unified notations is that the attachment point of I_1^w is identified with that of I_1^{w1} , regardless of whether we apply procedure I or II. As is apparent on (4.3), switching from procedure I to procedure II amounts on the universal cover to rotating

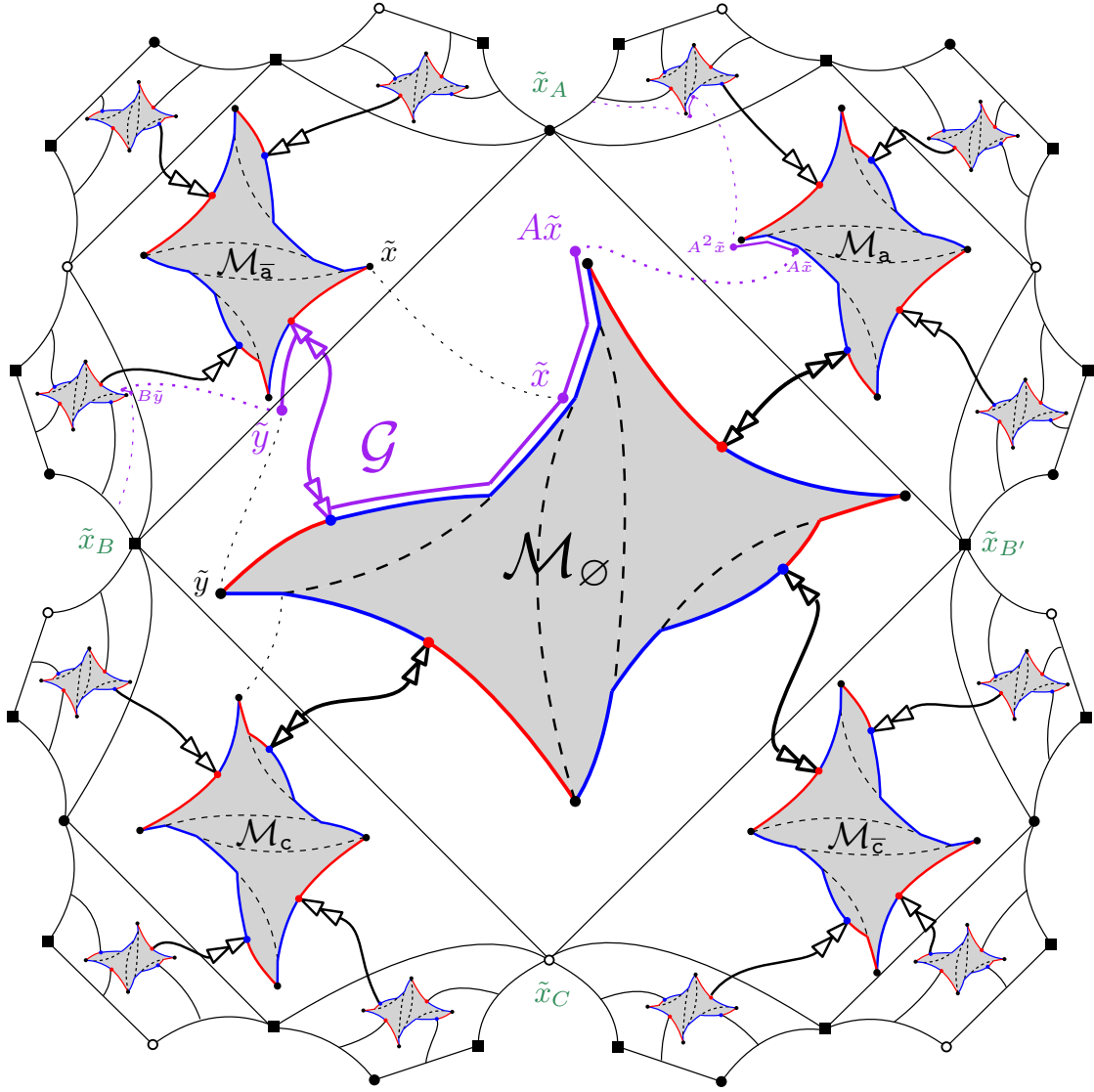


Figure 4.5: A visualization of the assembling procedure I in the universal cover of the triply punctured sphere. Inside each square S_w of the tiling of Figure 4.1, we place a copy \mathcal{M}_w of the partial gluing \mathcal{M} of Figure 4.4. By attaching these maps together via their attachment points as displayed with the arrows, and deforming appropriately to perform the identification of vertices, we obtain the universal cover of the map \mathcal{M}_I . To complete the assembling, we have to match and glue the red and blue edges of the ideal faces together (some identification between vertices are shown with dotted lines), thereby leaving only blue unmatched edges incident to ideal faces. Procedure II works just the same, except that we have to rotate each map \mathcal{M}_w by a quarter-turn clockwise. We display in purple the path \mathcal{G} and its vertices \tilde{x} , $A\tilde{x}$, $A^2\tilde{x}$, \tilde{y} , $B\tilde{y}$, as defined in Section 4.3 (in the displayed situation we have $\Delta_a, \Delta_{\bar{c}} > 0$ but $\Delta_{\bar{a}} = 0$). By Lemma 4.1, \mathcal{G} is a geodesic in \tilde{M} .

each \mathcal{M}_w by a quarter-turn clockwise. Furthermore, the red part of I_1^w and the blue part of I_1^{w1} are incident to the same special face, and appear successively counterclockwise around it. Thus, in the red-to-blue gluing operation, the red edges in I_1^w will first look for blue matches in I_1^{w1} . Observe that, in all this discussion, we can return from the universal cover to the sphere by dropping the copy superscript.

Let us first consider the case $1 = \mathbf{a}$: by (4.1), we see that the red part of $I_{\mathbf{a}}$ has $\Delta_{\mathbf{a}}$ fewer edges than the blue part of $I_{\bar{\mathbf{a}}}$, with

$$\text{procedure I: } \Delta_{\mathbf{a}} := e_1 + e_2, \quad \text{procedure II: } \Delta_{\mathbf{a}} := e_2. \quad (4.4)$$

Since $\Delta_{\mathbf{a}}$ is always nonnegative, when we complete the assembling of \mathcal{M} , the red part of $I_{\mathbf{a}}$ is thus completely glued to the beginning of the blue part of $I_{\bar{\mathbf{a}}}$ (starting at the attachment point). If $\Delta_{\mathbf{a}} > 0$, there remains an unmatched blue part of length $\Delta_{\mathbf{a}}$ which forms the contour of the boundary face ∂_A ; if $\Delta_{\mathbf{a}} = 0$, ∂_A is instead a boundary-vertex as explained in Section 3.1. Translated in the universal cover, the red part of $I_{\mathbf{a}}^w$ is completely glued to the beginning of the blue part of $I_{\bar{\mathbf{a}}}^{w\mathbf{a}}$ (starting at the attachment point). If $\Delta_{\mathbf{a}} > 0$, the remaining unmatched blue part of $I_{\bar{\mathbf{a}}}^{w\mathbf{a}}$ forms a lift of the contour of the boundary face ∂_A ; if $\Delta_{\mathbf{a}} = 0$, we only get an ‘‘exposed’’ blue vertex which we can place at an ideal corner of \tilde{S}' in order to form an ideal vertex of the map.

The case $1 = \mathbf{c}$ is entirely similar, the red part of $I_{\mathbf{c}}$ having $\Delta_{\mathbf{c}}$ fewer edges than the blue part of $I_{\bar{\mathbf{c}}}$, with

$$\text{procedure I: } \Delta_{\mathbf{c}} := e_1 + e_3, \quad \text{procedure II: } \Delta_{\mathbf{c}} := e_3. \quad (4.5)$$

The cases $1 = \bar{\mathbf{a}}$ and $1 = \bar{\mathbf{c}}$ are slightly more involved since they must be considered altogether to construct the boundary ∂_B . Let $\Delta_{\bar{\mathbf{a}}}$ (resp. $\Delta_{\bar{\mathbf{c}}}$) be the difference between the length of the blue part of $I_{\bar{\mathbf{a}}}$ (resp. $I_{\bar{\mathbf{c}}}$) and that of the red part of $I_{\mathbf{a}}$ (resp. $I_{\mathbf{c}}$). The relations (4.1) imply that $\Delta_{\mathbf{b}} := \Delta_{\bar{\mathbf{a}}} + \Delta_{\bar{\mathbf{c}}}$ is given by

$$\text{procedure I: } \Delta_{\mathbf{b}} := e_2 + e_3, \quad \text{procedure II: } \Delta_{\mathbf{b}} := 2e_1 + e_2 + e_3 \quad (4.6)$$

and is therefore always nonnegative, but the signs of $\Delta_{\bar{\mathbf{a}}}$ and $\Delta_{\bar{\mathbf{c}}}$ themselves are not fixed since they depend on the sizes of different diangles and triangles. We therefore have three generic situations:

- (i) $\Delta_{\bar{\mathbf{a}}}$ and $\Delta_{\bar{\mathbf{c}}}$ are both nonnegative,
- (ii) $\Delta_{\bar{\mathbf{a}}}$ is negative (hence $\Delta_{\bar{\mathbf{c}}}$ is positive),
- (iii) $\Delta_{\bar{\mathbf{c}}}$ is negative (hence $\Delta_{\bar{\mathbf{a}}}$ is positive).

Let us discuss these three situations, illustrated on Figure 4.6. In the situation (i), all the red edges of $I_{\bar{\mathbf{a}}}$ (resp. $I_{\bar{\mathbf{c}}}$) are matched to blue edges of $I_{\mathbf{a}}$ (resp. $I_{\mathbf{c}}$). This implies two things about the universal cover, one good and one bad. The good thing is that we only have ‘‘nearest neighbor’’ gluings, as in the cases $1 = \mathbf{a}, \mathbf{c}$ discussed before: all the red edges of $I_{\bar{\mathbf{a}}}^w$ (resp. $I_{\bar{\mathbf{c}}}^w$) are matched to blue edges of $I_{\bar{\mathbf{a}}}^{w\bar{\mathbf{a}}}$ (resp. $I_{\bar{\mathbf{c}}}^{w\bar{\mathbf{c}}}$). The bad thing is that, since there are some unmatched blue edges in both $I_{\mathbf{a}}$ and $I_{\mathbf{c}}$ (unless we are in

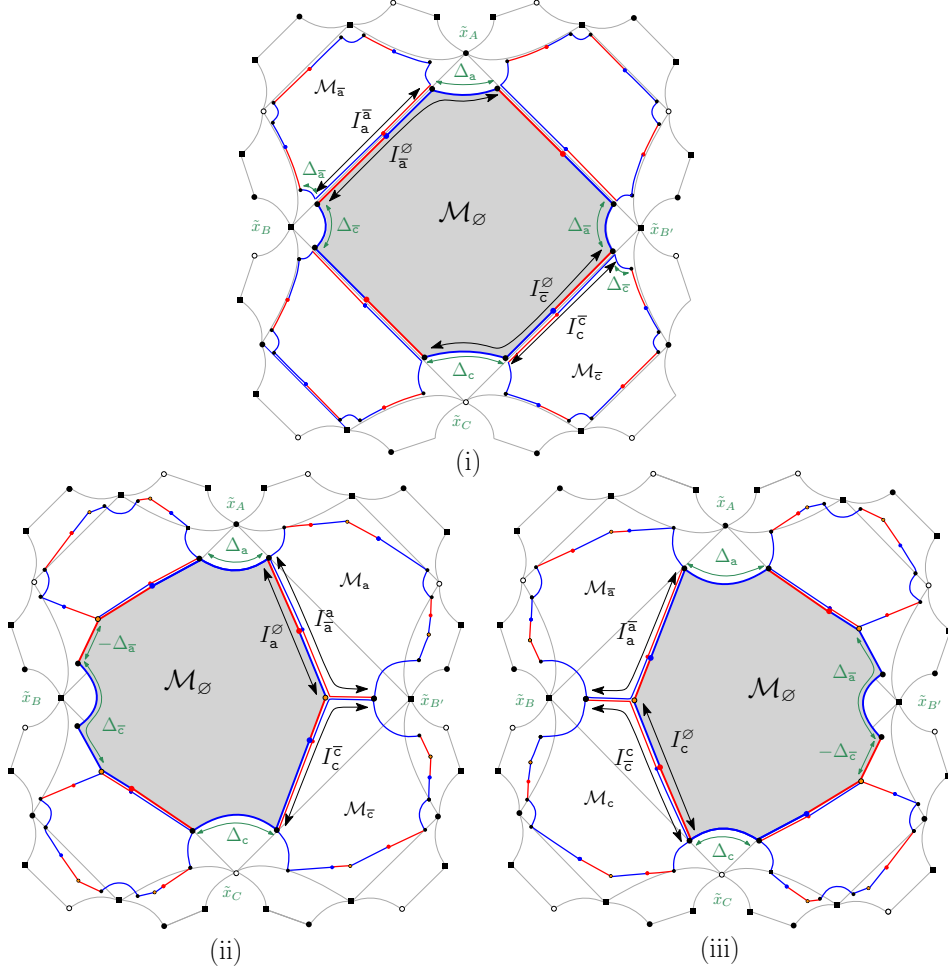


Figure 4.6: The three generic situations corresponding to the possible signs of $\Delta_{\bar{a}}$ and $\Delta_{\bar{c}}$: (i) $\Delta_{\bar{a}}, \Delta_{\bar{c}} \geq 0$, (ii) $\Delta_{\bar{a}} < 0$ and $\Delta_{\bar{c}} \geq 0$, (iii) $\Delta_{\bar{a}} \geq 0$ and $\Delta_{\bar{c}} < 0$. In case (ii), some of the red edges of $I_{\bar{a}}^{\bar{a}}$ are matched to blue edges of $I_c^{\bar{c}} = I_c^{\bar{c}}$, and similarly for case (iii) mutatis mutandis.

the degenerate situation where $\Delta_{\bar{a}}$ or $\Delta_{\bar{c}}$ vanishes), the lifts of the contour of ∂_B do not remain in a single copy $\mathcal{M}_{\bar{w}}$, but we have to consider two neighboring copies, say $\mathcal{M}_{\bar{w}}$ and $\mathcal{M}_{\bar{w}\bar{a}}$, to obtain such a lift as the concatenation of the unmatched blue parts of $I_{\bar{a}}^{\bar{w}}$ and $I_{\bar{c}}^{\bar{w}\bar{a}}$.

In the situation (ii), some red edges of $I_{\bar{a}}$ do not find blue matches in $I_{\bar{a}}$, and therefore find them in I_c . This implies two things about the universal cover, one bad and one good. The bad thing is that there are now “next nearest neighbor” gluings in the universal cover, namely some red edges of $I_{\bar{a}}^{\bar{w}}$ are matched to blue edges of $I_c^{\bar{w}\bar{b}}$, where we recall that $\bar{b} = \bar{a}\bar{c}$ is an element of length 2 in F . The good thing is, since all unmatched blue edges are found on I_c , the corresponding unmatched blue part of $I_c^{\bar{w}}$ forms a complete lift of the

contour of ∂_B that remains in the single copy $\mathcal{M}_{\mathbf{w}}$.

The situation (iii) is entirely similar to the situation (ii), upon interchanging the roles of \mathbf{a} and \mathbf{c} , and therefore changing \mathbf{b} into $\mathbf{b}' = \bar{\mathbf{c}}\bar{\mathbf{a}}$.

4.3. Tightness of the boundaries resulting from the assembling procedures

We are now in position to prove that the maps resulting from the assembling procedures have tight boundaries. Starting from three diangles and two triangles, we denote by \mathcal{M} the partially assembled map as defined in the previous subsection, and by M the completely assembled map (done according to procedure I or II). As we have seen, the universal cover \tilde{M} of M can be constructed directly by gluing infinitely many copies of \mathcal{M} along their boundaries.

A key ingredient in our proof is the path \mathcal{G} displayed on Figure 4.5 and defined as follows. It consists of two parts which are both “launched” from the attachment point between the copies \mathcal{M}_{\emptyset} and $\mathcal{M}_{\bar{\mathbf{a}}}$, and which go “towards” the ideal corners \tilde{x}_A and \tilde{x}_B , respectively, by following the blue boundaries. More precisely, the part towards \tilde{x}_A starts with the blue part of $I_{\bar{\mathbf{a}}}^{\emptyset}$, then continues with the unmatched blue part of $I_{\bar{\mathbf{a}}}^{\mathbf{a}}$, then that of $I_{\bar{\mathbf{a}}}^{\mathbf{a}^2}$, $I_{\bar{\mathbf{a}}}^{\mathbf{a}^3}$, etc. Let us denote by \tilde{x} the last vertex on the blue part of $I_{\bar{\mathbf{a}}}^{\emptyset}$ which is glued to the red part of $I_{\bar{\mathbf{a}}}^{\mathbf{a}}$. Then, our path passes through the vertices $A^n\tilde{x}$ for all $n \geq 0$ (the unmatched blue part of $I_{\bar{\mathbf{a}}}^{\mathbf{a}^n}$ going from $A^n\tilde{x}$ to $A^{n+1}\tilde{x}$). In the case $\Delta_{\mathbf{a}} = 0$, all the vertices $A^n\tilde{x}$ are identified and placed at the ideal corner \tilde{x}_A . In this case, \tilde{x}_A is reached in a finite number of steps by our path. As soon as $\Delta_{\mathbf{a}}$ is positive, our path is infinite but, as visible on Figure 4.5, it still “tends” to \tilde{x}_A in a sense, as it meets at \tilde{x} the contour of the ideal face containing \tilde{x}_A , and follows it counterclockwise onwards. The description of the part towards \tilde{x}_B is similar and just a bit more involved, for the reasons discussed at the end of Section 4.2: assume for instance that we are in case (i) with $\Delta_{\bar{\mathbf{a}}}, \Delta_{\bar{\mathbf{c}}} \geq 0$, then the path with the blue part of $I_{\bar{\mathbf{a}}}^{\bar{\mathbf{a}}}$, continues with the unmatched blue part of $I_{\bar{\mathbf{c}}}^{\mathbf{b}}$, then that of $I_{\bar{\mathbf{a}}}^{\mathbf{b}\bar{\mathbf{a}}}$, $I_{\bar{\mathbf{c}}}^{\mathbf{b}^2}$, $I_{\bar{\mathbf{a}}}^{\mathbf{b}^2\bar{\mathbf{a}}}$, etc. If $\Delta_{\mathbf{b}} > 0$, the path meets at a vertex denoted \tilde{y} the contour of the ideal face containing \tilde{x}_B , and follows it counterclockwise onwards, passing in particular through $B^n\tilde{y}$ for all $n \geq 0$. If $\Delta_{\mathbf{b}} = 0$, the path reaches \tilde{x}_B in a finite number of steps, and we set $\tilde{y} := \tilde{x}_B$. Then, the key property of \mathcal{G} is the following:

Lemma 4.1. *The path \mathcal{G} is a geodesic in \tilde{M} .*

Proof. Intuitively, the reason is that, in Figure 4.5, we glue the copies along (bi)geodesics. More formally, consider a path γ in \tilde{M} whose two endpoints are on \mathcal{G} : we need to show that the length of γ is at least that of the portion of \mathcal{G} having the same endpoints. Our proof is by induction on the number of copies visited by γ .

Precisely, we say that γ enters into k copies if it can be written as a concatenation of paths $\gamma_0\gamma_1 \dots \gamma_k\gamma_{k+1}$, where γ_0 and γ_{k+1} are portions of \mathcal{G} (which we do not include into the copy count) and, for all $i = 1, \dots, k$, γ_i is a path in the copy $\mathcal{M}_{\mathbf{w}_i}$. Without loss of generality, we may assume that the sequence $(\mathbf{w}_i)_{i=1}^k$ is consistent with the structure of gluings discussed at the end of Section 4.2, that is to say in the situation (i) we have $\mathbf{w}_{i+1}\mathbf{w}_i^{-1} \in \{\mathbf{a}, \bar{\mathbf{a}}, \mathbf{c}, \bar{\mathbf{c}}\}$ for all $i = 1, \dots, k-1$ and, in the situations (ii) and (iii), we must also allow the values $\mathbf{b}, \bar{\mathbf{b}}$ and $\mathbf{b}', \bar{\mathbf{b}}'$, respectively. Note that ideal vertices lead to

identifications between vertices belonging to distant copies, but we can always assume that the \mathbf{w}_i satisfy the above constraint by considering that a long-range identification corresponds to a concatenation of several paths γ_i of length zero. We may also assume that \mathbf{w}_1 and \mathbf{w}_k are both of the form \mathbf{a}^n , \mathbf{b}^n or $\mathbf{b}^n\bar{\mathbf{a}}$ for some $n \geq 0$, as these correspond to the copies “carrying” \mathcal{G} .

If γ enters into 0 copies, it is contained in \mathcal{G} and we are done. If it enters into $k \geq 1$ copies, we will show that we can modify it, without increasing its length, so that it enters into at most $k - 1$ copies. For this, we pick an i such that $|\mathbf{w}_i|$ is maximal. Let $\mathbf{l} \in \{\mathbf{a}, \bar{\mathbf{a}}, \mathbf{c}, \bar{\mathbf{c}}\}$ be the last letter of \mathbf{w}_i , with the convention that $\mathbf{l} = \mathbf{a}$ if $\mathbf{w}_i = \emptyset$. Then, from the structure of gluings discussed above, from the definition of \mathcal{G} , and from the maximality of $|\mathbf{w}_i|$, we see that γ_i has its two endpoints on the boundary interval $I_{\mathbf{l}}^{\mathbf{w}_i}$ which is geodesic in $\mathcal{M}_{\mathbf{w}_i}$. Let γ'_i be the portion of $I_{\mathbf{l}}^{\mathbf{w}_i}$ with the same endpoints as γ_i : γ_i cannot be shorter than γ'_i , so γ is not shorter than the path $\gamma' := \gamma_0 \dots \gamma_{i-1} \gamma'_i \gamma_{i+1} \dots \gamma_{k+1}$. We claim that γ' enters into (at most) $k - 1$ copies. Indeed, for $1 < i < k$, γ'_i can be viewed as a path on the boundaries of the copies $\mathcal{M}_{\mathbf{w}_{i-1}}$ and $\mathcal{M}_{\mathbf{w}_{i+1}}$ —which are necessarily the same in the situation (i), but could differ in the situations (ii) and (iii)—so that we may rewrite $\gamma_{i-1} \gamma'_i \gamma_{i+1}$ as the concatenation of (at most) two paths, each of them staying in one of these copies. The argument is the same for $i = 1$ or $i = k$, upon understanding that $\mathcal{M}_{\mathbf{w}_0}$ and $\mathcal{M}_{\mathbf{w}_{k+1}}$ refer to the path \mathcal{G} . \square

Remark 4.2. The projection of \mathcal{G} on the finite map M consists of a path connecting the projection x of \tilde{x} to the projection y of \tilde{y} —this path is *not* a geodesic in general—prolonged with infinitely many turns around ∂_A and ∂_B when these are boundary-faces.

We will need another technical lemma about \mathcal{G} and its two distinguished vertices \tilde{x} and \tilde{y} :

Lemma 4.3. *Suppose that ∂_A (resp. ∂_B) is a boundary-face of M , and let c be a cycle of M freely homotopic in S to, i.e. which can be continuously deformed into, the contour of ∂_A (resp. ∂_B), oriented counterclockwise. Then, c can be lifted to a path \tilde{c} in \tilde{M} going from a vertex \tilde{z} to the vertex $A\tilde{z}$ (resp. $B\tilde{z}$), with \tilde{z} belonging to \mathcal{G} and situated between \tilde{x} and \tilde{y} .*

Proof. If ∂_A is a boundary-face, we denote its contour by $\hat{\partial}_A$, which we orient counterclockwise and view as a loop rooted at the projection x of \tilde{x} on M . If c is freely homotopic to $\hat{\partial}_A$, there exists a path γ going from x to a point z_0 on c such that $\gamma c \gamma^{-1}$ and $\hat{\partial}_A$ are homotopic as loops rooted at x . Lifting these loops to \tilde{M} , we get paths with the same endpoints. Choosing the starting point to be \tilde{x} , the final point must be $A\tilde{z}$ (since it is the final point for the lift of $\hat{\partial}_A$), and we deduce that $\gamma c \gamma^{-1}$ lifts to $\tilde{\gamma} \tilde{c}_0 (A\tilde{\gamma})^{-1}$, where $\tilde{\gamma}$ is the lift of γ going from \tilde{x} to a vertex \tilde{z}_0 , and \tilde{c}_0 is a lift of c going from \tilde{z}_0 to $A\tilde{z}_0$.

If \tilde{z}_0 lies on \mathcal{G} we are done, otherwise we can tweak it as follows. Note that the paths $A^n \tilde{c}_0$, $n \in \mathbb{Z}$ are all lifts of c , with the property that the endpoint of $A^n \tilde{c}_0$ is the starting point of $A^{n+1} \tilde{c}_0$. The concatenation of these paths is a doubly infinite path \tilde{c}_∞ in \tilde{M} (whose projection to M circles around c indefinitely) which, by planarity, necessarily crosses \mathcal{G} at a vertex \tilde{z} situated between \tilde{x} and \tilde{y} . Indeed, as visible on Figure 4.5, the portion of \mathcal{G} between \tilde{x} and \tilde{y} separates the copies $\mathcal{M}_{\mathbf{w}}$ with a reduced word \mathbf{w} starting

with the letter \bar{a} , from the others. And, for $n \geq 0$ large enough, $A^{-n}\tilde{z}_0$ will be in the former set of copies, and $A^n\tilde{z}_0$ in the latter. The portion \tilde{c} of \tilde{c}_∞ between \tilde{z} and $A\tilde{z}$ is the wanted lift of c .

The reasoning in the case where ∂_B is a boundary-face and c is a cycle freely homotopic to its contour is entirely similar. \square

Proposition 4.4. *The map M , assembled according to procedure I or II, has tight boundaries.*

Proof. Let us first prove that the boundary ∂_A is tight. If it is a boundary-vertex this is a tautology, otherwise it is a boundary-face of length $\Delta_{\mathbf{a}} > 0$, and we need to show that any cycle c freely homotopic to its contour has length at least $\Delta_{\mathbf{a}}$. Let us lift c to a path \tilde{c} as in Lemma 4.3. Then, the length of c is at least $\tilde{d}(\tilde{z}, A\tilde{z})$ which, by the triangle inequality, satisfies

$$\tilde{d}(\tilde{z}, A\tilde{z}) \geq \tilde{d}(\tilde{z}, A\tilde{x}) - \tilde{d}(A\tilde{x}, A\tilde{z}). \quad (4.7)$$

As \mathcal{G} is a geodesic by Lemma 4.1, and as \tilde{x} lies between \tilde{z} and $A\tilde{x}$ on \mathcal{G} , we have

$$\tilde{d}(\tilde{z}, A\tilde{x}) = \tilde{d}(\tilde{z}, \tilde{x}) + \tilde{d}(\tilde{x}, A\tilde{x}) = \tilde{d}(\tilde{z}, \tilde{x}) + \Delta_{\mathbf{a}}. \quad (4.8)$$

But we have $\tilde{d}(\tilde{z}, \tilde{x}) = \tilde{d}(A\tilde{x}, A\tilde{z})$ since A is an automorphism of \tilde{M} , hence

$$\tilde{d}(\tilde{z}, A\tilde{z}) \geq \Delta_{\mathbf{a}} \quad (4.9)$$

as wanted. The proof for ∂_B is entirely similar, using again Lemma 4.3, and replacing in the above argument $\Delta_{\mathbf{a}}$ by $\Delta_{\mathbf{b}}$, A by B , and \tilde{x} by \tilde{y} . Finally, for ∂_C , we notice that throughout this section it plays a symmetric role to ∂_A , viewing all the figures upside down (i.e. rotated by 180 degrees). \square

To conclude this section, let us note that, symmetrically to the definition of \mathcal{G} , we may define another geodesic \mathcal{G}' that consists of two parts launched from the attachment point between the copies \mathcal{M}_\emptyset and $\mathcal{M}_{\bar{c}}$ and going towards the ideal corners \tilde{x}_C and $\tilde{x}_{B'}$, respectively. Then, the copy \mathcal{M}_\emptyset is delimited by the four geodesics \mathcal{G} , $A\mathcal{G}$, \mathcal{G}' and $C\mathcal{G}'$, upon removing their pairwise common parts. Furthermore, $A\mathcal{G}$ (resp. $C\mathcal{G}'$) may be viewed as a geodesic launched from the attachment point between \mathcal{M}_\emptyset and $\mathcal{M}_{\mathbf{a}}$ (resp. $\mathcal{M}_{\mathbf{c}}$).

5. Decomposing a map with three tight boundaries

In this section we complete the proof of Theorem 3.1: starting from an essentially bipartite planar map M with three tight boundaries $\partial_A, \partial_B, \partial_C$ of respective lengths $2a, 2b, 2c \geq 0$ on the triply punctured sphere S , we want to disassemble M into two bigeodesic triangles and three bigeodesic diangles with nonnegative exceedances, in a way that inverts the assembling procedure.

We already sketched in Section 3.4 the decomposition in the case of triply pointed maps ($a = b = c = 0$). In order to generalize it to the case $a, b, c \geq 0$, we have to find

an analog of the equilibrium conditions (3.3), which involve the distances d_{AB}, d_{BC}, d_{CA} between the boundary-vertices. When some boundaries are faces, we need appropriate analogs of these distances: it turns out that such analogs may be constructed using so-called Busemann functions defined on the universal cover \tilde{M} of the map M . From this, we will obtain the equilibrium vertices, from which we will launch leftmost bigeodesics giving the decomposition we are looking for.

Our presentation is done in several steps. First, we discuss in Section 5.1 some graph-theoretical properties of the infinite map \tilde{M} , via the notion of good embedding. Busemann functions, associated with infinite geodesics, are then introduced in Section 5.2. We then explain in Section 5.3 how tight boundaries give rise to specific Busemann functions on \tilde{M} . In Section 5.4, we adapt the notion of leftmost bigeodesic to \tilde{M} , and use it to state the crucial diangle lemma. We construct equilibrium vertices in Section 5.5, and use them to state the no less crucial triangle lemma. We apply all these tools in Sections 5.6 and 5.7 to exhibit the inverses of the assembling procedures I and II, respectively.

5.1. Graph-theoretical properties of the universal cover

Let us start by discussing some properties of the underlying graph of \tilde{M} , which is infinite. For this, it is useful to introduce the notion of “good embedding”.

Recall from Section 4.1 that the map \tilde{M} is obtained by lifting the map M in the universal cover \tilde{S} of the triply punctured sphere S , and that we constructed \tilde{S} as a square tiling $(S_w)_{w \in F}$ dual to the infinite 4-regular tree F . Let us denote by Σ the projection of the boundaries of the square S_\emptyset (hence of any square S_w) on the sphere S' : it is a path connecting x_A to x_C via x_B , see again Figure 4.1.

In general, the edges of \tilde{M} may connect vertices belonging to squares arbitrarily far from each other in F , since the edges of M may cross Σ in an arbitrarily complicated manner. We can simplify the situation by an appropriate deformation of the embedding of M in S (hence, of the embedding of \tilde{M} in \tilde{S}). More precisely, we say that we have a *good embedding* if every edge of M , with its endpoints excluded, is either entirely contained in Σ , or intersects it in at most one point. Note that, in the latter case, the endpoints may also belong to Σ . See again Figure 4.2 for an example.

Lemma 5.1. *Every map M with three boundaries admits a good embedding.*

Proof. Consider the first derived map M' of M , which is defined [Tut63] as the triangulation obtained by superimposing M with its dual—which creates a quadrangulation called the derived map [Sch15] of M —and splitting each quadrangle into two triangles by connecting each vertex of M to all neighboring dual vertices. The vertex set of M' can be partitioned into $\{W, W^*, W^\dagger\}$, where W , W^* and W^\dagger correspond respectively to the vertices, faces and edges of M , and the edges of M' correspond to the incidence relations in M . Note that the vertices of M' have even degree, and those in W^\dagger have degree four.

The boundaries $\partial_A, \partial_B, \partial_C$ of M become vertices in M' , which we can place at the punctures x_A, x_B, x_C of S . Let P be a simple path on M' connecting x_A to x_C via x_B , and going “straight” at every vertex in W^\dagger . Such a path always exists and, by deforming M' in such a way that P coincides with Σ , we get a good embedding of M . \square

When the embedding of M is good, which we will assume from now on, the lifted edges of \tilde{M} remains “local” with respect to the tiling $(S_w)_{w \in F}$, i.e. they may only connect vertices lying in the same square or in neighboring squares (i.e. squares $S_w, S_{w'}$ with $w^{-1}w' \in \{\mathbf{a}, \bar{\mathbf{a}}, \mathbf{c}, \bar{\mathbf{c}}\}$). In particular, when we remove the finitely many vertices belonging to the square S_\emptyset (including those possibly placed on its boundaries and at its ideal corners) and their incident edges, then \tilde{M} is disconnected in four infinite pieces. It follows that \tilde{M} has infinitely many ends in the graph-theoretical sense. These ends are in natural bijection with those of the infinite 4-regular tree F .

Recall that \tilde{M} has two possible types of vertices, namely regular vertices with finite degree, and ideal vertices (placed at ideal corners of \tilde{S}') with infinite degree. In the absence of ideal vertices (i.e. when M has only boundary-faces), the underlying graph of \tilde{M} is locally finite. In the presence of ideal vertices, we have the following weaker property:

Lemma 5.2. *Let v and v' be two vertices of \tilde{M} , and r a nonnegative integer. Then, the number of simple paths from v to v' having length at most r is finite.*

Proof. Since we have a good embedding, we may keep track of the squares visited by a path on \tilde{M} :

- when following an edge between regular vertices, we may either remain in the same square S_w , or *move* to a neighboring square $S_{w\mathbf{1}}$, $\mathbf{1} \in \{\mathbf{a}, \bar{\mathbf{a}}, \mathbf{c}, \bar{\mathbf{c}}\}$,
- when passing through an ideal vertex projecting to x_A (if there are any), we may *jump* from the square S_w to any square of the form $S_{w\mathbf{a}^n}$, with $n \in \mathbb{Z}$ arbitrary,
- similarly, when passing through an ideal vertex projecting to x_C (if there are any), we may jump from S_w to any square $S_{w\mathbf{c}^n}$, $n \in \mathbb{Z}$,
- finally, when passing through an ideal vertex projecting to x_B (if there are any), we may jump from S_w to squares of the form $S_{w\mathbf{b}^n}$, $S_{w\mathbf{a}\mathbf{b}^n}$, $S_{w\mathbf{b}^n\mathbf{c}}$ or $S_{w\mathbf{a}\mathbf{b}^n\mathbf{c}}$, with $n \in \mathbb{Z}$ and $\mathbf{b} = \bar{\mathbf{a}}\bar{\mathbf{c}}$ (see again Figure 4.1).

Without loss of generality, we may assume that the initial vertex v belongs to the square S_\emptyset . Then, we may reach after r steps only squares of the form $S_{w_1\mathbf{1}_1^{n_1}\dots w_s\mathbf{1}_s^{n_s}}$, where w_1, \dots, w_s are elements of F such that $|w_1| + \dots + |w_s| + s \leq 2r$, $\mathbf{1}_1, \dots, \mathbf{1}_s$ are equal to \mathbf{a}, \mathbf{b} or \mathbf{c} , and n_1, \dots, n_s are arbitrary integers. Hence, generally speaking, infinitely many squares may be reached.

However, here we fix the endpoint v' , hence the final square $S_{w_1\mathbf{1}_1^{n_1}\dots w_s\mathbf{1}_s^{n_s}}$. We claim that, on any simple path from v to v' with length at most r , we may only visit squares of the form $S_{v_1\mathbf{1}_1^{m_1}\dots v_s\mathbf{1}_s^{m_s}}$, where v_1, \dots, v_s are elements of F at bounded distance from the neutral element \emptyset , and m_1, \dots, m_s are integers such that either $|m_i| \leq r$, or $|m_i - n_i| \leq r$. The reason is that, if we perform a “big jump” (larger than r) at an ideal vertex, then we cannot “undo” the jump in less than r steps since we cannot revisit the same ideal vertex again—here we use the fact that F is a free group, whose Cayley graph is a tree. Therefore, the number of squares that may be visited is finite, and since each square contains finitely many vertices, the claim follows. \square

Note that Lemma 5.2 becomes false if, instead of simple paths, we consider general paths, or even nonbacktracking paths. Indeed, without the simplicity assumption, it is possible to do arbitrarily big jumps, then undo them.

Note also that we have not used the fact that the boundaries of M are tight, in fact all the discussion in this subsection remains valid without this assumption.

5.2. Infinite geodesics and Busemann functions

Next, we introduce the main tool that will allow us to decompose maps with tight boundary-faces. This tool is the notion of Busemann function, a classical object of metric geometry, see for instance Chapter 5 in [BBI01]. In the infinite map \tilde{M} , we define an *infinite geodesic* (also called a geodesic ray in metric geometry) as an infinite sequence $(\gamma(t))_{t \in \mathbb{N}}$ of vertices such that

$$\tilde{d}(\gamma(t), \gamma(t')) = |t - t'| \quad (5.1)$$

for all t, t' (recall that \tilde{d} denotes the graph distance in \tilde{M}). A *biinfinite geodesic* is defined in exactly the same way, except that the sequence is indexed by \mathbb{Z} instead of \mathbb{N} . To simplify our discussion, we overlook the fact that the map may be non simple, which would in all rigor require to specify which edges are visited by the geodesic.

With an infinite geodesic γ , we may associate its *Busemann function* B_γ which assigns to a vertex v the quantity

$$B_\gamma(v) = \lim_{t \rightarrow +\infty} \tilde{d}(v, \gamma(t)) - t. \quad (5.2)$$

This quantity is well-defined since the function $t \mapsto \tilde{d}(v, \gamma(t)) - t$ is nonincreasing, by virtue of the triangle inequality, and bounded from below by $-\tilde{d}(v, \gamma(0))$. In fact, since we are in a discrete metric space, we have $B_\gamma(v) = \tilde{d}(v, \gamma(t)) - t$ for t large enough. We also have $B_\gamma(\gamma(t)) = -t$ for all t .

It is not difficult to check that B_γ is a 1-Lipschitz function, changes parity along each edge since the map \tilde{M} is bipartite, and admits no local minimum: every vertex v has an adjacent vertex v' such that $B_\gamma(v') = B_\gamma(v) - 1$.

For a biinfinite geodesic γ , we define its Busemann function B_γ in the same way. Note that a change of parametrization $t \mapsto t + t_0$ of γ changes B_γ by a constant, so a Busemann function should really be viewed as “defined modulo a constant”. Note however that the change of parametrization $t \mapsto -t$ gives rise to a different Busemann function.

Lemma 5.3. *Let γ, γ' be two infinite geodesics, and suppose that there exists a finite set V_0 of vertices whose removal splits \tilde{M} in several connected components, such that γ and γ' eventually belong to different connected components (i.e. $\gamma(t)$ remains in one connected component and $\gamma'(t)$ in another for large enough t). Then, the function $B_\gamma + B_{\gamma'}$ admits a global minimum, which is reached at some $v_0 \in V_0$. Furthermore, there exists at least one biinfinite geodesic along which B_γ is strictly increasing and $B_{\gamma'}$ is strictly decreasing, and a vertex v , not necessarily in V_0 , belongs to such a geodesic if and only if it is a global minimum of $B_\gamma + B_{\gamma'}$.*

Proof. Let v_0 be a vertex at which $B_\gamma + B_{\gamma'}$ attains its minimum in the finite set V_0 . For a given v , take t large enough so that $B_\gamma(v) = \tilde{d}(v, \gamma(t)) - t$, $B_{\gamma'}(v) = \tilde{d}(v, \gamma'(t)) - t$, and so that $\gamma(t)$ and $\gamma'(t)$ are in different connected components after removing V_0 . By the triangle inequality, we have $B_\gamma(v) + B_{\gamma'}(v) \geq \tilde{d}(\gamma(t), \gamma'(t)) - 2t$, and we have $\tilde{d}(\gamma(t), \gamma'(t)) = \tilde{d}(\gamma(t), v_1) + \tilde{d}(v_1, \gamma'(t))$ for some $v_1 \in V_0$ since a geodesic path from $\gamma(t)$ to $\gamma'(t)$ necessarily meets V_0 at some vertex v_1 . We get

$$B_\gamma(v) + B_{\gamma'}(v) \geq (\tilde{d}(v_1, \gamma(t)) - t) + (\tilde{d}(v_1, \gamma'(t)) - t) \geq B_\gamma(v_1) + B_{\gamma'}(v_1), \quad (5.3)$$

which is at least $B_\gamma(v_0) + B_{\gamma'}(v_0)$. This proves the first claim.

Consider now an arbitrary minimizer v of $B_\gamma + B_{\gamma'}$. Since B_γ has no local minimum, we can construct an infinite path starting at v along which B_γ is strictly decreasing, and similarly we can construct another infinite path starting at v along which $B_{\gamma'}$ is strictly decreasing. It is straightforward to check that, reversing the direction of the second path and concatenating it with the first one, we get a biinfinite geodesic with the wanted property, and that conversely any such geodesic can only pass through minimizers of $B_\gamma + B_{\gamma'}$. \square

Note that, in this subsection, we have not used the fact that \tilde{M} is planar. In fact, our discussion (including Lemma 5.3) holds for an arbitrary infinite graph.

5.3. Busemann functions associated with tight boundaries

We will now exploit the assumption that M has tight boundaries. Consider a boundary of M , say ∂_A of length $2a$. As discussed in Section 4.1, ∂_A has a distinguished lift $\tilde{\partial}_A$ which is an ideal vertex if $a = 0$, and an ideal face if $a > 0$. In this latter case, we let γ_A be the biinfinite path on \tilde{M} obtained by following the contour of $\tilde{\partial}_A$ in the counterclockwise direction. Choosing a reference point $\gamma_A(0)$ arbitrarily, γ_A is parametrized by \mathbb{Z} .

Lemma 5.4. *If ∂_A is a tight boundary-face in M , then γ_A is a biinfinite geodesic in \tilde{M} .*

Proof. If we view the contour of ∂_A as a biinfinite sequence of vertices $(\lambda_A(t), t \in \mathbb{Z})$ obtained by cycling infinitely many times around ∂_A , then [CdVE10, Proposition 2.5]—which is closely related to the wrapping lemma of [BG14]—implies that any path of the form $(\lambda_A(t+l), 0 \leq t \leq m)$ for $l \in \mathbb{Z}$ and $m \in \mathbb{N}$ is shortest in its homotopy class with fixed endpoints (such a path is called ‘tight’ in [CdVE10], so that our terminology agrees). Then, as noted in [CdVE10, Section 2.1], this property is preserved by taking lifts in the universal cover (and in fact, even in arbitrary covers). Since γ_A is one of these lifts, and since \tilde{S} is simply connected, any two paths between the same vertices in \tilde{M} are homotopic, and we conclude that γ_A is a geodesic between any pair of points it visits, which is the definition of a biinfinite geodesic. \square

We may therefore define the function $\tilde{d}_A : V(\tilde{M}) \rightarrow \mathbb{Z}$ as follows:

- if $a = 0$, then we let \tilde{d}_A be the distance in \tilde{M} to the vertex \tilde{x}_A ,
- if $a > 0$, then we let $\tilde{d}_A = B_{\gamma_A}$ be the Busemann function associated with γ_A .

Let us record the relation

$$\tilde{d}_A(Av) = \tilde{d}_A(v) - 2a \quad (5.4)$$

valid for any vertex v of \tilde{M} , where $A \in \text{Aut}(p)$ is the automorphism defined in Section 4.1. This relation is immediate in the case $a = 0$; for $a > 0$ it follows from the definition of the Busemann function B_{γ_A} and the fact that $A(\gamma_A(t)) = \gamma_A(t + 2a)$ for any t .

In a completely similar manner, we define the functions \tilde{d}_B , \tilde{d}_C and $\tilde{d}_{B'}$, which obey relations similar to (5.4) mutatis mutandis. For later use, we record the following:

Lemma 5.5. *There exists a constant $k \in \mathbb{Z}$ such that, for any vertex v of \tilde{M} , we have*

$$\tilde{d}_{B'}(Av) = \tilde{d}_B(v) + k \quad (5.5)$$

and

$$\tilde{d}_B(Cv) = \tilde{d}_{B'}(v) - k + 2b. \quad (5.6)$$

Proof. The first relation is a straightforward consequence of the fact that $\tilde{\partial}_{B'} = A\tilde{\partial}_B$. The constant k is equal to 0 in the case $b = 0$ while, for $b > 0$, it satisfies $A\gamma_B(k) = \gamma_{B'}(0)$ (we could thus set it to 0 too by choosing the reference points on $\tilde{\partial}_B$ and $\tilde{\partial}_{B'}$ appropriately).

For the second relation, we note that $\tilde{\partial}_B = C\tilde{\partial}_{B'}$ hence there exists a constant k' such that $\tilde{d}_B(Cv) = \tilde{d}_{B'}(v) + k'$. But, by the relation $B = A^{-1}C^{-1}$, we have

$$\tilde{d}_B(v) = \tilde{d}_B(CABv) = \tilde{d}_{B'}(ABv) + k' = \tilde{d}_B(Bv) + k' + k = \tilde{d}_B(v) + k' + k - 2b. \quad (5.7)$$

hence $k' = -k + 2b$. □

Remark 5.6. In this paper, we only consider the Busemann functions obtained by following the contours of ideal faces counterclockwise. We surmise that considering the clockwise orientation might be useful to study “strictly tight” boundaries, i.e. boundaries whose contours are the unique paths of minimal length in their homotopy class.

5.4. Leftmost bigeodesics and the diangle lemma

Throughout this section, we consider specifically the pair of ideal vertices/faces $(\tilde{\partial}_A, \tilde{\partial}_B)$, but all the discussion can be adapted to any other pair, e.g. $(\tilde{\partial}_A, \tilde{\partial}_C)$, $(\tilde{\partial}_B, \tilde{\partial}_{B'})$, etc. We start by adapting the concepts of Section 2.1 to the context of the infinite map \tilde{M} and of Busemann functions.

Geodesics and bigeodesics. A *geodesic towards* $\tilde{\partial}_A$ is a path on \tilde{M} along which \tilde{d}_A is strictly decreasing, which stops at $\tilde{\partial}_A$ if $a = 0$, and which continues forever if $a > 0$ (so that \tilde{d}_A tends to $-\infty$ along the path). Such a path γ is indeed a geodesic, i.e. satisfies $\tilde{d}(\gamma(t), \gamma(t')) = |t - t'|$ for all t, t' in its interval of definition. A geodesic towards $\tilde{\partial}_B$ is defined similarly.

A *bigeodesic between* $\tilde{\partial}_A$ and $\tilde{\partial}_B$ is a path which is both a geodesic towards $\tilde{\partial}_A$ in one direction, and a geodesic towards $\tilde{\partial}_B$ in the other direction. Such bigeodesics always exist: this is clear when $b = 0$ (start at the vertex $\tilde{\partial}_B$ and follow a path along which \tilde{d}_A decreases) or similarly when $a = 0$; when $ab > 0$, we may invoke Lemma 5.3, with V_0 the

set of vertices lying in the square S_\emptyset (given a good embedding). We define the *distance* \tilde{d}_{AB} between $\tilde{\partial}_A$ and $\tilde{\partial}_B$ as

$$\tilde{d}_{AB} := \min_v \left(\tilde{d}_A(v) + \tilde{d}_B(v) \right). \quad (5.8)$$

This denomination is consistent with the fact that, for $a = b = 0$, \tilde{d}_{AB} is precisely the graph distance in \tilde{M} between \tilde{x}_A and \tilde{x}_B . For $ab > 0$, it is nothing but the minimal value of the function $B_{\gamma_A} + B_{\gamma_B}$ as considered in Lemma 5.3.

In the Poincaré disk representation of \tilde{S} , a geodesic towards $\tilde{\partial}_A$ forms a simple path which “ends” at the ideal point \tilde{x}_A , see again Figure 4.3. A bigeodesic between, say, $\tilde{\partial}_A$ and $\tilde{\partial}_B$, forms a simple path connecting the ideal points \tilde{x}_A and \tilde{x}_B . By planarity, this path splits the disk (hence \tilde{M}) in two regions, which we may distinguish as *left* and *right*, given an orientation of the bigeodesic (say, from $\tilde{\partial}_B$ to $\tilde{\partial}_A$). Note that the interiors of these regions may be disconnected, if the bigeodesic passes through an ideal vertex on its way.

Geodesic vertices. A *geodesic vertex* between $\tilde{\partial}_A$ and $\tilde{\partial}_B$ is a vertex belonging to a bigeodesic between $\tilde{\partial}_A$ and $\tilde{\partial}_B$. It is straightforward to check (see again Lemma 5.3 in the case $ab > 0$) that v is such a vertex if and only if

$$\tilde{d}_A(v) + \tilde{d}_B(v) = \tilde{d}_{AB}. \quad (5.9)$$

The quantity $\tilde{d}_A(v)$ is called the \tilde{d}_A -*latitude* of the geodesic vertex v between $\tilde{\partial}_A$ and $\tilde{\partial}_B$.

Lemma 5.7. *For any $r \in \mathbb{Z}$, the set $I_{AB}(r)$ of geodesic vertices between $\tilde{\partial}_A$ and $\tilde{\partial}_B$ having \tilde{d}_A -latitude r is finite.*

Proof. If $a = b = 0$ then this is a corollary of Lemma 5.2. Suppose now that $a > 0$. Given a good embedding, any bigeodesic between $\tilde{\partial}_A$ and $\tilde{\partial}_B$ must visit a vertex in the square $S_{\mathbf{a}^n}$, for any $n \geq 0$. Let us denote by r_n the maximal \tilde{d}_A -latitude of a geodesic vertex belonging to $S_{\mathbf{a}^n}$, then $r_{n+1} = r_n - 2a < r_n$ by (5.4). Hence there exists an m such that $r_m < r$. If $b = 0$, we see that any geodesic vertex of \tilde{d}_A -latitude r belongs to a geodesic (hence simple) path between $\tilde{\partial}_B$ and a vertex of $S_{\mathbf{a}^m}$, so there are finitely many of them by Lemma 5.2. If $b > 0$, adapting the previous reasoning shows that there exists an ℓ such that the minimal \tilde{d}_A -latitude of a geodesic vertex in $S_{\mathbf{b}^\ell}$ is larger than r . Therefore, any geodesic vertex of \tilde{d}_A -latitude r belongs to a geodesic (hence simple) path between a vertex of $S_{\mathbf{a}^m}$ and a vertex of $S_{\mathbf{b}^\ell}$, and again there are finitely many of them by Lemma 5.2. \square

Leftmost bigeodesic via a geodesic vertex. Given a geodesic vertex v between $\tilde{\partial}_A$ and $\tilde{\partial}_B$, we may, as in Section 2, “launch” from v the leftmost geodesics towards $\tilde{\partial}_A$ and $\tilde{\partial}_B$ (the planarity of \tilde{M} is used to identify the first edges of these leftmost geodesics, as in the finite case). The only potential difficulty is that these geodesics may encounter ideal vertices of infinite degree. However, by Lemma 5.7, only finitely many edges through a given ideal boundary point make \tilde{d}_A and \tilde{d}_B decrease, therefore, when there are any, there

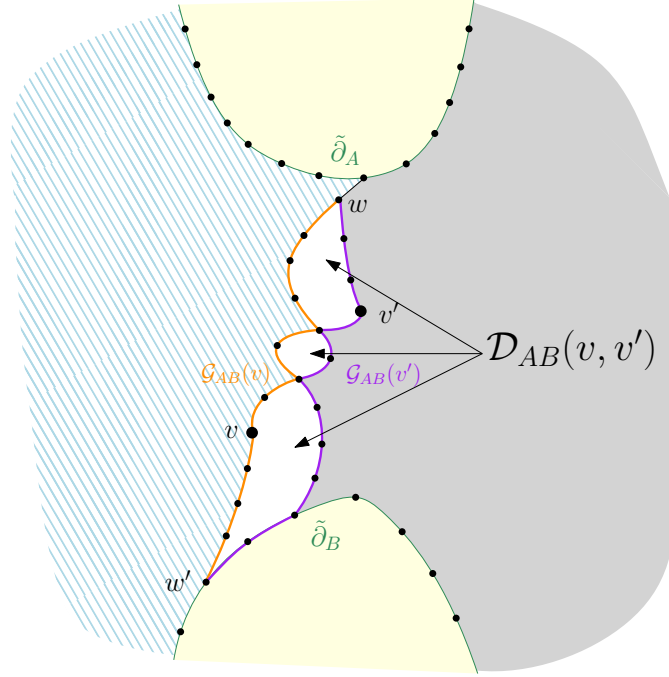


Figure 5.1: Illustration of the diangle lemma: we consider two geodesic vertices v and v' between $\tilde{\partial}_A$ and $\tilde{\partial}_B$, such that v' lies on the right of the leftmost bigeodesic $\mathcal{G}_{AB}(v)$ (shown in orange), and such that $\tilde{d}_A(v) \geq \tilde{d}_A(v')$. Then, $\mathcal{G}_{AB}(v)$ and $\mathcal{G}_{AB}(v')$ (shown in purple) delimit a region $\mathcal{D}_{AB}(v, v')$ (shown in white) which is a bigeodesic diangle of nonnegative exceedance $\tilde{d}_A(v) - \tilde{d}_A(v')$.

is always a leftmost one to be picked. Since v is a geodesic vertex, the concatenation of these two geodesics, oriented all the way from $\tilde{\partial}_B$ to $\tilde{\partial}_A$, forms a bigeodesic between $\tilde{\partial}_A$ and $\tilde{\partial}_B$ which we call the *leftmost bigeodesic via v* and denote $\mathcal{G}_{AB}(v)$. Note that the leftmost geodesic towards $\tilde{\partial}_A$ eventually merges with it: this is obvious for $a = 0$ since the ideal vertex $\tilde{x}_A = \tilde{\partial}_A$ is reached in finitely many steps; for $a > 0$, setting γ_A as in Section 5.3, then the leftmost geodesic from v merges with γ_A at the vertex $\gamma_A(t)$ for the smallest value of t such that $\tilde{d}_A(v) = \tilde{d}(v, \gamma_A(t)) - t$. Of course, a similar property holds for the leftmost geodesic towards $\tilde{\partial}_B$.

The diangle lemma. Consider two geodesic vertices v and v' between $\tilde{\partial}_A$ and $\tilde{\partial}_B$, such that v' lies on the right of the leftmost bigeodesic $\mathcal{G}_{AB}(v)$ (oriented from $\tilde{\partial}_B$ to $\tilde{\partial}_A$) or on it, and such that $\tilde{d}_A(v) \geq \tilde{d}_A(v')$. This situation is illustrated on Figure 5.1.

We claim that the leftmost bigeodesic $\mathcal{G}_{AB}(v')$ remains on the right of $\mathcal{G}_{AB}(v)$. Indeed, as we start from v' and follow a geodesic towards $\tilde{\partial}_A$, it is not possible to pass to the left of $\mathcal{G}_{AB}(v)$, since the latter consists of a leftmost geodesic towards $\tilde{\partial}_A$ and we started on its right. Furthermore, when we actually follow the leftmost geodesic from v' towards $\tilde{\partial}_A$, then we will eventually meet $\mathcal{G}_{AB}(v)$ at a vertex w (since all leftmost geodesics towards $\tilde{\partial}_A$

eventually merge with it), and follow it onwards. Similarly, as we start from v' and follow the leftmost geodesic towards $\tilde{\partial}_B$, it is again not possible to pass to the left of $\mathcal{G}_{AB}(v)$, hence $\mathcal{G}_{AB}(v')$ stays to the right of $\mathcal{G}_{AB}(v)$. In particular, v lies on the left of $\mathcal{G}_{AB}(v')$, hence on the right of $\mathcal{G}_{BA}(v')$ (oriented from $\tilde{\partial}_A$ to $\tilde{\partial}_B$). As we have $\tilde{d}_B(v') \geq \tilde{d}_B(v)$, we see that v and v' play a completely symmetric role, upon exchanging the roles of A and B and viewing Figure 5.1 upside-down. We denote by w' the vertex at which $\mathcal{G}_{AB}(v)$ and $\mathcal{G}_{AB}(v')$ merge when going towards $\tilde{\partial}_B$. Note that it is possible that $\mathcal{G}_{AB}(v)$ and $\mathcal{G}_{AB}(v')$ have intermediate contacts at vertices of \tilde{d}_A -latitude strictly included between $\tilde{d}_A(v')$ and $\tilde{d}_A(v)$.

We now consider the closed region $\mathcal{D}_{AB}(v, v')$ delimited by $\mathcal{G}_{AB}(v)$ and $\mathcal{G}_{AB}(v')$ (precisely, the region which is on the right of $\mathcal{G}_{AB}(v)$ and on the left of $\mathcal{G}_{AB}(v')$, when orienting them from $\tilde{\partial}_B$ to $\tilde{\partial}_A$), which we prune at w and w' to remove their (possibly infinite) common parts towards $\tilde{\partial}_A$ and $\tilde{\partial}_B$. Note that $\mathcal{D}_{AB}(v, v')$ is connected but its interior may be disconnected when there are intermediate contacts between $\mathcal{G}_{AB}(v)$ and $\mathcal{G}_{AB}(v')$. As a degenerate case, it is possible to have $\mathcal{G}_{AB}(v) = \mathcal{G}_{AB}(v')$, and then $\mathcal{D}_{AB}(v, v')$ consists of a segment joining $v = w'$ to $v' = w$.

Lemma 5.8 (Diangle lemma). *$\mathcal{D}_{AB}(v, v')$ is a bigeodesic diangle of nonnegative exceedance $\tilde{d}_A(v) - \tilde{d}_A(v')$.*

Proof. We have to check that $\mathcal{D}_{AB}(v, v')$ satisfies the axioms of Section 2.3. First we observe that it is by construction a finite map with one boundary-face (the interior of a closed cycle on \tilde{M} always contains finitely many vertices, edges and faces).

Then, to make the correspondence with the notations of Section 2.3, we take $w_{12} = v$, $w_{21} = v'$, $v_1 = w$ and $v_2 = w'$ (see again Figure 2.2) and the corners c_1, c_{12}, c_2, c_{21} are selected in a natural manner. The boundary intervals $[c_1, c_2]$ and $[c_2, c_1]$ are geodesic since they correspond to parts of the bigeodesics $\mathcal{G}_{AB}(v)$ and $\mathcal{G}_{AB}(v')$. The boundary intervals $[c_{12}, c_2]$ and $[c_{21}, c_1]$ are strictly geodesic since $\mathcal{G}_{AB}(v)$ and $\mathcal{G}_{AB}(v')$ are actually *leftmost* bigeodesics: no geodesic between v and w' can enter into $\mathcal{D}_{AB}(v, v')$, and similarly between v' and w . Finally, w (resp. w') is by definition the only vertex common to $[c_{21}, c_1]$ and $[c_1, c_2]$ (resp. $[c_{12}, c_2]$ and $[c_2, c_1]$). \square

So far, our construction depends on the choice of geodesic vertices v and v' satisfying the aforementioned properties that v' is on the right of $\mathcal{G}_{AB}(v)$ and that $\tilde{d}_A(v) \geq \tilde{d}_A(v')$. However, given two latitudes $r \geq r'$ such that the sets $I_{AB}(r)$ and $I_{AB}(r')$, as defined in Lemma 5.7, are both nonempty, there exists a canonical choice of such vertices. Indeed, we may consider the *leftmost* element v of $I_{AB}(r)$, defined as the only vertex $v \in I_{AB}(r)$ such that the region on the left of $\mathcal{G}_{AB}(v)$ (again oriented from $\tilde{\partial}_B$ to $\tilde{\partial}_A$) contains no other element of $I_{AB}(r)$. Similarly, we choose v' to be the *rightmost* element of $I_{AB}(r')$. Clearly v' is on the right of $\mathcal{G}_{AB}(v)$, which actually passes through the leftmost element of $I_{AB}(r')$. This choice of v and v' makes $\mathcal{D}_{AB}(v, v')$ the largest possible, as in the case of triply pointed maps discussed in Section 3.4, and we will always encounter such maximal diangles in the following.

5.5. Equilibrium vertices and the triangle lemma

In the previous subsection, we have only considered the pair $(\tilde{\partial}_A, \tilde{\partial}_B)$. Let us now add $\tilde{\partial}_C$ in the game: our purpose is to construct a bigeodesic triangle \mathcal{T}_{ABC} which, interestingly, is canonical in the sense that it is entirely determined by the triplet of distinguished ideal corners $(\tilde{x}_A, \tilde{x}_B, \tilde{x}_C)$ of \tilde{S}' . Indeed, as discussed in Section 4.1, this triplet distinguishes the triplet $(\tilde{\partial}_A, \tilde{\partial}_B, \tilde{\partial}_C)$ of ideal vertices/faces of \tilde{M} .

Recall the definition (5.8) of the distance \tilde{d}_{AB} between $\tilde{\partial}_A$ and $\tilde{\partial}_B$, and define \tilde{d}_{BC} and \tilde{d}_{CA} similarly. Inspired by the equilibrium conditions (3.3), we define r_A, r_B and r_C by

$$\tilde{d}_{AB} = r_A + r_B, \quad \tilde{d}_{BC} = r_B + r_C, \quad \tilde{d}_{CA} = r_C + r_A. \quad (5.10)$$

Note that r_A, r_B and r_C may now be negative, since the “renormalized” distances $\tilde{d}_{AB}, \tilde{d}_{BC}$ and \tilde{d}_{CA} may be negative in the presence of ideal faces. From the very definition of Busemann functions and from the bipartiteness of \tilde{M} , we get that the quantity $\tilde{d}_A(v) + \tilde{d}_B(v)$ has the same parity for all v , which is also necessarily the parity of \tilde{d}_{AB} . We immediately deduce that $\tilde{d}_{AB} + \tilde{d}_{BC} + \tilde{d}_{CA}$ is even, hence r_A, r_B and r_C are integers.

We claim that the sets $I_{AB}(r_A)$ (as defined in Lemma 5.7), $I_{BC}(r_B)$ and $I_{CA}(r_C)$ are always nonempty: this is true when $\tilde{\partial}_A, \tilde{\partial}_B, \tilde{\partial}_C$ are all ideal faces, since the bigeodesics between them are infinite and therefore pass through geodesic vertices of any latitude; this is also true when $\tilde{\partial}_A, \tilde{\partial}_B, \tilde{\partial}_C$ are all ideal vertices, as $I_{AB}(r_A)$ projects to the set S_{AB} considered in Figure 3.4 and similarly for the other sets; the other cases are left to the reader.

Furthermore, even though we had to choose a reference point along $\tilde{\partial}_A$ to define the Busemann function \tilde{d}_A when $a > 0$, and similarly for $\tilde{\partial}_B$ and $\tilde{\partial}_C$, the sets $I_{AB}(r_A), I_{BC}(r_B)$ and $I_{CA}(r_C)$ do not depend on these choices. Indeed, as we change the reference point along $\tilde{\partial}_A$, say, \tilde{d}_A is changed by a constant, but r_A gets changed by the same constant. We also have the identification $I_{AB}(r_A) = I_{BA}(r_B)$.

We now define v_{AB} to be the rightmost element of $I_{AB}(r_A)$ (again orienting from $\tilde{\partial}_B$ to $\tilde{\partial}_A$), and define v_{BC} and v_{CA} similarly by permuting A, B, C cyclically. We call v_{AB}, v_{BC} and v_{CA} *equilibrium vertices*, as they satisfy

$$\begin{aligned} \tilde{d}_A(v_{AB}) &= \tilde{d}_A(v_{CA}) = r_A, \\ \tilde{d}_B(v_{AB}) &= \tilde{d}_B(v_{BC}) = r_B, \\ \tilde{d}_C(v_{BC}) &= \tilde{d}_C(v_{CA}) = r_C. \end{aligned} \quad (5.11)$$

By the previous paragraph, the equilibrium vertices are intrinsic to \tilde{M} .

Consider now the leftmost bigeodesics $\mathcal{G}_{AB}(v_{AB}), \mathcal{G}_{BC}(v_{BC})$ and $\mathcal{G}_{CA}(v_{CA})$. We will show that they delimit a region \mathcal{T}_{ABC} which is a bigeodesic triangle. For this, we first state some technical lemmas.

Lemma 5.9. *Let v be a vertex strictly to the left of the leftmost bigeodesic $\mathcal{G}_{AB}(v_{AB})$. Then, we have $\tilde{d}_C(v) > r_C$.*

Proof. Since \tilde{x}_C is on the right of $\mathcal{G}_{AB}(v_{AB})$, any geodesic from v towards $\tilde{\partial}_C$ must cross $\mathcal{G}_{AB}(v_{AB})$, at a vertex denoted w such that $\tilde{d}_C(v) > \tilde{d}_C(w)$. As w is a geodesic vertex

between $\tilde{\partial}_A$ and $\tilde{\partial}_B$, we have $\tilde{d}_A(w) + \tilde{d}_B(w) = \tilde{d}_{AB} = r_A + r_B$, and therefore we have either $\tilde{d}_A(w) \leq r_A$ or $\tilde{d}_B(w) \leq r_B$. In the former case, the definition of \tilde{d}_{CA} implies that $\tilde{d}_C(w) + \tilde{d}_A(w) \geq \tilde{d}_{CA} = r_C + r_A$ hence $\tilde{d}_C(w) \geq r_C$. The same conclusion holds in the latter case, using rather \tilde{d}_{BC} . \square

Corollary 5.10. *Unless we have $v_{AB} = v_{BC} = v_{CA}$, the vertices v_{BC} and v_{CA} are both strictly to the right of $\mathcal{G}_{AB}(v_{AB})$.*

Proof. Since v_{BC} and v_{CA} are both at \tilde{d}_C -latitude r_C , they cannot be strictly on the left of $\mathcal{G}_{AB}(v_{AB})$ by the previous lemma. If one of them, say v_{BC} , is on $\mathcal{G}_{AB}(v_{AB})$, then it is equal to v_{AB} since these two vertices are at the same \tilde{d}_B -latitude r_B . But then, $v_{AB} = v_{BC}$ belongs to $I_{CA}(r_C)$, and is clearly the rightmost element v_{CA} of that set. \square

Reasoning as in the discussion of the diangle lemma, we deduce from Corollary 5.10 that $\mathcal{G}_{BC}(v_{BC})$ and $\mathcal{G}_{CA}(v_{CA})$ remain on the right of $\mathcal{G}_{AB}(v_{AB})$. Furthermore, the two bigeodesics $\mathcal{G}_{AB}(v_{AB})$ and $\mathcal{G}_{CA}(v_{CA})$ merge at a vertex v_A when following them towards $\tilde{\partial}_A$, but are disjoint before. Similarly, we introduce the merging vertices v_B and v_C of the bigeodesics going towards $\tilde{\partial}_B$ and $\tilde{\partial}_C$, respectively.

We now consider the cycle on \tilde{M} obtained by following $\mathcal{G}_{AB}(v_{AB})$ from v_A to v_B , then $\mathcal{G}_{BC}(v_{BC})$ until v_C , and finally $\mathcal{G}_{CA}(v_{CA})$ until we return to v_A . It is a simple counterclockwise cycle which delimits a region denoted \mathcal{T}_{ABC} . See the left of Figure 5.2 for an illustration (ignoring the right of this figure for now). Note that \mathcal{T}_{ABC} is reduced to a single vertex if and only if $v_{AB} = v_{BC} = v_{CA}$. This situation happens when there exists a vertex which is a geodesic vertex between $\tilde{\partial}_A$ and $\tilde{\partial}_B$, between $\tilde{\partial}_B$ and $\tilde{\partial}_C$, and between $\tilde{\partial}_C$ and $\tilde{\partial}_A$, all at the same time. Such a vertex, if it exists, is necessarily unique by planarity².

Lemma 5.11 (Triangle lemma). *\mathcal{T}_{ABC} is a bigeodesic triangle.*

Proof. To make the correspondence with the notations of Section 2.4, we take $v_1 = v_A$, $v_{12} = v_{AB}$, etc. (see again Figure 2.5), and the corners c_1, c_{12}, \dots are selected in a natural manner. It is then straightforward to check that \mathcal{T}_{ABC} satisfies all the axioms defining bigeodesic triangles, since it is delimited by leftmost bigeodesics, and every geodesic from v_A to v_B inside \mathcal{T}_{ABC} must pass through v_{AB} as we chose it to be the rightmost element of $I_{AB}(r_A)$, and similarly for v_{BC} and v_{CA} . \square

We have constructed the bigeodesic triangle \mathcal{T}_{ABC} associated with the triplet of ideal corners $(\tilde{x}_A, \tilde{x}_B, \tilde{x}_C)$ of \tilde{S}' , but we can adapt the construction to any other triplet. Note however that our construction depends at several places (e.g. in Lemma 5.9) on the fact that \tilde{x}_A, \tilde{x}_B and \tilde{x}_C appear in counterclockwise order along the ideal boundary of \tilde{S}' , and we shall therefore assume the same order for other triplets. Specifically, we will consider later on the triangles $\mathcal{T}_{ACB'}$, $\mathcal{T}_{ABB'}$ and $\mathcal{T}_{BCB'}$ corresponding to such triplets.

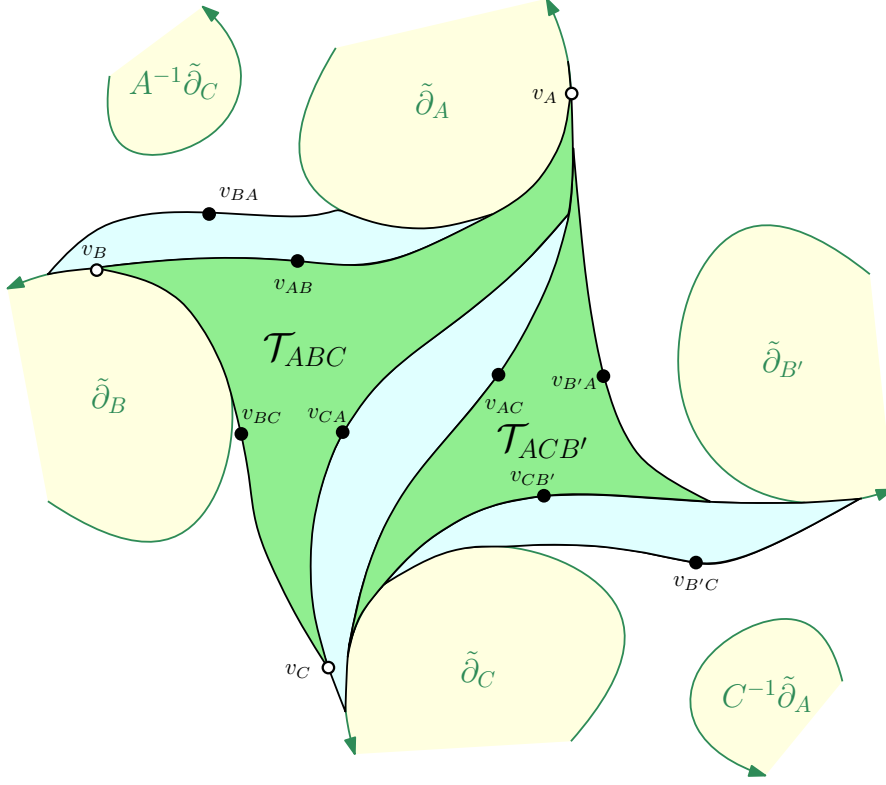


Figure 5.2: Illustration of the decomposition of a map of type I. Cutting along the leftmost bigeodesics launched from the equilibrium vertices (shown in black), we delimit the two geodesic triangles \mathcal{T}_{ABC} and $\mathcal{T}_{ACB'}$ (shown in green), and three geodesic diangles of nonnegative exceedances (shown in light blue). Altogether, these five regions form the domain $\mathcal{M}_{ACB'}$ of Lemma 5.13, containing exactly one preimage of each inner face of M .

5.6. Decomposing a map of type I

Let us consider the bigeodesic triangles \mathcal{T}_{ABC} and $\mathcal{T}_{ACB'}$, as constructed in the previous subsection. From the fact that $\tilde{x}_A, \tilde{x}_B, \tilde{x}_C$ and $\tilde{x}_{B'}$ are the four ideal corners of a fundamental domain of \tilde{S} , it is tempting to identify \mathcal{T}_{ABC} and $\mathcal{T}_{ACB'}$ with the two triangles appearing in the assembling procedure. For this, we need to make sure that they do not overlap. Recall the notations from Section 5.5, which we complete with notations pertaining to the triangle $\mathcal{T}_{ACB'}$: we let r'_A, r'_C and r'_B be the integers such that

$$\tilde{d}_{AC} = r'_A + r'_C, \quad \tilde{d}_{CB'} = r'_C + r'_B, \quad \tilde{d}_{B'A} = r'_B + r'_A, \quad (5.12)$$

and we let $v_{AC}, v_{CB'}$ and $v_{B'A}$ be the corresponding equilibrium vertices, see Figure 5.2. Then, the triangles \mathcal{T}_{ABC} and $\mathcal{T}_{ACB'}$ do not overlap if the leftmost bigeodesic $\mathcal{G}_{AC}(v_{AC})$

²Two such vertices may exist on the sphere (consider the situation $v_{AB} = v_{BC} = v_{CA}$ and $v_{BA} = v_{CB} = v_{AC}$ on Figure 3.4), but here we are in the disk with $\tilde{\partial}_A, \tilde{\partial}_B$ and $\tilde{\partial}_C$ on the (ideal) boundary.

remains on the right of $\mathcal{G}_{AC}(v_{CA})$ (oriented from $\tilde{\partial}_C$ to $\tilde{\partial}_A$). We may ensure this by invoking the diangle lemma (Lemma 5.8), and more precisely by identifying the region delimited by these two bigeodesics with the diangle $\mathcal{D}_{AC}(v_{CA}, v_{AC})$ as defined (mutatis mutandis) in Section 5.4. But, for this, the assumption of the diangle lemma must be satisfied, namely we must have $\tilde{d}_A(v_{CA}) \geq \tilde{d}_A(v_{AC})$, i.e. $r_A \geq r'_A$.

Lemma 5.12. *The difference $r_A - r'_A$ of \tilde{d}_A -latitude between v_{CA} and v_{AC} is equal to $a + c - b$.*

Proof. By the equilibrium conditions (5.10) and (5.12), we have

$$r_A - r'_A = \frac{(\tilde{d}_{AB} - \tilde{d}_{B'A}) - (\tilde{d}_{BC} - \tilde{d}_{CB'})}{2}. \quad (5.13)$$

Therefore, we must compare \tilde{d}_{AB} to $\tilde{d}_{B'A}$, and \tilde{d}_{BC} to $\tilde{d}_{CB'}$. For this, we will use the symmetries of \tilde{M} . Consider first the action of A on the Busemann functions. By (5.4) and (5.5), we have

$$\begin{aligned} \tilde{d}_{B'A} &= \min_v \left(\tilde{d}_{B'}(v) + \tilde{d}_A(v) \right) = \min_v \left(\tilde{d}_{B'}(Av) + \tilde{d}_A(Av) \right) \\ &= \min_v \left(\tilde{d}_B(v) + k + \tilde{d}_A(v) - 2a \right) = \tilde{d}_{AB} + k - 2a. \end{aligned} \quad (5.14)$$

Similarly, considering now the action of C , the analog of (5.4) for C and (5.6) imply

$$\tilde{d}_{BC} = \min_v \left(\tilde{d}_B(v) + \tilde{d}_C(v) \right) = \min_v \left(\tilde{d}_B(Cv) + \tilde{d}_C(Cv) \right) = \tilde{d}_{CB'} - k + 2b - 2c. \quad (5.15)$$

Plugging these relations into (5.13) gives the wanted difference $a + c - b$. \square

We conclude that \mathcal{T}_{ABC} and $\mathcal{T}_{ACB'}$ do not overlap when $a + c - b \geq 0$. However, as we are trying to find a decomposition of M (and not just \tilde{M}), we actually want the stronger property that the *projections* of \mathcal{T}_{ABC} and $\mathcal{T}_{ACB'}$ on M do not overlap. This property is ensured by the following:

Lemma 5.13. *Let $v_{BA} := A^{-1}v_{B'A}$ and $v_{B'C} := C^{-1}v_{BC}$, and let $\mathcal{M}_{ABCB'}$ be the domain delimited by the bigeodesics $\mathcal{G}_{AB}(v_{BA})$, $\mathcal{G}_{BC}(v_{BC})$, $\mathcal{G}_{CB'}(v_{B'C})$ and $\mathcal{G}_{B'A}(v_{B'A})$, pruned from their common parts (see again Figure 5.2). Then, $\mathcal{M}_{ABCB'}$ contains exactly one preimage of each inner face of M .*

Furthermore, when M is of type I, then both triangles \mathcal{T}_{ABC} and $\mathcal{T}_{ACB'}$ are contained in $\mathcal{M}_{ABCB'}$, and their complement consists of the three geodesic diangles $\mathcal{D}_{AC}(v_{CA}, v_{AC})$, $\mathcal{D}_{AB}(v_{BA}, v_{AB})$ and $\mathcal{D}_{B'C}(v_{CB'}, v_{B'C})$, with nonnegative exceedances equal to $a + c - b$, $b + a - c$ and $c + b - a$, respectively.

Proof. The first claim means that $\mathcal{M}_{ABCB'}$ is essentially a fundamental domain for the action of $\text{Aut}(p)$. Indeed, the bigeodesics delimiting $\mathcal{M}_{ABCB'}$ can be viewed as paths connecting the ideal points \tilde{x}_A , \tilde{x}_B , \tilde{x}_C and $\tilde{x}_{B'}$: the bigeodesic $\mathcal{G}_{AB}(v_{BA})$ connects \tilde{x}_A and \tilde{x}_B and the bigeodesic $\mathcal{G}_{B'A}(v_{B'A})$ is (upon reversing its orientation) its image by

A , connecting \tilde{x}_A and $\tilde{x}_{B'}$. Similarly, $\mathcal{G}_{CB'}(v_{B'C})$ connects \tilde{x}_C and $\tilde{x}_{B'}$ and $\mathcal{G}_{BC}(v_{BC})$ is (upon reversing its orientation) its image by C connecting \tilde{x}_C and \tilde{x}_B . This pattern mimics precisely that of the four sides of the square S_\emptyset in Figure 4.1, even though the topology of the quadrangle $\mathcal{M}_{ABCB'}$ is not necessarily that of a square as it may have pinch points if two of its boundaries come into contact. The similitude with S_\emptyset (whose sides do reach the ideal points) may be further improved by adding to $\mathcal{M}_{ABCB'}$ the common parts of its boundary geodesics so as to eventually reach \tilde{x}_A , \tilde{x}_B , \tilde{x}_C and $\tilde{x}_{B'}$ (possibly after infinitely many steps). We are still left with a final (but somewhat irrelevant) slight difference with the situation of Section 4.1: when, say, ∂_A is a boundary-face, the projection on the sphere $p(\mathcal{G}_{AB}(v_{BA})) = p(\mathcal{G}_{B'A}(v_{B'A}))$ actually never reaches the puncture x_A , but rather wraps eventually around ∂_A forever. This issue can be fixed by stopping the path at the first time it hits ∂_A , replacing the final part with a segment entering inside ∂_A to reach x_A (and doing similar fixes at ∂_B and ∂_C if needed). All in all, the above differences do not concern the inner faces of M , which therefore lift to unique preimages in $\mathcal{M}_{ABCB'}$.

We now turn to the second claim. We have seen that $\mathcal{T}_{ACB'}$ is on the right of \mathcal{T}_{ABC} when $a + c - b \geq 0$, and each of these triangles has one side in common with $\mathcal{M}_{ABCB'}$ (namely along $\mathcal{G}_{BC}(v_{BC})$ for \mathcal{T}_{ABC} and along $\mathcal{G}_{B'A}(v_{B'A})$ for $\mathcal{T}_{ACB'}$). Checking that both triangles are contained in $\mathcal{M}_{ABCB'}$ therefore boils down to checking that their other sides are well placed, namely that the boundary $\mathcal{G}_{AB}(v_{AB})$ of \mathcal{T}_{ABC} is on the right of boundary $\mathcal{G}_{AB}(v_{BA})$ of $\mathcal{M}_{ABCB'}$ and that the boundary $\mathcal{G}_{CB'}(v_{B'C})$ of $\mathcal{M}_{ABCB'}$ is on the right of the boundary $\mathcal{G}_{CB'}(v_{CB'})$ of $\mathcal{T}_{ACB'}$. But this can be done exactly in the same way as for proving that $\mathcal{G}_{AC}(v_{AC})$ is on the right of $\mathcal{G}_{AC}(v_{CA})$, via the diangle lemma. Indeed, the reasoning done at the beginning of this subsection—including Lemma 5.12—pertains to the quadruplet of ideal corners $(\tilde{x}_A, \tilde{x}_B, \tilde{x}_C, \tilde{x}_{B'})$, and relies on the key relations $\tilde{x}_{B'} = A\tilde{x}_B = C^{-1}\tilde{x}_B$. But, at a fundamental level, A , B and C play a completely symmetric role, and redoing our reasoning with the quadruplets $(\tilde{x}_B, \tilde{x}_C, \tilde{x}_A, \tilde{x}_{C'})$ and $(\tilde{x}_{B'}, \tilde{x}_A, \tilde{x}_C, \tilde{x}_{A'})$, with $\tilde{x}_{C'} := B\tilde{x}_C = A^{-1}\tilde{x}_C$ and $\tilde{x}_{A'} := B'\tilde{x}_A = C^{-1}\tilde{x}_A$, we find that the remaining pieces of the puzzle of Figure 5.2 are the bigeodesic diangles $\mathcal{D}_{AB}(v_{BA}, v_{AB})$ and $\mathcal{D}_{B'C}(v_{CB'}, v_{B'C})$ of respective exceedances $b + a - c$ and $c + b - a$, which are indeed nonnegative since M is assumed of type I. \square

Proposition 5.14. *The procedure which, to the map M of type I, associates the two bigeodesic triangles \mathcal{T}_{ABC} and $\mathcal{T}_{ACB'}$, and the three bigeodesic diangles $\mathcal{D}_{AC}(v_{CA}, v_{AC})$, $\mathcal{D}_{AB}(v_{BA}, v_{AB})$ and $\mathcal{D}_{B'C}(v_{CB'}, v_{B'C})$, is the inverse of the assembling procedure I.*

Proof. By comparing Figures 4.5 and 5.2, it is plain that disassembling a map M of type I by cutting its universal cover \tilde{M} along leftmost bigeodesics as in Figure 5.2, then reassembling the pieces following procedure I as in Figures 4.4 and 4.5, restores M after projecting \tilde{M} on S by p .

It remains to check that, conversely, if we assemble two triangles and three diangles together, then disassemble the result, we recover the original pieces. We thus start with two triangles and three diangles, and perform a partial gluing, as described in the Figure 4.4 of Section 4.1. We note that the obtained “bigeodesic quadrangle” \mathcal{M} is of the

same form as that, $\mathcal{M}_{ABC B'}$, displayed on Figure 5.2. Working directly on the universal cover, we then have to glue copies \mathcal{M}_w of \mathcal{M} along the scheme of Figure 4.5.

Let us for now forget the decomposition interpretation of Figure 5.2 described in its caption and reinterpret it instead as the result of the procedure described in Figure 4.5, once completed by a gluing of all the red and blue intervals facing each other. We may then view the light blue and green domains in this figure as representing the copy \mathcal{M}_\emptyset of \mathcal{M} , together with its diangle/triangle components. We may also view the vertices v_{AB}, \dots as the associated attachment points of \mathcal{M}_\emptyset and of its internal components.

With this new interpretation of the figure, we already know from Lemma 4.1 that the four sides of the quadrangle \mathcal{M}_\emptyset lie along four geodesic paths in \tilde{M} : the bigeodesic denoted \mathcal{G} in Section 4.3, its image by A , and a symmetric bigeodesic \mathcal{G}' (launched from the attachment point between the copies \mathcal{M}_\emptyset and \mathcal{M}_ε and going towards the ideal corners \tilde{x}_C and $\tilde{x}_{B'}$) and its image by C . Clearly, \mathcal{G} is a bigeodesic between $\tilde{\partial}_A$ and $\tilde{\partial}_B$ and it is in fact the leftmost bigeodesic $\mathcal{G}_{AB}(v_{BA})$ launched from v_{BA} (which is de facto a geodesic vertex). This is a straightforward consequence of the fact that, from v_{BA} to $\tilde{\partial}_A$ (respectively to $\tilde{\partial}_B$), \mathcal{G} is glued to only red segments on its left. Similarly, \mathcal{G}' is the leftmost bigeodesic $\mathcal{G}_{CB'}(v_{B'C})$. Since $v_{B'A} = Av_{AB}$ and $v_{BC} = Cv_{B'C}$, the two other sides of \mathcal{M}_\emptyset are the leftmost bigeodesics $\mathcal{G}_{B'A}(v_{B'A})$ and $\mathcal{G}_{BC}(v_{BC})$. From the definition of bigeodesic diangles and triangles, the paths passing via v_{AB}, v_{CA}, v_{AC} and $v_{CB'}$ are clearly leftmost bigeodesics within \mathcal{M}_\emptyset and coalesce with either \mathcal{G} or \mathcal{G}' outside of \mathcal{M}_\emptyset , hence they are leftmost bigeodesics in \tilde{M} which we thus identify as $\mathcal{G}_{AB}(v_{AB}), \mathcal{G}_{CA}(v_{CA}), \mathcal{G}_{AC}(v_{AC})$ and $\mathcal{G}_{CB'}(v_{CB'})$.

To recover the original interpretation of Figure 5.2, it remains to show that v_{AB}, v_{BC} and v_{CA} are actually the equilibrium vertices for $\tilde{\partial}_A, \tilde{\partial}_B$ and $\tilde{\partial}_C$, while $v_{AC}, v_{CB'}$ and $v_{B'A}$ are the equilibrium vertices for $\tilde{\partial}_A, \tilde{\partial}_C$ and $\tilde{\partial}_{B'}$. Since \mathcal{T}_{ABC} is a bigeodesic triangle, we deduce that v_{AB} and v_{CA} have the same \tilde{d}_A -latitude, v_{AB} and v_{BC} the same \tilde{d}_B -latitude and v_{BC} and v_{CA} the same \tilde{d}_C -latitude. Since these vertices are all geodesic vertices (so that, e.g. $\tilde{d}_A(v_{AB}) + \tilde{d}_B(v_{AB}) = \tilde{d}_{AB} = r_A + r_B$), we deduce that they obey the relation (5.11) imposed on equilibrium vertices. Otherwise stated, the vertices v_{AB}, v_{BC} and v_{CA} belong to the respective sets $I_{AB}(r_A), I_{BC}(r_B)$ and $I_{CA}(r_C)$, as defined in Section 5.5. Furthermore, since these vertices are the three attachment points of a bigeodesic triangle, they are necessarily the rightmost elements of their respective sets, hence they are indeed the equilibrium vertices associated with $(\tilde{\partial}_A, \tilde{\partial}_B, \tilde{\partial}_C)$, and \mathcal{T}_{ABC} indeed coincides with the triangle constructed in Section 5.5. Performing the same reasoning on the triangle denoted $\mathcal{T}_{ACB'}$, we eventually recover precisely the original decomposition interpretation of Figure 5.2, as described in its caption. Proposition 5.14 follows. \square

We conclude this section with two remarks. First, when M has no inner face, \tilde{M} has only ideal faces and is actually a tree. We find that the triangles \mathcal{T}_{ABC} and $\mathcal{T}_{ACB'}$ are reduced to single vertices, while the diangles are reduced to segments, thereby inverting the assembling of Figure 3.3 for type I. Second, in the case $a = b = c = 0$, the current disassembling procedure coincides with that of Section 3.4. Indeed, we only have ideal vertices in this case, so that \tilde{d}_{AB} is just the graph distance between $\tilde{\partial}_A$ and $\tilde{\partial}_B$ in \tilde{M} and coincides with the graph distance d_{AB} between ∂_A and ∂_B in M , and similarly for

the other pairs of ideal vertices. The decomposition of \tilde{M} which we perform here just projects to the decomposition of M performed in Section 3.4 (note that, in that section, the vertices denoted v_{AB} , v_{BC} and v_{CA} are the projections of those which we consider here, while v_{BA} , v_{CB} and v_{AC} are the projections of $v_{B'A}$, $v_{C'B'}$ and v_{AC} respectively).

5.7. Decomposing a map of type II

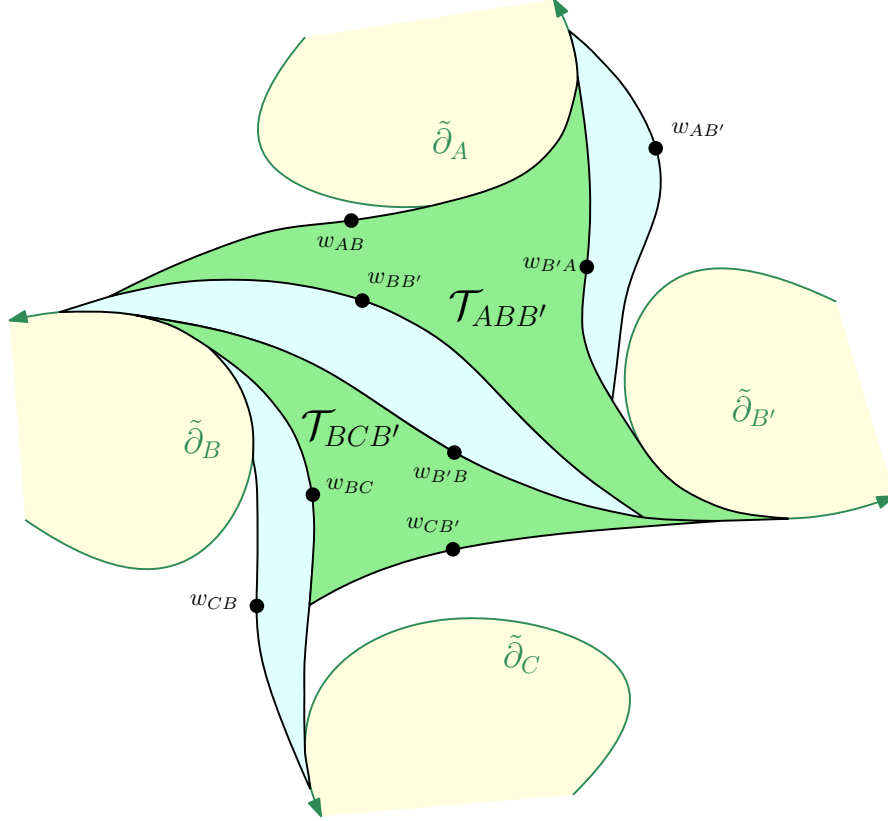


Figure 5.3: Illustration of the decomposition of a map of type II. The two geodesic triangles $\mathcal{T}_{ABB'}$ and $\mathcal{T}_{BCB'}$ (shown in green) and the three bigeodesic diangles (shown in light blue) form the domain $\mathcal{M}'_{ABCB'}$ of Lemma 5.15.

Suppose now that we have a map M of type II. Without loss of generality, we may assume that ∂_B is the longest boundary, i.e. we have $b \geq a+c$. Then, the decomposition of the previous subsection might fail, since now $\tilde{d}_A(v_{CA}) - \tilde{d}_A(v_{AC}) = r_A - r'_A = a+c-b \leq 0$, hence it is not possible in general to apply the diangle lemma (it could happen that the bigeodesics $\mathcal{G}_{AC}(v_{CA})$ and $\mathcal{G}_{AC}(v_{AC})$ cross each other).

Then, the trick is to “perform a flip” and, instead of the triangles \mathcal{T}_{ABC} and $\mathcal{T}_{ACB'}$, to consider rather the triangles $\mathcal{T}_{ABB'}$ and $\mathcal{T}_{BCB'}$, see Figure 5.3. The equilibrium vertices of $\mathcal{T}_{ABB'}$ (resp. $\mathcal{T}_{BCB'}$) are denoted w_{AB} , $w_{BB'}$ and $w_{B'A}$ (resp. w_{BC} , $w_{CB'}$ and $w_{B'B}$). We now have the following counterpart of Lemma 5.13:

Lemma 5.15. *Let $w_{AB'} := Aw_{AB}$ and $w_{CB} := Cw_{CB'}$, and let $\mathcal{M}'_{ABC B'}$ be the domain delimited by the bigeodesics $\mathcal{G}_{AB}(w_{AB})$, $\mathcal{G}_{BC}(w_{CB})$, $\mathcal{G}_{CB'}(w_{CB'})$ and $\mathcal{G}_{B'A}(w_{AB'})$, pruned from their common parts (see again Figure 5.3). Then, $\mathcal{M}'_{ABC B'}$ contains exactly one preimage of each inner face of M .*

Furthermore, when M is of type II, then both triangles $\mathcal{T}_{ABB'}$ and $\mathcal{T}_{BCB'}$ are contained in $\mathcal{M}'_{ABC B'}$, and their complement consists of the three geodesic diangles $\mathcal{D}_{BB'}(w_{B'B}, w_{BB'})$, $\mathcal{D}_{AB'}(w_{B'A}, w_{AB'})$ and $\mathcal{D}_{BC}(w_{CB}, w_{BC})$, with nonnegative exceedances equal to $b - a - c$, $2a$ and $2c$, respectively.

Proof. The first claim is similar to that of Lemma 5.13, and is proved in the same way.

For the second claim, we apply again the diangle lemma, and all boils down to proving that

$$\begin{aligned}\tilde{d}_B(w_{B'B}) - \tilde{d}_B(w_{BB'}) &= b - a - c, \\ \tilde{d}_A(w_{B'A}) - \tilde{d}_A(w_{AB'}) &= 2a, \\ \tilde{d}_C(w_{BC}) - \tilde{d}_C(w_{CB}) &= 2c.\end{aligned}\tag{5.16}$$

For the first relation, by considering the equilibrium conditions in $\mathcal{T}_{ABB'}$ and $\mathcal{T}_{BCB'}$ we find that

$$\tilde{d}_B(w_{B'B}) - \tilde{d}_B(w_{BB'}) = \frac{(\tilde{d}_{BC} - \tilde{d}_{AB}) - (\tilde{d}_{CB'} - \tilde{d}_{B'A})}{2}\tag{5.17}$$

and we observe that the right-hand side is nothing but the opposite of that of (5.13). Thus, by Lemma 5.12, it is equal to $b - a - c$ as wanted. For the second relation of (5.16), we simply note that $\tilde{d}_A(w_{AB}) = \tilde{d}_A(w_{B'A})$ by the definition of equilibrium vertices, and that $\tilde{d}_A(w_{AB'}) = \tilde{d}_A(w_{AB}) - 2a$ by (5.4). For the third relation, we proceed in the same way, with C instead of A . \square

Proposition 5.16. *The procedure which, to the map M of type II, associates the two bigeodesic triangles $\mathcal{T}_{ABB'}$ and $\mathcal{T}_{BCB'}$, and the three bigeodesic diangles $\mathcal{D}_{BB'}(w_{B'B}, w_{BB'})$, $\mathcal{D}_{AB'}(w_{B'A}, w_{AB'})$ and $\mathcal{D}_{BC}(w_{CB}, w_{BC})$, is the inverse of the assembling procedure II.*

The proof is entirely similar to that of Proposition 5.14. Note that, when M has no inner face, \tilde{M} has only ideal faces and is actually a tree. We find that the triangles $\mathcal{T}_{ABB'}$ and $\mathcal{T}_{BCB'}$ are reduced to single vertices, while the diangles are reduced to segments, thereby inverting the assembling of Figure 3.3 for type II. The proof of Theorem 3.1 is now complete.

6. Equivalence with the Eynard-Collet-Fusy formula, and limiting statistics in random maps with boundaries

In this section, we discuss the relation of our work with the Eynard-Collet-Fusy (ECF) formula for (quasi-)bipartite maps with three boundaries—see [Eyn16, Proposition 3.3.1] and [CF12]—and we show that it entails interesting properties of the statistics of distances and areas in random maps and their scaling limits.

Let L_1, L_2, L_3 be positive integers or half-integers whose sum is an integer. Let G_{L_1, L_2, L_3} be the generating function of essentially bipartite planar maps with three (non necessarily tight) rooted boundary-faces of degrees $2L_1, 2L_2, 2L_3$, counted with a weight t per vertex and a weight g_{2k} per inner face of degree $2k$. Here, a boundary-face is said *rooted* if one its incident corners is distinguished. We also let R be the generating series defined at (1.2), and we introduce the notation

$$\alpha(2L) := \frac{(2L)!}{[L]![L - \frac{1}{2}]!}, \quad L \in \frac{1}{2}\mathbb{Z}. \quad (6.1)$$

The ECF formula states that

$$G_{L_1, L_2, L_3} = \alpha(2L_1)\alpha(2L_2)\alpha(2L_3) \cdot R^{L_1+L_2+L_3} \frac{d \ln(R)}{dt}. \quad (6.2)$$

We will show in Section 6.2 how one can recover this formula from Theorem 1.1. To this end, we first establish in Section 6.1 some facts about the structure of minimal cycles homotopic to the boundaries in general pairs of pants. For the record, and since this will be useful for the probabilistic considerations of Section 6.3, we also recall the formula for the generating function G_{L_1, L_2} of essentially bipartite *annular maps*, namely maps with two rooted boundary-faces of lengths $2L_1$ and $2L_2$, with L_1, L_2 positive integers or half-integers whose sum is an integer:

$$G_{L_1, L_2} = \frac{\alpha(2L_1)\alpha(2L_2)}{L_1 + L_2} \cdot R^{L_1+L_2}. \quad (6.3)$$

This formula appears in various places in the literature, for instance it is the case $r = 2$ of [CF12, Theorem 1.1], see also [Bud17, Proposition 4] or [Cur19, Theorem 3.12], and [Bou19, Equation (2.1)] for a derivation based on the slice decomposition.

6.1. The structure of outermost minimal separating cycles

Let M be a planar map with three boundary-faces $\partial_1, \partial_2, \partial_3$, that are *not* supposed to be tight. We consider the problem of finding cycles homotopic to the boundaries ∂_i of M , with minimal length. The optimization problems of finding shortest paths with certain topological constraints on surfaces have been investigated in the literature on effective geometry and computer science. In particular, some of the ideas used in this section are similar to [CdVL07, CdVE10]. We mention that the discussion below generalizes easily to maps with more than three boundaries.

As in Section 4, we may and will assume that M is a map on the triply punctured sphere S , and we denote the punctures by x_1, x_2, x_3 . For $i \in \{1, 2, 3\}$, let $\mathcal{C}_{\min}^{(i)}(M)$ be the set of cycles in M that are freely homotopic to the contour of ∂_i in the punctured sphere S , and that have minimal possible length. This minimal length will be denoted by $2\ell_i(M)$, where $\ell_i(M)$ is a positive integer or half-integer. Note that, when M is essentially bipartite, $2\ell_i(M)$ has the same parity as the degree of ∂_i . Our goal is to collect a number of facts about the structure of $\mathcal{C}_{\min}^{(i)}(M)$. In particular, we will see that it carries a natural order relation which makes it a lattice.

As in the preceding sections, it will be useful to work on the universal cover \tilde{M} of M introduced in Section 4, which is a map on the universal cover $p : \tilde{S} \rightarrow S$. We will however use a slightly different index notation, replacing $\partial_A, \partial_B, \partial_C$ with $\partial_1, \partial_2, \partial_3$, x_A, x_B, x_C with x_1, x_2, x_3 . The automorphisms A, B, C are renamed A_1, A_2, A_3 , and the distinguished ideal corners $\tilde{x}_A, \tilde{x}_B, \tilde{x}_C$ are renamed $\tilde{x}_1, \tilde{x}_2, \tilde{x}_3$, see for instance Figure 4.1 for a reminder of the former notation (we will not use $\tilde{x}_{B'}$ here).

The boundary-faces of M are lifted in \tilde{M} to faces of infinite degrees, similarly to Figure 4.2, but whose contours are now not necessarily geodesic, and not even necessarily simple curves, since the boundaries of M are not assumed to be tight. From the “concrete” construction of \tilde{M} in Section 4, for $i \in \{1, 2, 3\}$, we can naturally distinguish a particular lift of ∂_i by choosing $\tilde{\partial}_i$ to be the infinite face of \tilde{M} that is incident to the ideal boundary point \tilde{x}_i . Note that $\tilde{\partial}_i$ is invariant under the automorphism A_i . If c^i is a cycle that is homotopic to the contour $\tilde{\partial}_i$ of ∂_i , then we can reason exactly as in the beginning of the proof of Lemma 4.3, which did not make use of the fact that the boundaries are tight. Namely, we let γ be a path from some arbitrary point x on $\tilde{\partial}_i$ to some point z on c^i such that $\gamma c^i \gamma^{-1}$ and $\tilde{\partial}_i$ are homotopic as loops rooted at x , and then lift those two paths to obtain a path \tilde{c}_0^i from a vertex \tilde{z} in \tilde{M} to $A_i \tilde{z}$ that is a lift of c^i . The concatenation of the paths $A_i^n \tilde{c}_0^i, n \in \mathbb{Z}$, seen up to increasing reparametrization, is then a biinfinite path \tilde{c}^i whose projection via p is a path that circles indefinitely around c^i , and which we call a *biinfinite lift* of c^i . Moreover, \tilde{c}^i is invariant under A_i . Let U_0 be the finite set of words \mathbf{w} such that \tilde{c}_0^i visits the domains $S_{\mathbf{w}}$, in the former notation of Section 4.1. Then by invariance under A_i , \tilde{c}^i visits $A_i^n S_{\mathbf{w}}, n \in \mathbb{Z}, \mathbf{w} \in U_0$. Now, from the way in which domains are connected together, we see that all domains of the form $A_i^n S_{\emptyset}, n \in \mathbb{Z}$ must be visited, so that \tilde{c}^i remains at bounded “distance” from $\tilde{\partial}_i$ (where distance is measured in terms of number of domains $S_{\mathbf{w}}$ to cross). In this sense, \tilde{c}^i converges to the ideal boundary point \tilde{x}_i , that is incident to the infinite face $\tilde{\partial}_i$. Consequently, if $j \neq i$ and c^i, c^j are two cycles that are respectively freely homotopic to the contours of ∂_i and ∂_j , their biinfinite lifts \tilde{c}^i, \tilde{c}^j defined as above converge to two different ideal boundary points.

Now, if \hat{c}^i is another biinfinite lift of c^i , there is an automorphism W such that $\hat{c}^i = W \tilde{c}^i$. If $W \in \{A_i^n, n \in \mathbb{Z}\}$, we have $\hat{c}^i = \tilde{c}^i$, and otherwise, \hat{c}^i is a distinct infinite path that is invariant under the automorphisms $W A_i^n W^{-1}, n \in \mathbb{Z}$. In the latter case, this infinite path visits domains of the form $W A_i^n S_{\mathbf{w}}$ where $n \in \mathbb{Z}$ and \mathbf{w} belongs to a finite set of words, which implies that \hat{c}^i converges to the ideal corner $W \tilde{x}_i$, distinct from \tilde{x}_i . For this reason, we can single out the biinfinite lift \tilde{c}^i constructed above, which converges to the distinguished ideal boundary vertex \tilde{x}_i , and call it the *canonical biinfinite lift* of c^i .

Now fix $i \in \{1, 2, 3\}$, let $c^i \in \mathcal{C}_{\min}^{(i)}(M)$, and let \hat{c}^i be any biinfinite lift of c^i in \tilde{M} , passing through an arbitrary point \hat{z} projecting to a point of c^i . Similarly to Lemma 5.4 above, the minimality of the length of c^i , and Proposition 2.5 and Lemma 2.1 in [CdVE10], imply the following result.

Lemma 6.1. *The path \hat{c}^i is a biinfinite geodesic in \tilde{M} , separating \tilde{S} into two connected components.*

Note that we can view the two components of $\tilde{M} \setminus \hat{c}^i$ as the “left” and “right” component, since \tilde{M} is oriented, and we can assume that c^i circles counterclockwise around the

puncture x_i . Given the fact that the latter (which we view as a point “outside” the surface) belongs to the region of the complement of c^i located to its left, we call the left region of $\tilde{M} \setminus \hat{c}^i$ the outer domain of \hat{c}^i , and the right region the inner domain. Note that both domains of \hat{c}^i determine \hat{c}^i as their boundaries, by Jordan’s theorem.

We now define a partial order relation on $\mathcal{C}_{\min}^{(i)}(M)$. Let $c_1^i, c_2^i \in \mathcal{C}_{\min}^{(i)}(M)$, and $\tilde{c}_1^i, \tilde{c}_2^i$ be their canonical biinfinite lifts. We write $c_1^i \preceq^{(i)} c_2^i$ if the outer domain of \tilde{c}_1^i is included in the outer domain of \tilde{c}_2^i . The fact that this indeed defines a partial order is easy and left to the reader.

Lemma 6.2. *If c_1^i, c_2^i are elements of $\mathcal{C}_{\min}^{(i)}(M)$, and if $\tilde{c}_1^i, \tilde{c}_2^i$ are their canonical lifts, then the intersection and union of their outer domains are simply connected and bounded by two paths which we denote by $\tilde{c}_1^i \wedge \tilde{c}_2^i$ and $\tilde{c}_1^i \vee \tilde{c}_2^i$. In turn, these two paths project via p to two cycles $c_1^i \wedge c_2^i$ and $c_1^i \vee c_2^i$ on M , which are the infimum and supremum of $\{c_1^i, c_2^i\}$ for the order $\preceq^{(i)}$. In particular, $(\mathcal{C}_{\min}^{(i)}(M), \preceq^{(i)})$ is a lattice.*

Again, the proof of this statement is easy and relies on the observation that two consecutive intersections of the paths \tilde{c}_1^i and \tilde{c}_2^i must arise in increasing order for the parametrization of both paths, and be linked by arcs of same lengths, by the geodesic property.

As a consequence, since $(\mathcal{C}_{\min}^{(i)}(M), \preceq^{(i)})$ is clearly a finite lattice, it admits a smallest element $c_{(i)}$, called the outermost minimal cycle homotopic to the contour of ∂_i . It also admits a maximal element, although we are not going to use this one in the sequel. As a final observation, we state the following.

Lemma 6.3. *For every $i, j \in \{1, 2, 3\}$, the cycles $c_{(i)}, c_{(j)}$ do not cross each other, but may however have edges in common. For $i = j$ this means that the cycle $c_{(i)}$ cannot be self-crossing, but may possibly visit some edges more than once.*

Remark 6.4. Though intuitively clear, this lemma has some subtlety to it. In particular, the fact that $c_{(i)}$ may visit some edges twice does happen, see for instance the contour of ∂_B on the example displayed in Figure 4.2. The proof of the lemma consists in showing that the outer domains of two distinct biinfinite lifts of $c_{(i)}$ and $c_{(j)}$ cannot overlap. For $i = j$, this entails that the self-contacts of $c_{(i)}$, if there are any, can occur only “from the inner side”. More precisely, the outer region of $c_{(i)}$, which is comprised of the edges of \tilde{M} that can be attained from ∂_i without crossing $c_{(i)}$, can be seen as a map with two boundaries, one of which is the contour of ∂_i , and the other being a *simple* boundary that results from cutting along $c_{(i)}$. This remark will be useful in the next section.

Proof. In this proof, we let $A = A_i$ to simplify the notation. If $c_{(i)}$ and $c_{(j)}$ cross each other, then we can lift them into biinfinite geodesics $\tilde{c}_{(i)}, \hat{c}_{(j)}$ in the universal cover that also cross each other, where we choose the first lift to be the canonical lift of $c_{(i)}$, which is invariant under A . Note that $\hat{c}_{(j)}$ is not necessarily the canonical lift of $c_{(j)}$, as it is determined by the choice of a lift of an intersection point of $c_{(i)}$ and $c_{(j)}$. Necessarily, these two geodesic biinfinite lifts must converge to two distinct ideal boundary points. Therefore, whenever $\hat{c}_{(j)}$ enters the outer region of $\tilde{c}_{(i)}$, it has to eventually leave it. This

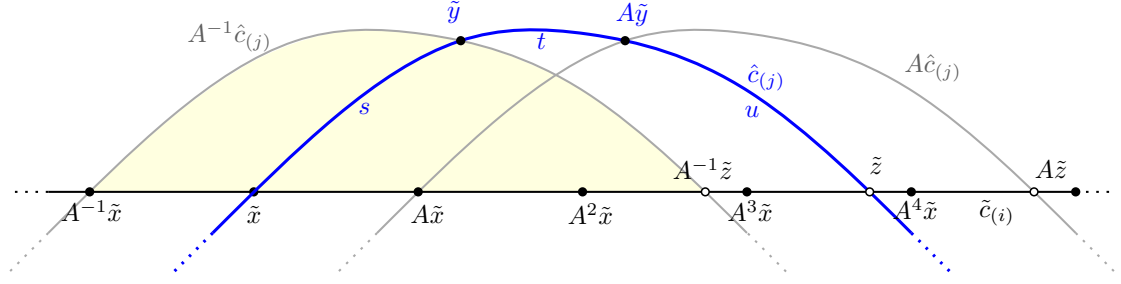


Figure 6.1: Illustration of the proof of Lemma 6.3. The bottom black line is the biinfinite geodesic $\tilde{c}_{(i)}$, whose outer domain, represented as the upper-half of the picture, is visited by the blue path $\hat{c}_{(j)}$. The proof consists in showing that the portion of the blue arc between \tilde{y} and $A\tilde{y}$ projects via p to a cycle of $\mathcal{C}_{\min}^{(i)}(M)$ which is strictly smaller than its minimal element, a contradiction.

reasoning holds also when $i = j$ and $c_{(i)}$ has a self-crossing, upon noting that $\tilde{c}_{(i)}$ and $\hat{c}_{(i)}$ denote two lifts of $c_{(i)}$ which are necessarily different, since they are simple paths that cross each other.

So there is then a subpath of $\hat{c}_{(j)}$ within the outer region of $\tilde{c}_{(i)}$, say between the two points \tilde{x} and \tilde{z} , meaning that $\hat{c}_{(j)}$ is entirely contained in the open outer region of $\tilde{c}_{(i)}$ between these points. Now assume without loss of generality that \tilde{z} belongs to the portion of $\tilde{c}_{(i)}$ between $A^n\tilde{x}$ and $A^{n+1}\tilde{x}$ for some $n \geq 0$, and distinct from $A^n\tilde{x}$. If $n = 0$ we arrive at a contradiction, because we can follow the arc of $\hat{c}_{(j)}$ between points \tilde{x} and \tilde{z} , then the arc of $\tilde{c}_{(i)}$ between \tilde{z} and $A\tilde{x}$ to form a new geodesic arc \tilde{c} between \tilde{x} and $A\tilde{x}$ that is contained in the (closed) outer domain of $\tilde{c}_{(i)}$, and therefore projects via p to a cycle that is strictly smaller than $c_{(i)}$ in $\mathcal{C}_{\min}^{(i)}(M)$.

Next, let us assume that $n \geq 1$. Let $2\ell = 2\ell_i(M)$ be the length of the cycle $c_{(i)}$, that is in particular the length of the arc of $\tilde{c}_{(i)}$ between $A^m\tilde{x}$ and $A^{m+1}\tilde{x}$ for every $m \in \mathbb{Z}$. In particular, the length of the arc of $\tilde{c}_{(i)}$ between \tilde{x} and \tilde{z} equals $2n\ell + \ell'$ for some $\ell' \in (0, 2\ell]$, and this is also the distance between its extremities since $\tilde{c}_{(i)}$ is a geodesic path.

Then the arc of $\hat{c}_{(j)}$ between \tilde{x} and \tilde{z} enters the Jordan domain (see the yellow domain in Figure 6.1) formed by the arcs of $\tilde{c}_{(i)}$ and $A^{-1}\hat{c}_{(j)}$ between the points $A^{-1}\tilde{x}$ and $A^{-1}\tilde{z}$, and has to leave it through some point \tilde{y} since \tilde{z} is not in this domain. Since we assumed that the arc of $\hat{c}_{(j)}$ between \tilde{x} and \tilde{z} is entirely contained in the outer domain of $\tilde{c}_{(i)}$, it must be that \tilde{y} belongs to the arc of $A^{-1}\hat{c}_{(j)}$ between $A^{-1}\tilde{x}$ and $A^{-1}\tilde{z}$. Now by applying the automorphism A , $A\tilde{y}$ has to be the intersection point of the arc of $\hat{c}_{(j)}$ between \tilde{x} and \tilde{z} with the arc of $A\hat{c}_{(j)}$ between $A\tilde{x}$ and $A\tilde{z}$. In particular, $\hat{c}_{(j)}$ contains an arc (between \tilde{y} and $A\tilde{y}$) that is strictly contained in the outer domain of $\tilde{c}_{(i)}$. Since one of its extremity is the image of the other by A , this arc projects to a cycle c of M that is homotopic to the boundary ∂_i . So if we can show that its length is 2ℓ (in fact, we will show that this length can be at most 2ℓ , which is even better!), we will obtain that c is in $\mathcal{C}_{\min}^{(i)}(M)$ but $c \prec^{(i)} c_{(i)}$, a contradiction.

So let t be the length of the arc of $\hat{c}_{(j)}$ between \tilde{y} and $A\tilde{y}$, and let s, u be the lengths of the arcs between \tilde{x} and \tilde{y} , and between $A\tilde{y}$ and \tilde{z} respectively. Then u is also the length of the arc of $A^{-1}\hat{c}_{(j)}$ between \tilde{y} and $A^{-1}\tilde{z}$.

Now the length of the concatenation of the arc of $\hat{c}_{(j)}$ between \tilde{x} and \tilde{y} , the arc of $A^{-1}\hat{c}_{(j)}$ between \tilde{y} and $A^{-1}\tilde{z}$, and the arc of $\tilde{c}_{(i)}$ between $A^{-1}\tilde{z}$ and \tilde{z} equals $s + u + 2\ell$, and has to be greater than or equal to the distance between its extremities \tilde{x} and \tilde{z} , which is $2n\ell + \ell'$ as mentioned above. Therefore, we obtain $s + u \geq 2(n-1)\ell + \ell'$. On the other hand, since $\hat{c}_{(j)}$ is a geodesic path, this distance $2n\ell + \ell'$ is also equal to $s + t + u$, which is at least $t + 2(n-1)\ell + \ell'$. So we obtain that $t \leq 2\ell$, as wanted. \square

6.2. A re-derivation of the ECF formula for pairs of pants

We now use the above discussion to introduce a bijective decomposition of planar maps with three boundary-faces which are not necessarily tight. Let M be such a map, with boundaries denoted $\partial_1, \partial_2, \partial_3$ as before. For every $i = 1, 2, 3$, we let $c_{(i)}$ be the minimal element of $(\mathcal{C}_{\min}^{(i)}(M), \preceq^{(i)})$, as defined in the previous subsection. By Lemma 6.3, these cycles cannot cross, so they split the map M into four parts $M^{(0)}, M^{(1)}, M^{(2)}, M^{(3)}$ where, for $i = 1, 2, 3$, $M^{(i)}$ is the part of M delimited by the (non self-crossing) cycle $c_{(i)}$ and containing the face ∂_i , while $M^{(0)}$ is the remainder of the map delimited by the three cycles $c_{(1)}, c_{(2)}, c_{(3)}$. By Remark 6.4, for $i \in \{1, 2, 3\}$, we may view $M^{(i)}$ as a map with two boundaries, one being given by the contour of ∂_i , and the other being a simple boundary resulting from cutting along $c_{(i)}$.

In order to be consistent with the ECF formula, the boundary-faces of M are assumed to be rooted. This induces a canonical rooting of the boundary-faces of $M^{(0)}$ by, say, considering the leftmost shortest path starting at the root of ∂_i and ending on $c_{(i)}$.

To characterize the resulting maps, we need an extra definition: a boundary-face is said *strictly tight* if its contour is the unique cycle of minimal length in its homotopy class. A strictly tight boundary-face is to a tight boundary-face what a (red) strictly geodesic boundary interval is to a (blue) geodesic boundary interval, as we defined in Section 2.1.

Proposition 6.5. *Let $L_1, L_2, L_3, l_1, l_2, l_3$ be positive integers or half-integers. Then, the mapping $M \mapsto (M^{(0)}, M^{(1)}, M^{(2)}, M^{(3)})$ is a bijection between:*

- *the set of planar maps M which have three rooted boundary-faces of lengths $2L_1, 2L_2, 2L_3$ and whose minimal separating cycles have lengths $2\ell_i(M) = 2l_i$,*
- *and the set of quadruplets $(M^{(0)}, M^{(1)}, M^{(2)}, M^{(3)})$ made of a planar map $M^{(0)}$ with three rooted tight boundary-faces of lengths $2l_1, 2l_2, 2l_3$, and of three annular maps $M^{(1)}, M^{(2)}, M^{(3)}$ where, for $i = 1, 2, 3$, the map $M^{(i)}$ has a rooted boundary of length $2L_i$ and a strictly tight unrooted boundary of length $2l_i$.*

The map M is essentially bipartite if and only if $M^{(0)}, M^{(1)}, M^{(2)}, M^{(3)}$ are essentially bipartite. (In this case, M exists if and only if $L_1 + L_2 + L_3, L_1 - l_1, L_2 - l_2$ and $L_3 - l_3$ are all nonnegative integers.)

Proof. The tightness properties of the boundaries of $M^{(0)}, M^{(1)}, M^{(2)}, M^{(3)}$ result from the fact that $c_{(i)}$ is the minimal element of $\mathcal{C}_{\min}^{(i)}(M)$ for $i = 1, 2, 3$.

The mapping is a bijection since we may conversely (re)assemble a map M from a quadruplet. Note that there are a priori $(2l_1) \cdot (2l_2) \cdot (2l_3)$ ways to perform the (re)assembling, but only one of them is consistent with the rootings. Indeed, in $M^{(i)}$ we consider the leftmost shortest path starting with the root and ending on the unrooted boundary, and this singles out the position at which we must align the root on the i -th boundary of $M^{(0)}$. \square

We refer to the areas (number of faces) of the annular maps $M^{(1)}, M^{(2)}, M^{(3)}$ as the *exterior areas* of M , denoted by $A_1(M), A_2(M), A_3(M)$ respectively, and to the area of the map $M^{(0)}$ as the *interior area* of M , denoted by $A_0(M)$. In this way, the exterior area $A_i(M)$ ($i = 1, 2, 3$) is the minimal area bounded by the contour of ∂_i and by a cycle homotopic to it of minimal possible length³.

For the purposes of the next section, we also consider the case where M is an annular map whose two boundary-faces ∂_1, ∂_2 are rooted and not necessarily tight. The contours of the two boundaries are now homotopic, hence there is now a single set $\mathcal{C}_{\min}(M)$ of separating cycles of minimal length (this length is denoted $2\ell(M)$). In this set we may find two “extremal cycles”, closest to ∂_1 and to ∂_2 respectively. By splitting M along these two cycles, we obtain three pieces $M^{(0)}, M^{(1)}, M^{(2)}$, where $M^{(0)}$ is a map with two rooted tight boundary-faces both of length $2\ell(M)$, while $M^{(1)}$ and $M^{(2)}$ have one rooted boundary-face and another strictly tight unrooted boundary-face of length $2\ell(M)$. This decomposition yields a bijection analogous to that of Proposition 6.5. We define the interior and exterior areas of M accordingly: for $i = 0, 1, 2$, we let $A_i(M)$ be the area of $M^{(i)}$.

We now recall known enumerative results about the annular maps with (strictly) tight boundaries considered above. We mention that these results may be obtained by specializing [BF12, Theorem 34] or [BG14, Equations (9.18) and (9.19)], which deal with the more general setting of maps with girth/irreducibility constraints, but we refer to [Bou19, Section 2.2] for a more elementary presentation in the current setting. It uses a slice decomposition expressed in the universal covers of the annular maps, similarly to the present paper.

Proposition 6.6 (see e.g. [Bou19, Theorem 2.1]). *Let L, l be positive integers or half-integers such that $L - l$ is a nonnegative integer. Then, the generating function of essentially bipartite annular maps with a rooted boundary-face of degree $2L$ and a strictly tight unrooted boundary-face of degree $2l$, counted with a weight g_{2k} per inner face of degree $2k$ and a weight t per vertex not incident to the unrooted boundary, is given by $\binom{2L}{L-l} R^{L-l}$, where R is as usual defined by (1.2).*

The generating function of essentially bipartite annular maps with two tight rooted boundary-faces of degree $2l$, counted with a weight g_{2k} per inner face of degree $2k$ and a weight t per vertex is equal to $2lR^{2l}$.

³As was pointed to one of the authors by Marco Mazzucchelli, this area is related to the notion of *flat topology* (here “flat” stands for the musical symbol b) on homology classes introduced by Whitney and Federer in geometric measure theory, see for instance the Introduction in [MN16].

We now re-derive the ECF formula (6.2). Indeed, the last two propositions imply that the generating function G_{L_1, L_2, L_3} of essentially bipartite planar maps with three rooted boundary-faces of lengths $2L_1, 2L_2, 2L_3$ is equal to

$$\sum_{\substack{2l_1, 2l_2, 2l_3 > 0 \\ L_i - l_i \in \mathbb{Z}}} \binom{2L_1}{L_1 - l_1} R^{L_1 - l_1} \binom{2L_2}{L_2 - l_2} R^{L_2 - l_2} \binom{2L_3}{L_3 - l_3} R^{L_3 - l_3} (2l_1)(2l_2)(2l_3) T_{l_1, l_2, l_3}$$

where the factors $2l_i$ account for the extra rooting of the faces in the tight maps counted by T_{l_1, l_2, l_3} . Using Theorem 1.1 and the hypergeometric identity $\sum_{2l > 0} (2l) \binom{2L}{L-l} = \alpha(2L)$, we recover precisely (6.2).

Similarly, the generating function of essentially bipartite annular maps with two rooted boundary-faces of lengths $2L_1, 2L_2$ is equal to

$$G_{L_1, L_2} = \sum_{\substack{2l > 0 \\ L_1 - l \in \mathbb{Z}}} \binom{2L_1}{L_1 - l} R^{L_1 - l} \binom{2L_2}{L_2 - l} R^{L_2 - l} (2l) R^{2l} \quad (6.4)$$

and we recover (6.3) by another hypergeometric identity.

6.3. Scaling limits of separating loop statistics

In this section we show how our results can be used to deduce statistical properties of random annular maps and pairs of pants with a large area. This will be done by deriving a scaling limit result for the minimum cycle lengths, as well as for the exterior and interior areas of the associated decomposition. For simplicity, we focus on the simplest case of bipartite quadrangulations, for which $g_{2k} = g\delta_{k,2}$, although our results should have extensions to much more general models of random maps.

Let us recall some classical probability densities:

$$p_a(x) = \frac{1}{\sqrt{2\pi a}} e^{-x^2/2a}, \quad x \in \mathbb{R} \quad (6.5)$$

the Gaussian density (of variance $a > 0$),

$$q_x(a) = \frac{x}{a} p_a(x) = \frac{x}{\sqrt{2\pi a^3}} e^{-x^2/2a}, \quad a > 0 \quad (6.6)$$

the stable-1/2 density (with parameter $x > 0$), and

$$r_a(x) = x \sqrt{\frac{2\pi}{a}} p_a(x) = \frac{x}{a} e^{-x^2/2a}, \quad x \geq 0 \quad (6.7)$$

the size-biased Gaussian absolute value density, also known as Rayleigh density (with parameter $a > 0$). All the random variables considered below will be defined on some common probability space $(\Omega, \mathcal{F}, \mathbb{P})$.

Theorem 6.7. *Let M^n be a uniformly random quadrangulation with two rooted boundaries of lengths $2L_1^n$ and $2L_2^n$ and n inner faces, where the integers $L_i^n, i \in \{1, 2\}$ satisfy $L_i^n \sim \mathcal{L}_i \sqrt{2n}$ as $n \rightarrow \infty$ for some $\mathcal{L}_1, \mathcal{L}_2 \in (0, \infty)$. Then we have the following convergence in distribution for the rescaled minimal half-length of a separating cycle and for the rescaled exterior/interior areas of M^n :*

$$\left(\left(\frac{2}{n} \right)^{1/4} \ell(M^n), \frac{A_1(M^n)}{n}, \frac{A_0(M^n)}{\sqrt{2n}} \right) \longrightarrow (\mathcal{R}, \mathcal{A}, \mathcal{B}). \quad (6.8)$$

Here \mathcal{R} and \mathcal{A} are independent random variables, \mathcal{R} follows a Rayleigh law of parameter $\mathcal{L}_{\text{eff}} = (\mathcal{L}_1^{-1} + \mathcal{L}_2^{-1})^{-1}$ and \mathcal{A} has density $q_{\mathcal{L}_1}(a)q_{\mathcal{L}_2}(1-a)/q_{\mathcal{L}_1+\mathcal{L}_2}(1)$ for $a \in (0, 1)$. Finally, the random variable \mathcal{B} has conditional density $q_{\mathcal{R}}$ given $(\mathcal{R}, \mathcal{A})$, and in particular it is independent of \mathcal{A} .

Remark 6.8. Note that this theorem implies in particular that $A_0(M^n)/n \rightarrow 0$ in probability, and so $(A_1(M^n) + A_2(M^n))/n \rightarrow 1$ in probability. One can also be more explicit by computing the Laplace transform of the Rayleigh random variable, which yields

$$\mathbb{E}[e^{-u\mathcal{B}}] = \sqrt{2\pi}(2u\mathcal{L}_{\text{eff}})^{1/4} e^{u\mathcal{L}_{\text{eff}}} \Pi(\sqrt{2u\mathcal{L}_{\text{eff}}}), \quad (6.9)$$

where $\Pi(x) = \int_x^\infty p_1(y)dy$ is the Gaussian tail distribution function.

Theorem 6.9. *Let M^n be a uniformly random quadrangulation with three rooted boundaries of lengths $2L_1^n, 2L_2^n$ and $2L_3^n$ and n inner faces, where the integers $L_i^n, i \in \{1, 2, 3\}$ satisfy $L_i^n \sim \mathcal{L}_i \sqrt{2n}$ as $n \rightarrow \infty$ for some $\mathcal{L}_1, \mathcal{L}_2, \mathcal{L}_3 \in (0, \infty)$. Then we have the following convergence in distribution for the rescaled minimal half-lengths of separating cycles in each homotopy class and for the rescaled exterior/interior areas of M^n :*

$$\left(\left(\frac{2}{n} \right)^{1/4} \ell_i(M^n), \frac{A_i(M^n)}{n} \right)_{i \in \{1, 2, 3\}} \longrightarrow (\mathcal{R}_i, \mathcal{A}_i)_{i \in \{1, 2, 3\}}. \quad (6.10)$$

Here $\mathcal{R}_1, \mathcal{R}_2, \mathcal{R}_3$ are independent random variables, respectively with Rayleigh distribution of parameter $\mathcal{L}_1, \mathcal{L}_2$ and \mathcal{L}_3 , and $(\mathcal{A}_1, \mathcal{A}_2, \mathcal{A}_3)$ is a random vector, independent of $(\mathcal{R}_1, \mathcal{R}_2, \mathcal{R}_3)$, with density

$$\left(\int_0^1 \frac{q_{\mathcal{L}_1+\mathcal{L}_2+\mathcal{L}_3}(x)}{2\sqrt{1-x}} dx \right)^{-1} \frac{q_{\mathcal{L}_1}(a_1)q_{\mathcal{L}_2}(a_2)q_{\mathcal{L}_3}(a_3)}{2\sqrt{1-a_1-a_2-a_3}} \quad (6.11)$$

on the simplex $\{(a_1, a_2, a_3) \in (0, \infty)^3 : a_1 + a_2 + a_3 < 1\}$.

Remark 6.10. That (6.11) is indeed a probability density is an easy exercise using the semigroup property of the stable densities. The reason why we put a constant 2 in the denominator is that it allows to view it as the conditional probability density function of four independent random variables $(\xi_0, \xi_1, \xi_2, \xi_3)$ where ξ_i follows a stable(1/2) law with parameter \mathcal{L}_i for $i \in \{1, 2, 3\}$, and ξ_0 follows a Beta(1,1/2) random variable, given the singular event that $\sum_{i=0}^3 \xi_i = 1$. Note also that the integral of the normalizing constant can be computed from the explicit form of $q_x(a)$, which after a change of variables $y = (1-x)/x$ yields $\int_0^1 q_{\mathcal{L}}(x)dx/\sqrt{1-x} = \exp(-\mathcal{L}^2/2)$.

Remark 6.11. Note that in both statements, we have the remarkable property that the areas of the regions cut by the minimal length curves homotopic to the boundaries are independent of these respective lengths. We also note that in the setting of Theorem 6.9, the quantity $\min(\ell_1(M), \ell_2(M), \ell_3(M))$ is also the length $\ell_{\min}(M)$ of the shortest non contractible cycle in M . An immediate consequence of this observation is that $(2/n)^{1/4} \ell_{\min}(M^n)$ converges in distribution to a random variable with Rayleigh distribution of parameter $\mathcal{L}_{\text{eff}} = (\mathcal{L}_1^{-1} + \mathcal{L}_2^{-1} + \mathcal{L}_3^{-1})^{-1}$. Remarkably, this extends word by word the conclusion of Theorem 6.7, and asks the question whether this further generalizes to maps with four boundaries or more.

Remark 6.12. It is tempting to believe that these two theorems have consequences for Brownian surfaces, that are the scaling limits in the Gromov-Hausdorff sense of (say) random quadrangulations with a fixed topology [Bet16, BM22]. In particular, we expect that for the Brownian annulus ($k = 2$), which is known [Bet16] to be homeomorphic to a two-punctured sphere, there is a unique cycle of minimal length separating the two boundaries, and that this cycle has a Rayleigh distribution with parameter $(\mathcal{L}_1^{-1} + \mathcal{L}_2^{-1})^{-1}$. By letting the size of the second boundary \mathcal{L}_2 go to infinity, we naturally expect to find the *infinite Brownian disk* with boundary length \mathcal{L}_1 introduced in [BMR19], a random metric space homeomorphic to the complement of the open unit disk in the plane. We conjecture that the shortest non-contractible loop in this space has length distributed as a Rayleigh law of parameter \mathcal{L}_1 . This would be relevant in work by Riera [Rie22] on the isoperimetric profile of the Brownian plane, but will be investigated elsewhere.

Let us prove these results. Since we are focusing on the case of quadrangulations, from now on we will restrict the generating function $R = R(t, (g_{2k}, k \geq 1))$ to the special case $g_{2k} = g\delta_{k,2}$, yielding explicitly

$$R = \frac{1 - \sqrt{1 - 12gt}}{6g}. \quad (6.12)$$

This implies the following well-known asymptotic enumeration formulas:

$$[g^n]R|_{t=1} \sim \frac{12^n}{\sqrt{\pi n^3}}, \quad [g^n] \frac{d \ln(R/t)}{dt} \Big|_{t=1} \sim \frac{12^n}{2\sqrt{\pi n}}. \quad (6.13)$$

From now on we will always implicitly assume that the vertex parameter t is set to 1. The coefficients of R and its powers admit some convenient probabilistic representations that we recall quickly here. Let $P_n(k) = 2^{-n} \binom{n}{(n+k)/2}$ be the probability that a simple random walk starting from 0 equals k at time n . It satisfies a local limit theorem (the summation index being due to parity reasons)

$$\sum_{k \in 2\mathbb{Z}+n} |\sqrt{n}P_n(k) - 2p_1(k/\sqrt{n})| \xrightarrow{n \rightarrow \infty} 0. \quad (6.14)$$

Let also $Q_k(n) = (k/n)P_n(k)$ be the probability that the simple random walk first hits $-k$ at time n . Then

$$\sum_{n \in 2\mathbb{N}+k} |k^2 Q_k(n) - 2q_1(n/k^2)| \xrightarrow{k \rightarrow \infty} 0. \quad (6.15)$$

Then (6.12) and Lagrange's inversion formula imply that for every $n, k \geq 0$,

$$[g^n]R^k = 12^n 2^k Q_k(2n + k). \quad (6.16)$$

Proof of Theorem 6.7. The number of annular quadrangulations $\mathcal{Q}(n; L_1^n, L_2^n)$ with boundaries of lengths $2L_1^n, 2L_2^n$ and with n inner quadrangles is given by (6.3): letting $\underline{L}^n = L_1^n + L_2^n$ and $\underline{\mathcal{L}} = \mathcal{L}_1 + \mathcal{L}_2$, this is

$$\#\mathcal{Q}(n; L_1^n, L_2^n) = \frac{\alpha(2L_1^n)\alpha(2L_2^n)}{\underline{L}^n} [g^n]R^{\underline{L}^n} \underset{n \rightarrow \infty}{\sim} \frac{12^n 8^{\underline{L}^n}}{n} \cdot \frac{\sqrt{\underline{\mathcal{L}}_1 \underline{\mathcal{L}}_2}}{\pi \underline{\mathcal{L}}} q_{\underline{\mathcal{L}}}(1), \quad (6.17)$$

where the asymptotic formula is obtained from (6.16) and by applying (6.15) as well as the easy asymptotics $\alpha(2l) \sim 4^l \sqrt{l/\pi}$, also a consequence of (6.14). Now, by the same discussion as that leading to (6.4), the number of quadrangulations $M \in \mathcal{Q}(n; L_1^n, L_2^n)$ that have $\ell(M) = l$, $A_0(M) = n_0$, $A_1(M) = n_1$, hence $A_2(M) = n_2 := n - n_0 - n_1$, is given by

$$[g^{n_1}] \binom{2L_1^n}{L_1^n - l} R^{L_1^n - l} [g^{n_2}] \binom{2L_2^n}{L_2^n - l} R^{L_2^n - l} [g^{n_0}] 2l R^{2l}. \quad (6.18)$$

We rewrite this in ‘‘probabilistic’’ form as

$$12^n 8^{\underline{L}^n} 2l P_{2L_1^n}(-2l) P_{2L_2^n}(-2l) Q_{L_1^n - l}(2n_1 + L_1^n - l) Q_{L_2^n - l}(2n_2 + L_2^n - l) Q_{2l}(2n_0 + 2l). \quad (6.19)$$

Letting now $n_1 = \lfloor na \rfloor$ for some $a \in (0, 1)$, $l = \lfloor (n/2)^{1/4} \lambda \rfloor$ and $n_0 = \lfloor b\sqrt{2n} \rfloor$, for some $\lambda, b > 0$, we can use the local limit theorems to get the following asymptotics:

$$2l P_{2L_1^n}(-2l) P_{2L_2^n}(-2l) \underset{n \rightarrow \infty}{\sim} \frac{\sqrt{\underline{\mathcal{L}}_1 \underline{\mathcal{L}}_2}}{\pi \underline{\mathcal{L}}} \left(\frac{2}{n}\right)^{1/4} r_{\mathcal{L}^{\text{eff}}}(\lambda), \quad (6.20)$$

$$Q_{L_1^n - l}(2n_1 + L_1^n - l) Q_{L_2^n - l}(2n_2 + L_2^n - l) \underset{n \rightarrow \infty}{\sim} \frac{1}{n^2} q_{\mathcal{L}_1}(a) q_{\mathcal{L}_2}(1 - a), \quad (6.21)$$

$$Q_{2l}(2n_0 + 2l) \underset{n \rightarrow \infty}{\sim} \frac{1}{\sqrt{2n}} q_{\lambda}(b). \quad (6.22)$$

Taking a quotient with (6.17), this implies that for l, n_1, n_0 as above,

$$\mathbb{P}(\ell(M^n) = l, A_1(M^n) = n_1, A_0(M^n) = n_0) \underset{n \rightarrow \infty}{\sim} \left(\frac{2}{n}\right)^{1/4} r_{\mathcal{L}^{\text{eff}}}(\lambda) \frac{1}{n} \frac{q_{\mathcal{L}_1}(a) q_{\mathcal{L}_2}(1 - a)}{q_{\underline{\mathcal{L}}}(1)} \frac{1}{\sqrt{2n}} q_{\lambda}(b). \quad (6.23)$$

Since the function of λ, a, b appearing in the right hand side (after removing the factors involving n) is a probability density function on $\mathbb{R}_+ \times (0, 1) \times (0, \infty)$, we easily conclude by Scheffé's lemma. \square

Proof of Theorem 6.9. The number of quadrangulations $\mathcal{Q}(n; L_1^n, L_2^n, L_3^n)$ with three boundaries of perimeters $2L_1^n, 2L_2^n, 2L_3^n$ and with n inner quadrangles is given by the ECF

formula: letting $\underline{L}^n = L_1^n + L_2^n + L_3^n$ and $\underline{\mathcal{L}} = \mathcal{L}_1 + \mathcal{L}_2 + \mathcal{L}_3$, this is

$$\begin{aligned} \#\mathcal{Q}(n; L_1^n, L_2^n, L_3^n) &= \alpha(2L_1^n)\alpha(2L_2^n)\alpha(2L_3^n)[g^n]R^{\underline{L}^n} \frac{d \ln R}{dt} \\ &\underset{n \rightarrow \infty}{\sim} 4^{\underline{L}^n} \frac{\sqrt{L_1^n L_2^n L_3^n}}{\pi^{3/2}} [g^n]R^{\underline{L}^n} \frac{d \ln R}{dt} \end{aligned} \quad (6.24)$$

The coefficient to extract in the right-hand side is given by a convolution of the form

$$\begin{aligned} [g^n]R^k \frac{d \ln R}{dt} &= \sum_{m=0}^n [g^m]R^k [g^{n-m}] \frac{d \ln R}{dt} \\ &= 12^n 2^k \sum_{m=0}^n Q_{\underline{L}^n}(2m+k) [g^{n-m}] \frac{1}{12^{n-m}} \frac{d \ln R}{dt}, \end{aligned} \quad (6.25)$$

where we have used again the probabilistic representation for the coefficients of R^k . For our present purposes we should take $k = \underline{L}^n \sim \underline{\mathcal{L}}\sqrt{2n}$, but later we will also need the asymptotic behaviour of the same quantity, where k is of smaller order $n^{1/4}$. So let us start with this simpler case, assuming that $k = k(n)$ is bounded by $Kn^{1/4}$ for some $K > 0$.

Note that, by the asymptotics (6.13), the coefficients $c_m = [g^m]12^{-m} \frac{d \ln R}{dt}$ involving the logarithmic derivative of R are uniformly bounded by some constant C , and equivalent to $1/2\sqrt{\pi m}$ as $m \rightarrow \infty$. So if we fix $\beta \in (1/2, 1)$, we can rewrite using (6.13) the sum arising in (6.25) as

$$\sum_{m=0}^{n^\beta} Q_k(2m+k) \frac{(1+\epsilon_n)}{2\sqrt{\pi n}} + r_n \quad (6.26)$$

where ϵ_n is a sequence depending only on n and converging to 0, and $r_n \geq 0$ is a remainder term which is bounded by $C \sum_{m > n^\beta} Q_k(2m+k)$. Our choice of β and the fact that $k \leq Kn^{1/4}$ then implies that $r_n \rightarrow 0$. So in this case,

$$[g^n]R^k \frac{d \ln R}{dt} \sim \frac{12^n 2^k}{2\sqrt{\pi n}}. \quad (6.27)$$

Now, for the slightly more delicate case where $k = \underline{L}^n$, we rewrite the sum in (6.25) as

$$\frac{1}{(\underline{L}^n)^2} \left[\sum_{m=0}^n c_{n-m} \left((\underline{L}^n)^2 Q_{\underline{L}^n}(2m + \underline{L}^n) - 2q_1 \left(\frac{2m + \underline{L}^n}{(\underline{L}^n)^2} \right) \right) + 2 \sum_{m=0}^n c_{n-m} q_1 \left(\frac{2m + \underline{L}^n}{(\underline{L}^n)^2} \right) \right]$$

and note that by boundedness of (c_m) and the local limit theorem (6.15), the first sum converges to 0 in absolute value. It remains to deal with the second sum. We introduce some $\beta \in (1/2, 1)$ and split the sum according to whether $m \leq n - n^\beta$ or $n - n^\beta < m \leq n$. In the first case we can use the asymptotics (6.13) and a comparison with an integral to obtain

$$\sum_{m=0}^{n-n^\beta} c_{n-m} q_1 \left(\frac{2m + \underline{L}^n}{(\underline{L}^n)^2} \right) \sim \sqrt{n} \int_0^1 \frac{q_1(a/\underline{\mathcal{L}}^2)}{2\sqrt{\pi(1-a)}} da, \quad (6.28)$$

while the sum over $n - n^\beta < m \leq n$ is clearly $O(n^{-\beta})$ by bounding the coefficients c_{n-m} by C and using the fact that q_1 is bounded near $1/\underline{\mathcal{L}}^2$. Putting things together, we obtain

$$\#\mathcal{Q}(n; L_1^n, L_2^n, L_3^n) \underset{n \rightarrow \infty}{\sim} (8n)^{1/4} \frac{12^n 8^{L^n}}{\pi^2} \sqrt{\mathcal{L}_1 \mathcal{L}_2 \mathcal{L}_3} \int_0^1 \frac{q_{\underline{\mathcal{L}}}(t)}{2\sqrt{1-t}} dt. \quad (6.29)$$

By Propositions 6.5 and 6.6 and Theorem 1.1, the number of quadrangulations $M \in \mathcal{Q}(n; L_1^n, L_2^n, L_3^n)$ such that $\ell_i(M) = l_i$ and $A_i(M) = n_i$ for $i \in \{1, 2, 3\}$ is equal to (letting $n_0 = n - n_1 - n_2 - n_3$)

$$\prod_{i=1}^3 [g^{n_i}] (2l_i) \binom{2L_i^n}{L_i^n - l_i} R^{L_i^n - l_i} \times [g^{n_0}] R^{\underline{l}} \frac{d \ln R}{dt} = \\ 12^n 8^{L^n} \prod_{i=1}^3 (2l_i) P_{2L_i^n}(-2l_i) Q_{L_i^n - l_i}(2n_i + L_i^n - l_i) \times \frac{1}{12^{n_0} 2^{\underline{l}}} [g^{n_0}] R^{\underline{l}} \frac{d \ln R}{dt} \quad (6.30)$$

where $\underline{l} = l_1 + l_2 + l_3$ and where we have used once again the probabilistic representation of the coefficients. Here the first two extracted coefficients count the number of annular quadrangulations with a rooted boundary of perimeter $2L_i^n$, and a strictly tight boundary of length $2l_i$, and the last one counts the number of (quadrangulated) pairs of pants with tight boundaries of perimeters $2l_i$, $i \in \{1, 2, 3\}$. Proposition 6.5 states that the boundaries of these pairs of pants should be marked, and we have absorbed the corresponding factors $2l_i$ in the product before. We let $l_i = \lfloor (n/2)^{1/4} \lambda_i \rfloor$ and $n_i = \lfloor na_i \rfloor$ for some $\lambda_i > 0$ and $a_i > 0$, $i \in \{1, 2, 3\}$, such that $a_0 = 1 - (a_1 + a_2 + a_3) > 0$. Then, the local limit theorems give the asymptotics

$$2l_i P_{2L_i^n}(-2l_i) \xrightarrow{n \rightarrow \infty} \sqrt{\frac{2\mathcal{L}_i}{\pi}} r_{\mathcal{L}_i}(\lambda_i), \quad (6.31)$$

$$Q_{L_i^n - l_i}(2n_i + L_i^n - l_i) \underset{n \rightarrow \infty}{\sim} \frac{1}{n} q_{\mathcal{L}_i}(a_i). \quad (6.32)$$

Together with (6.27), this implies by taking a quotient with (6.17) that for l_i, n_i as above,

$$\mathbb{P}(\ell_i(M^n) = l_i, A_i(M^n) = n_i, i \in \{1, 2, 3\}) \underset{n \rightarrow \infty}{\sim} \\ \prod_{i=1}^3 \left(\frac{2}{n}\right)^{1/4} r_{\mathcal{L}_i}(\lambda_i) \times \frac{1}{n^3} \left(\int_0^1 \frac{q_{\underline{\mathcal{L}}}(a)}{2\sqrt{1-a}} da\right)^{-1} \frac{q_{\mathcal{L}_1}(a_1) q_{\mathcal{L}_2}(a_2) q_{\mathcal{L}_3}(a_3)}{2\sqrt{1-a_1-a_2-a_3}}. \quad (6.33)$$

Since the function of λ_i, a_i appearing in the right hand side (after removing the factors involving n) is a probability density function on $(\mathbb{R}_+)^3 \times \{(a_1, a_2, a_3) \in (0, \infty)^3 : a_1 + a_2 + a_3 < 1\}$, we conclude by Scheffé's lemma. \square

7. Conclusion

In this work, we have enumerated bijectively essentially bipartite planar maps with three tight boundaries, relying on a geometric decomposition of these objects in terms of elementary pieces with certain geodesic boundaries.

Let us mention a number of natural extensions of the present work that we plan on studying in the future. The most natural extension consists in considering maps with more than three boundaries and/or higher genus. We first remark that the discussion of Section 6.1, hence Proposition 6.5, extend easily to arbitrary topologies: a map M of genus g having n boundary-faces which are not necessarily tight can be decomposed bijectively into a tuple $(M^{(0)}, M^{(1)}, \dots, M^{(n)})$, where $M^{(0)}$ is a map of genus g with n tight boundary-faces, and where $M^{(1)}, \dots, M^{(n)}$ are “funnels”, namely annular maps with one strictly tight boundary-face, as defined in Section 6.2. This decomposition is closely related to the Joukowski transform considered in [Eyn16, Section 3.1.3.1]. Using enumerative results coming from topological recursion, we can show that the generating function of essentially bipartite maps of genus g with n tight boundary-faces of prescribed lengths $2\ell_1, \dots, 2\ell_n$ is a quasi-polynomial generalizing the lattice count polynomial of [Nor10] (which we recover when setting the weights for inner faces to zero). This will be discussed in a forthcoming paper.

Furthermore, it would be interesting to address the problem of the enumeration of maps of genus g with n tight boundaries by a bijective approach. One might think at first that our decomposition into bigeodesic triangles and diangles could easily be extended without fundamental changes beyond the case $(g, n) = (0, 3)$ considered in the present paper. A closer look however shows that a number of new technical questions arise in the general case: for instance, controlling the exceedances of the diangles is not as simple as for pairs of pants where these exceedances are entirely fixed by the boundary lengths. More important, making sure that the bigeodesics used in the decomposition do not cross, and therefore lead to independent building blocks, is more challenging for more boundaries or higher genus.

Still, we hope that the tight pairs of pants introduced in this work, or small variations thereof, will serve as new elementary pieces intervening in the decomposition of such maps with higher topological complexity. Indeed, pants decompositions are the canonical way to describe all Riemann surfaces, by cutting them along separating cycles. In the context of maps, in order to get a canonical decomposition, one needs to specify along which cycles we cut. In this respect, minimal separating cycles are the natural candidates, but we must specify which of these minimal cycles we choose among certain ordered sets \mathcal{C} of such cycles. In Section 6.1, we explained why the choice of “outermost” elements in the ordered set \mathcal{C} was crucial to avoid possible crossings of the various cutting cycles. If we now wish to split a map into two components, the ordering of the set \mathcal{C} of separating cycles is reversed when viewed from both components and choosing its outermost element from both sides therefore produces some overlap between the components, hence a decomposition into non independent elements. To avoid such overlap, we must instead choose innermost elements from both sides (so that the overlapping region now becomes an independent building block), or at least from one side. We then face again the problem that, if we choose only innermost elements, different cycles around a pair of pants may cross each other. A probable solution is to consider a mixed prescription, with both outermost and innermost elements, which would involve as building blocks pairs of pants with, say, one strictly tight boundary and two tight ones. The question of their enumeration is therefore an issue that we hope to better understand in the future.

As we noticed above, Theorems 6.7 and 6.9 imply that minimal separating cycles in random maps with the topology of the annulus or of the pair of pants admit Rayleigh statistics in the scaling limit, with a parameter that depends in a similar and simple way on the boundary lengths. One can naturally wonder whether these statistics also arise for more boundaries or in higher genera. However, for four boundaries or more, the minimal separating cycles are not necessarily separating only one boundary from all the others, and it is likely that more complicated statistics would arise.

Another direction of study would be to control distances between the boundaries. This program was achieved in the case of three boundary-vertices in [BG08] for planar quadrangulations and in [FG14] for general planar maps. As discussed in Appendix B, the results of [BG08] provide an explicit expression for the generating function $X_{s,t}$ (respectively $Y_{s,t,u}$) of balanced bigeodesic diangles (respectively bigeodesic triangles) with all inner faces of degree 4 and with, say red intervals of lengths $s' \leq s$ and $t' \leq t$ (respectively of lengths $s' \leq s$, $t' \leq t$ and $u' \leq u$). Together with the generating function R_s for elementary slices with (red) right boundary of length $s' < s - 1$ ($s \geq 1$), known since the very introduction of slices in [BG12], it seems that we have all the ingredients (at least for quadrangulations) for a proper refined enumeration of pairs of pants with a control on the (properly defined) geodesic distances between their boundary-faces or boundary-vertices. Indeed, the lengths s, t, u above, characterizing the various building blocks, eventually fix the desired distances.

A final framework where our method is likely to apply is that of planar irreducible maps or maps with girth constraints, for which an interesting connection with Weil-Petersson volumes was recently pointed out by Budd [Bud22a, Bud22b]. Recall that the *girth* is the length of the shortest cycle in the map and that a map is *d-irreducible* if its girth is at least d and any cycle of length d is the contour of an inner face. In [BG14], a slice decomposition was devised to enumerate such families of maps with one or two boundaries. We expect that this decomposition may be extended to three boundaries along lines similar to those of the present paper.

A. A slice-theoretic enumeration of triply pointed maps

Recursion relation for R . Call R the generating function of elementary slices (i.e. tight slices of width 1). Let us show that R satisfies the recursion relation (1.2), which determines it uniquely as a formal power series in t and in the g_{2k} 's. We use the notations of Figure 2.1 for tight slices, specialized to the case where the interval $[c', c'']$ reduces to a single oriented “base edge” e . Assuming that the slice is not reduced to e , we may consider its base face f incident to e on its left, and look at the (clockwise) contour path of f from v' (incident to c') to v'' (incident to c''): this path has length $2k - 1$ if f has degree $2k$. Calling v the apex of the slice (vertex incident to c), we may record the relative distances $\ell_i = d(v', v) - d(v_i, v)$ for the successively visited vertices v_i , $i = 0, \dots, 2k - 1$, along the contour path from $v_0 = v'$ to $v_{2k-1} = v''$. The sequence $((i, \ell_i))_{0 \leq i \leq 2k-1}$ defines a directed path \mathcal{P} of length $2k - 1$ in \mathbb{Z}^2 from $(0, \ell_0) = (0, 0)$ to $(2k - 1, \ell_{2k-1}) = (2k - 1, 1)$, with k ascending steps with $\ell_i - \ell_{i-1} = +1$ and $k - 1$ descending steps with $\ell_i - \ell_{i-1} = -1$. Let

us now, for each visited vertex v_i , cut the slice along the leftmost geodesic \mathcal{G}_i from v_i to v . This results into a decomposition of the slice into k components which are elementary slices, in correspondence with the k ascending steps of \mathcal{P} . More precisely, to each step with $\ell_i - \ell_{i-1} = +1$ is associated an elementary slice delimited by \mathcal{G}_{i-1} and \mathcal{G}_i , whose base edge connects v_{i-1} (at distance $d(v, v') - \ell_{i-1}$ from v) to v_i (at distance $d(v, v') - \ell_{i-1} - 1$ from v) and whose apex is the first meeting point of \mathcal{G}_{i-1} and \mathcal{G}_i towards v . As for a step with $\ell_i - \ell_{i-1} = -1$, it does not give rise to any component in the decomposition since \mathcal{G}_i starts by following (counterclockwise) the contour of f from v_i (at distance $d(v, v') - \ell_i$ from v) to v_{i-1} (at distance $d(v, v') - \ell_i - 1$ from v) and then merges with \mathcal{G}_{i-1} , so that no faces lie in-between \mathcal{G}_{i-1} and \mathcal{G}_i .

Starting conversely from the directed path \mathcal{P} above, viewed as a sequence of edges all colored in red, and from the k elementary slice components S_1, \dots, S_k , we may recover the original slice by: (i) gluing the (blue) base edge of S_j to (and above) the (red) edge associated with the j -th ascending step of \mathcal{P} , then (ii) gluing each blue boundary edge of a slice S_j to the the first available red edge, if any, facing it on its left (this edge may belong to the red boundary of a preceding slice component or be associated with a descending step of \mathcal{P}) and finally (iii) closing \mathcal{P} by adding an extra base edge e so as to form the base face f of degree $2k$.

Once translated in the language of generating functions, the above bijective decomposition yields the relation (1.2), where the first term t accounts for the elementary slice reduced to a single edge and the k -th term in the sum accounts for elementary slices with a base face of degree $2k$, with g_{2k} the weight of this face, the factor $\binom{2k-1}{k}$ the number of possible oriented paths \mathcal{P} of length $2k - 1$ with k ascending steps, and the factor R^k the generating function for the k elementary slice components.

Proof of the relation $T_{0,0,0} = d \ln(R/t)/dt$. Take an elementary slice not reduced to a single edge. Upon gluing its two intervals $[c, c']$ and $[c', c]$ (see again Figure 2.1 for the notations), we get a bipartite planar map with both a marked oriented edge e (corresponding to the interval $[c', c'']$ of length 1 oriented from c' to c'') and a marked vertex v (corresponding to the vertex incident to c) which is closer to the endpoint than to the origin of e . Conversely, starting from a bipartite planar map with a marked oriented edge e and a marked vertex v closer to the endpoint than to the origin of e , the elementary slice leading to this marked map by the above gluing is easily recovered by cutting the map along the leftmost geodesic towards v starting with e . In the generating function $R - t$ of elementary slices not reduced to a single edge, the vertex incident to c' receives a weight t while that incident to c receives no weight. We immediately deduce that $(R - t)/t$ is the generating function of planar bipartite maps with a marked oriented edge e and a marked vertex v closer to the endpoint than to the origin of e , where neither v nor the origin v' of e (necessarily distinct from v) receive the weight t . Alternatively, by first choosing v' then e , $(R - t)/t$ is the generating function of planar bipartite maps with two distinct marked vertices v and v' (which receive no weight t) and a marked edge e incident to v' and whose other extremity is at distance $d(v', v) - 1$ from v . If we now wish to compute instead the generating function B of doubly pointed maps, without the

marked edge e , we may proceed as follows: consider, for a map with two marked distinct vertices v and v' the (non-empty) counterclockwise sequence of edges from v' to a vertex at distance $d(v', v) - 1$ from v , and cut the map along the leftmost geodesics towards v starting with these successive edges. This results in a non-empty cyclic sequence of a particular type of elementary slices, all not reduced to a single edge, which are such that all the non-boundary edges incident to the vertex v' incident to the corner c' lead to vertices at a distance larger than $d(v', v)$ from v , the vertex incident to c . Call N the generating function of these particular elementary slices (with the same weighting convention as for regular tight slices). We deduce the relation $B = -\ln(1 - N/t)$ (note that in B , maps are counted with symmetry factors: a planar map with two marked distinct vertices may have a k -fold symmetry by “rotating” around the axis of the two marked vertices. It then receives the weight $1/k$). As for the maps counted by $(R - t)/t$, the additional marked edge e provides an origin for the cyclic sequence so that the above cutting now results in a non-empty linear sequence of the same particular tight slices. We now deduce the relation $(R - t)/t = N/t/(1 - N/t)$, from which we eventually get $B = \ln(R/t)$. Since in B the two marked vertices have no weight, taking a derivative with respect to t in B amounts to the marking of a third vertex on the map, distinct from the already marked ones. We deduce that $T_{0,0,0} = dB/dt = d\ln(R/t)/dt = d\ln R/dt - t^{-1}$.

B. Connection with well-labeled maps

We discuss here the connection between our decomposition into bigeodesic diangles and triangles and another decomposition introduced in [BG08] to characterize the three-point function of planar maps. We restrict our discussion to the case of quadrangulations, i.e. maps whose all inner faces have degree 4, and to the case where the three boundaries are boundary-vertices. As first noted in [Mie09], such triply pointed planar quadrangulations may be bijectively encoded by so-called planar *well-labeled maps*, which are maps whose vertices carry integer labels with the constraint that

- the difference of labels between any two neighboring vertices is 0 or ± 1 .

For convenience, the corners of a well-labeled map receive the label of their incident vertex.

More precisely, as shown in [Mie09], and in [BG08] in the specific case that we consider here, one may establish a one-to-one correspondence between planar quadrangulations with three distinct vertices v_A , v_B and v_C and planar well-labeled maps with (generically) three faces f_A , f_B and f_C satisfying the additional constraint that

- C1. the frontier between any two faces of the map (i.e. the set of vertices and edges incident to both faces) is non-empty and the minimum label on this frontier is 0.

In the non-generic case where one of the three boundary-vertices is a geodesic vertex between the other two, one of the faces in the well-labeled map degenerates into a single vertex, and some of the arguments presented below must be adapted.

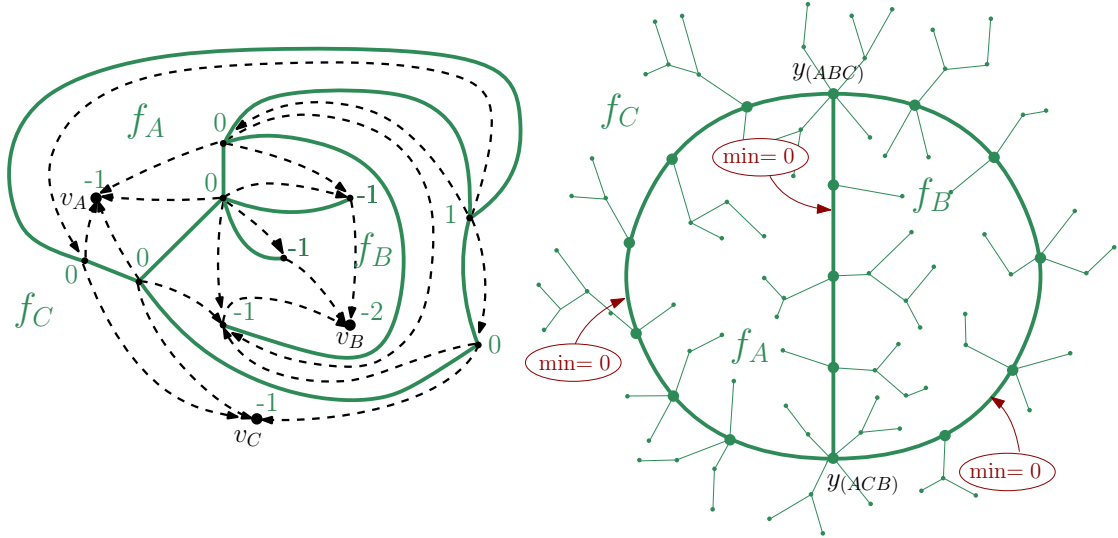


Figure B.1: Left: The construction of a quadrangulation with three boundary-vertices v_A , v_B and v_C from a well-labeled map with three faces f_A , f_B and f_C , as obtained by connecting each corner to its successor. Here $r_B = 2$ and $r_A = r_C = 1$. Right: Schematic picture of a 3-face well-labeled map satisfying C1. Its skeleton is indicated by thick edges. Each frontier between two given faces carries minimal label 0.

Given a planar well-labeled map with three faces satisfying C1, the associated triply pointed quadrangulation is easily recovered as follows: calling $1 - r_i$ the minimum label among vertices incident to the face f_i ($i \in \{A, B, C\}$), we add a new vertex v_i with label $-r_i$ in this face. Within each face, we then connect each corner with label ℓ to its *successor*, which is the first encountered corner with label $\ell - 1$ when going counterclockwise around the face (i.e. with the face on the left). See the left of Figure B.1 for an example. We finally remove the labels as well as the original edges of the well-labeled map. In particular, the vertices of the quadrangulation are identified with those of the well-labeled map, plus the three added vertices v_A , v_B and v_C .

An important property relating the well-labeled map to its associated quadrangulation is the following:

- Any vertex v incident to f_i ($i \in \{A, B, C\}$) with label $\ell(v)$ is at a distance $r_i + \ell(v)$ from v_i in the quadrangulation (the property extends trivially to v_i itself since $\ell(v_i) = -r_i$).

From this property, it is then easily shown that those vertices of the frontier between f_i and f_j which carry the (minimal) label 0 are precisely the geodesic vertices between v_i and v_j (for $i \neq j \in \{A, B, C\}$) at distance r_i from v_i and r_j from v_j .

The generic topology of a planar well-labeled map with three faces satisfying C1 is shown on the right of Figure B.1. Its *skeleton*, obtained by iteratively removing all the

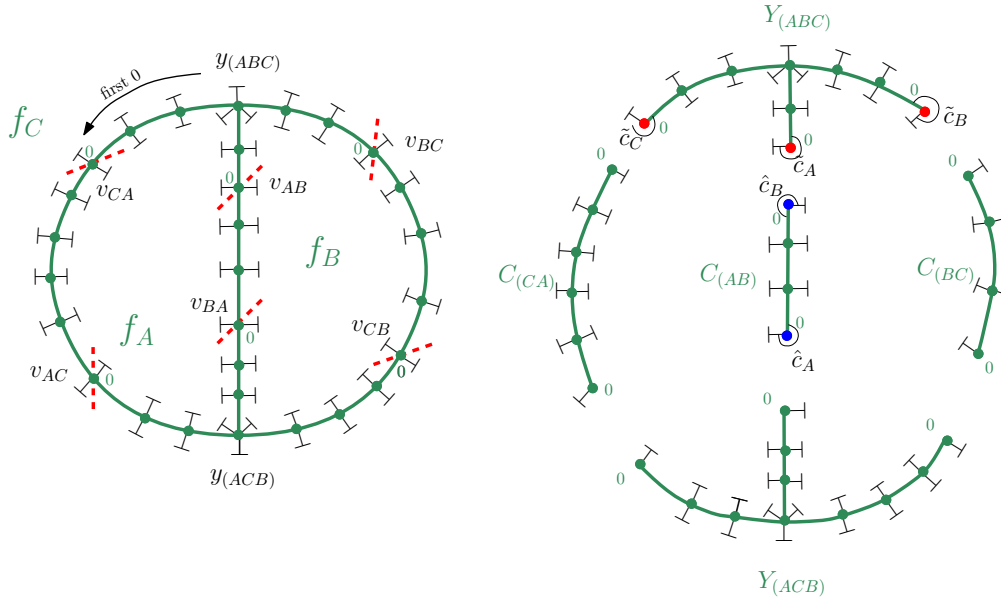


Figure B.2: Schematic picture of the decomposition of a well-labeled map with three faces satisfying C1 into five well-labeled components, two Y-diagrams and three chains, by cutting each branch of the skeleton at their extremal vertices labeled 0 as shown by dashed red lines. The \perp signs indicate attached well-labeled subtrees. The cutting singles out two corners \hat{c}_A and \hat{c}_B on the chain $C_{(AB)}$. Similarly, three corners $\tilde{c}_A, \tilde{c}_B, \tilde{c}_C$ are singled out on the Y-diagram $Y_{(ABC)}$.

leaves of the map so that all remaining vertices have degree at most 2, has exactly two 3-valent vertices $y_{(ABC)}$ and $y_{(BAC)}$ and three linear branches between them made of 2-valent vertices, each branch corresponding to a frontier between two faces. From C1, each of the three branches carries a minimal label 0. The full well-labeled map is made of this skeleton and a number of attached well-labeled subtrees.

We may now perform a canonical decomposition of the map as in [BG08, Section 4.3]. Namely, consider the branch at the frontier between, say f_A and f_B and call v_{AB} (respectively v_{BA}) the vertex with label 0 closest to $y_{(ABC)}$ (respectively closest to $y_{(ACB)}$). We define v_{BC}, v_{CB} and v_{CA}, v_{AC} by cyclic permutation. Clearly, from the above discussion, v_{AB} and v_{BA} are the extremal elements of S_{AB} in the sense of Figure 3.4. We may then cut the map at all the v_{ij} vertices, resulting in five well-labeled tree components: the first two components, containing one of the vertices $y_{(ABC)}$ or $y_{(BAC)}$, will be referred to as *Y-diagrams* and called $Y_{(ABC)}$ and $Y_{(BAC)}$ accordingly. The last three components, lying in-between v_{ij} and v_{ji} for some $i \neq j \in \{A, B, C\}$, will be called *chains* and denoted $C_{(ij)}$. In the cutting process, we must specify to which component we attach the subtrees incident to the cutting vertices v_{ij} . We use the convention shown on the left of Figure B.2. This is dictated by the fact that we wish to retain in, say the chain $C_{(AB)}$

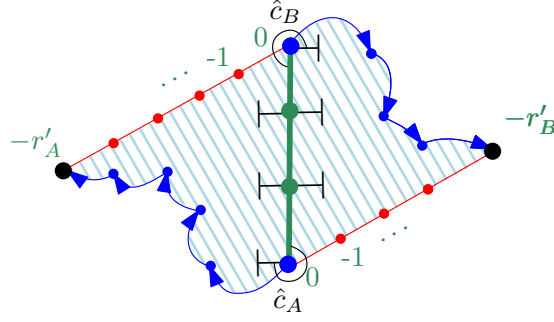


Figure B.3: Schematic picture of the balanced bigeodesic diangle encoded by the well-labeled chain $C_{(AB)}$ (see text). Its attachment points are the big blue dots.

the subtree incident to v_{BA} which follows clockwise the leftmost corner incident to v_{BA} in the face f_A of the original well-labeled map, as this subtree may carry the successor of this corner. This choice of cutting singles out de facto two corners at the extremities of the chain $C_{(AB)}$: a corner \hat{c}_A at v_{BA} and a corner \hat{c}_B at v_{AB} , see the right of Figure B.2. Note that we may identify those vertices of the chain originally in f_A (respectively f_B) as the vertices lying in-between \hat{c}_A and \hat{c}_B (respectively in-between \hat{c}_B and \hat{c}_A) when going clockwise around the chain. Similarly, the cutting process marks three corners $\tilde{c}_A, \tilde{c}_B, \tilde{c}_C$ preceding the retained subtrees at the end of the branches of Y-diagram $Y_{(ABC)}$, see the right of Figure B.2. By construction, the well-labeled chains have nonnegative labels on the unique path linking their extremal corners, the latter having label zero, while for Y-diagrams, all labels along the paths linking the three extremal corners are strictly positive, except for the corners themselves, which have label zero.

We now claim that the two Y-diagrams and the three chains resulting from the decomposition of the well-labeled map precisely encode the two bigeodesic triangles and the three bigeodesic diangles resulting from our decomposition of the associated triply pointed quadrangulation. To see this, consider for instance the well-labeled chain $C_{(AB)}$. We may associate to this chain a balanced bigeodesic diangle with attachment points v_{AB} and v_{BA} as follows: calling $1 - r'_A$ (respectively $1 - r'_B$) the minimal label of the chain between \hat{c}_A and \hat{c}_B (respectively between \hat{c}_B and \hat{c}_A) when going clockwise around the chain (with $r'_A \leq r_A$ and $r'_B \leq r_B$), we attach to \hat{c}_B a new branch, called the A -branch, made of r'_A vertices with labels decreasing from -1 to $-r'_A$ and to \hat{c}_A a new branch, the B -branch, made of r'_B vertices with labels decreasing from -1 to $-r'_B$. These branches are represented as red lines in Figure B.3. Each corner of the chain, except those incident to the new vertices of the two added red branches, is then connected to its successor, possibly lying on the newly added red branch (note that going counterclockwise around the external face corresponds to going clockwise around the chain). The resulting object is a map with one boundary-face and four boundary intervals, alternating between blue (geodesic) intervals, corresponding to the sequence of successors of \hat{c}_A and that of \hat{c}_B , and red (strictly geodesic) intervals, corresponding to the A - and the B -branch. This is nothing but a bigeodesic diangle with attachment points v_{AB} and v_{BA} , which is more-

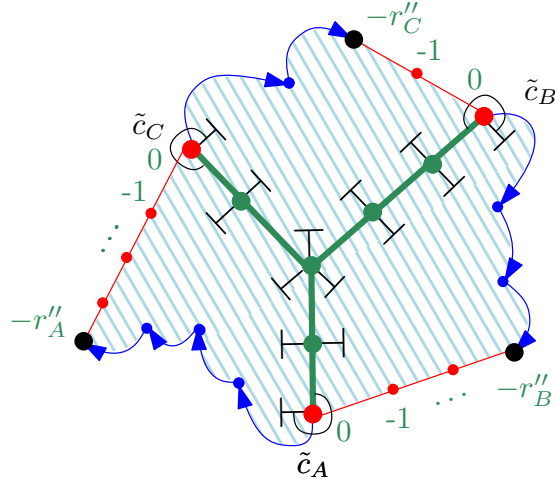


Figure B.4: Schematic picture of the bigeodesic triangle encoded by the well-labeled Y-diagram $Y_{(ABC)}$ (see text). Its attachment points are the big red dots.

over balanced, with a blue and a red interval of the same length r'_A and the other two of the same length r'_B . We can repeat the process to build balanced bigeodesic diangles from the chains $C_{(BC)}$ and $C_{(CA)}$. As for the well-labeled Y-diagrams, say for instance $Y_{(ABC)}$: calling $1 - r''_A$ the minimal label between \tilde{c}_A and \tilde{c}_C , we attach a new red A -branch of length r''_A to the corner \tilde{c}_C . We do the same by cyclic permutations of the letters A, B, C . This gives rise to the red lines in Figure B.4. Finally, we connect as before each corner not along the added red branches to its successor (possibly lying on the newly added red branches). This clearly creates a bigeodesic triangle: the fact that the attachment points of this triangles are “red” points in our terminology is due to the fact that we chose the extremal 0 labels on each frontier so that any geodesic between v_i and v_j ($i \neq j \in \{A, B, C\}$) within the triangle, which must cross a vertex with label 0, has to pass via the appropriate attachment vertex. The other triangle is obtained similarly from $Y_{(ACB)}$.

We now claim that gluing the three bigeodesic diangles and two bigeodesic triangles associated to the three well-labeled chains and the two well-labeled Y-diagrams according to our procedure I clearly reproduces the quadrangulation associated with the well-labeled map at hand before its decomposition. This simply results from the fact that the sequences of successors within the full well-labeled map after gluing match precisely with the sequences of successors within each of its five well-labeled components after identification of the glued blue and red intervals, see Figure B.5. The paths along which the bigeodesic diangles and triangles are glued induce paths in the resulting quadrangulation, that correspond precisely to leftmost geodesics launched from the cutting points v_{ij} ($i \neq j \in \{A, B, C\}$) towards the vertices v_i at the extremity of the added red i -branches of the various well-labeled components which have the smallest label, necessarily equal to $-r_i$.

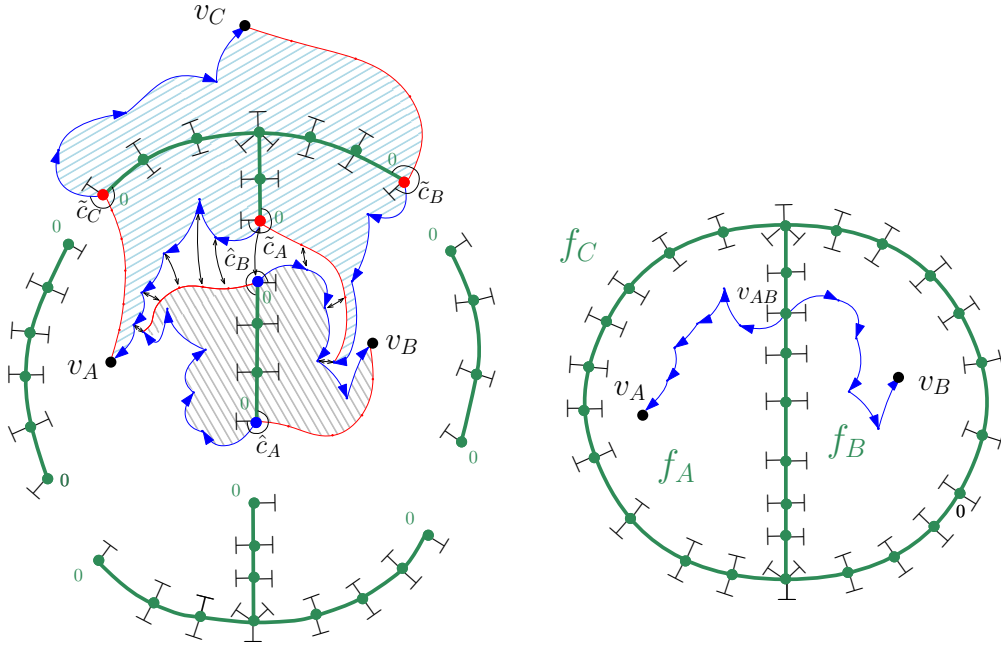


Figure B.5: The gluing of the bigeodesic triangle encoded by the Y-diagram Y_{ABC} and the bigeodesic diangle encoded by the chain $C_{(AB)}$ occurs along leftmost geodesics launched from v_{AB} in the original quadrangulation and correspond to sequences of successors both in the well-labeled components (left) and in the well-labeled map (right).

To conclude, we have a bijective correspondence between (i) balanced bigeodesic diangles and well-labeled chains, and (ii) bigeodesic triangles and well-labeled Y-diagrams. With this correspondence, our decomposition of planar quadrangulations with three boundary-vertices matches precisely that of [BG08] for the associated well-labeled maps with three faces.

As a direct enumerative consequence, we identify X and Y as the generating functions of properly weighted well-labeled chains and Y-diagrams. More precisely, if we let t and $g = g_4$ be the inner vertex and face weights in the triply pointed quadrangulation, each vertex of a well-labeled chain or Y-diagram receives the weight t and each edge the weight g . To include the possible degenerate cases (for instance the case of well-labeled maps with two faces obtained whenever one of the boundary-vertices is geodesic between the other two), the vertex map, with label 0, must be considered as a well-labeled Y-diagram as well as a well-labeled chain. Viewed as well-labeled object generating functions, X and Y are easily obtained as the power series in t solutions (see [BG08] for a detailed derivation) of

$$R = t + 3gR^2, \quad X = t + \frac{1}{t}gR^2X \left(1 + \frac{1}{t^2}gR^2X\right) \quad Y = t + \frac{1}{t^6}g^3R^6X^3Y, \quad (\text{B.1})$$

where R is the generating function of well-labeled planted trees with root label 0. Note

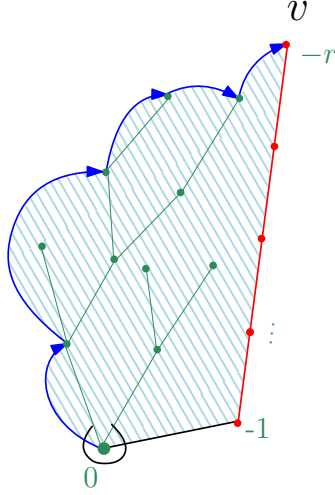


Figure B.6: The elementary slice encoded by a well-labeled planted tree with root label 0 (see text).

that R matches our definition (1.2) for $g_{2k} = g \delta_{k,2}$, i.e. is also the generating function of elementary slices with 4-valent inner faces only. That well-labeled planted trees encode elementary slices is obtained along the same lines as before: calling $1 - r$ the smallest label in the tree, we attach to the root-corner a branch of length r with vertices having decreasing labels $-1, \dots, -r$ as in Figure B.6. Connecting each corner not incident to one of the new added vertices to its successor creates a map with a single boundary face, with 4-valent inner faces, having a blue (geodesic) interval from the extremity v of the added branch to the root vertex counterclockwise around the map, and a geodesic interval from the root vertex to v , whose portion which goes from the new added vertex with label -1 to v is strictly geodesic (hence represented in red). This is precisely an elementary slice.

A simple parametrization of X and Y is obtained by introducing the power series x solution of

$$x = \frac{gR^2}{t} (1 + x + x^2) \quad (\text{B.2})$$

as it allows to write

$$X = t \frac{1 - x^3}{1 - x}, \quad Y = \frac{t}{1 - x^3}. \quad (\text{B.3})$$

References

- [AB12] M. Albenque and J. Bouttier. Constellations and multicontinued fractions: application to Eulerian triangulations. In *24th International Conference on Formal Power Series and Algebraic Combinatorics (FPSAC 2012)*, Discrete Math. Theor. Comput. Sci. Proc., AR, pages 805–816. Assoc. Discrete Math. Theor. Comput. Sci., Nancy, 2012, arXiv:1112.6379 [math.CO].
- [AB13] J. Ambjørn and T. G. Budd. Trees and spatial topology change in causal dynamical triangulations. *J. Phys. A*, 46(31):315201, 33, 2013, arXiv:1302.1763 [hep-th].
- [ADJ97] J. Ambjørn, B. Durhuus, and T. Jonsson. *Quantum geometry: a statistical field theory approach*. Cambridge Monographs on Mathematical Physics. Cambridge University Press, Cambridge, 1997.
- [AJM90] J. Ambjørn, J. Jurkiewicz, and Y. M. Makeenko. Multiloop correlators for two-dimensional quantum gravity. *Phys. Lett. B*, 251(4):517–524, 1990.
- [BBI01] D. Burago, Y. Burago, and S. Ivanov. *A course in metric geometry*, volume 33 of *Graduate Studies in Mathematics*. American Mathematical Society, Providence, RI, 2001.
- [BDFG04] J. Bouttier, P. Di Francesco, and E. Guitter. Planar maps as labeled mobiles. *Electron. J. Combin.*, 11(1):R69, 2004, arXiv:math/0405099 [math.CO].
- [Bet16] J. Bettinelli. Geodesics in Brownian surfaces (Brownian maps). *Ann. Inst. Henri Poincaré Probab. Stat.*, 52(2):612–646, 2016, arXiv:1401.3602 [math.PR].
- [BF12] O. Bernardi and E. Fusy. Unified bijections for maps with prescribed degrees and girth. *J. Combin. Theory Ser. A*, 119(6):1351–1387, 2012, arXiv:1102.3619 [math.CO].
- [BFG14] J. Bouttier, É. Fusy, and E. Guitter. On the two-point function of general planar maps and hypermaps. *Ann. Inst. Henri Poincaré D*, 1(3):265–306, 2014, arXiv:1312.0502 [math.CO].
- [BG08] J. Bouttier and E. Guitter. The three-point function of planar quadrangulations. *J. Stat. Mech. Theory Exp.*, (7):P07020, 39, 2008, arXiv:0805.2355 [math-ph].
- [BG09a] J. Bouttier and E. Guitter. Confluence of geodesic paths and separating loops in large planar quadrangulations. *J. Stat. Mech. Theory Exp.*, (3):P03001, 44, 2009, arXiv:0811.0509 [math-ph].
- [BG09b] J. Bouttier and E. Guitter. Distance statistics in quadrangulations with a boundary, or with a self-avoiding loop. *J. Phys. A*, 42(46):465208, 2009, arXiv:0906.4892 [math-ph].

- [BG12] J. Bouttier and E. Guitter. Planar maps and continued fractions. *Comm. Math. Phys.*, 309(3):623–662, 2012, arXiv:1007.0419 [math.CO].
- [BG14] J. Bouttier and E. Guitter. On irreducible maps and slices. *Combin. Probab. Comput.*, 23(6):914–972, 2014, arXiv:1303.3728 [math.CO].
- [BM17] J. Bettinelli and G. Miermont. Compact Brownian surfaces I: Brownian disks. *Probab. Theory Related Fields*, 167(3-4):555–614, 2017, arXiv:1507.08776 [math.PR].
- [BM22] J. Bettinelli and G. Miermont. Compact Brownian surfaces II: Orientable surfaces, 2022+. In preparation.
- [BMR19] E. Baur, G. Miermont, and G. Ray. Classification of scaling limits of uniform quadrangulations with a boundary. *Ann. Probab.*, 47(6):3397–3477, 2019, arXiv:1608.01129 [math.PR].
- [Bou19] J. Bouttier. Planar maps and random partitions. Habilitation à diriger des recherches, Université Paris-Sud, 2019, arXiv:1912.06855 [math-ph].
- [Bud17] T. Budd. Peeling of random planar maps. Lecture notes for a mini-course given at the Mini-school on Random Maps and the Gaussian Free Field, ENS de Lyon, 2017. <https://hef.ru.nl/~tbudd/docs/mappeeling.pdf>.
- [Bud22a] T. Budd. Irreducible metric maps and Weil-Petersson volumes. *Communications in Mathematical Physics*, 394(2):887–917, 2022, arXiv:2012.11318 [math-ph].
- [Bud22b] T. Budd. On polynomials counting essentially irreducible maps. *Electron. J. Combin.*, 29(2):P2.45, 2022, arXiv:2006.15701 [math.CO].
- [CdVE10] E. Colin de Verdière and J. Erickson. Tightening nonsimple paths and cycles on surfaces. *SIAM J. Comput.*, 39(8):3784–3813, 2010.
- [CdVL07] E. Colin de Verdière and F. Lazarus. Optimal pants decompositions and shortest homotopic cycles on an orientable surface. *J. ACM*, 54(4):Art. 18, 27, 2007.
- [CF12] G. Collet and E. Fusy. A simple formula for the series of bipartite and quasi-bipartite maps with boundaries. In *24th International Conference on Formal Power Series and Algebraic Combinatorics (FPSAC 2012)*, Discrete Math. Theor. Comput. Sci. Proc., AR, pages 607–618. Assoc. Discrete Math. Theor. Comput. Sci., Nancy, 2012, arXiv:1205.5215 [math.CO].
- [Cur19] N. Curien. Peeling random planar maps. Lecture notes for the Saint-Flour Probability Summer School, 2019. <https://www.math.u-psud.fr/~curien/enseignement.html>.

- [DFGZJ95] P. Di Francesco, P. Ginsparg, and J. Zinn-Justin. 2D gravity and random matrices. *Phys. Rep.*, 254(1-2):133, 1995, arXiv:hep-th/9306153.
- [Eyn16] B. Eynard. *Counting surfaces*, volume 70 of *Progress in Mathematical Physics*. Birkhäuser/Springer, [Cham], 2016. CRM Aisenstadt chair lectures.
- [FG14] E. Fusy and E. Guitter. The three-point function of general planar maps. *J. Stat. Mech. Theory Exp.*, (9):p09012, 39, 2014, arXiv:1403.3514 [math.CO].
- [IT92] Y. Imayoshi and M. Taniguchi. *An introduction to Teichmüller spaces*. Springer-Verlag, Tokyo, 1992. Translated and revised from the Japanese by the authors.
- [LG13] J.-F. Le Gall. Uniqueness and universality of the Brownian map. *Ann. Probab.*, 41(4):2880–2960, 2013, arXiv:1105.4842 [math.PR].
- [LGM12] J.-F. Le Gall and G. Miermont. Scaling limits of random trees and planar maps. In *Probability and statistical physics in two and more dimensions*, volume 15 of *Clay Math. Proc.*, pages 155–211. Amer. Math. Soc., Providence, RI, 2012, arXiv:1101.4856 [math.PR].
- [Mie09] G. Miermont. Tessellations of random maps of arbitrary genus. *Ann. Sci. Éc. Norm. Supér. (4)*, 42(5):725–781, 2009, arXiv:0712.3688 [math.PR].
- [Mie14] G. Miermont. Aspects of random maps. Lecture notes for the Saint-Flour Probability Summer School, 2014. <http://perso.ens-lyon.fr/gregory.miermont/coursSaint-Flour.pdf>.
- [Mil18] J. Miller. Liouville quantum gravity as a metric space and a scaling limit. In *Proceedings of the International Congress of Mathematicians—Rio de Janeiro 2018. Vol. IV. Invited lectures*, pages 2945–2971. World Sci. Publ., Hackensack, NJ, 2018, arXiv:1712.01571 [math.PR].
- [MN16] F. C. Marques and A. Neves. Topology of the space of cycles and existence of minimal varieties. In *Surveys in differential geometry 2016. Advances in geometry and mathematical physics*, volume 21 of *Surv. Differ. Geom.*, pages 165–177. Int. Press, Somerville, MA, 2016.
- [Nor10] P. Norbury. Counting lattice points in the moduli space of curves. *Mathematical Research Letters*, 17(3):467–481, 2010, arXiv:0801.4590 [math.AG].
- [Rie22] A. Riera. Isoperimetric inequalities in the Brownian plane. *The Annals of Probability*, 50(5):2013–2055, 2022, arXiv:2103.14573 [math.PR].
- [Sch15] G. Schaeffer. Planar maps. In *Handbook of enumerative combinatorics*, Discrete Math. Appl. (Boca Raton), pages 335–395. CRC Press, Boca Raton, FL, 2015. <http://www.lix.polytechnique.fr/~schaeffe/Biblio/HB.pdf>.

- [Sti12] J. Stillwell. *Geometry of Surfaces*. Universitext. Springer New York, 2012.
- [Thu97] W. P. Thurston. *Three-dimensional geometry and topology. Vol. 1*, volume 35 of *Princeton Mathematical Series*. Princeton University Press, Princeton, NJ, 1997. Edited by Silvio Levy.
- [Tut63] W. T. Tutte. A census of planar maps. *Canadian J. Math.*, 15:249–271, 1963.
- [Tut68] W. T. Tutte. On the enumeration of planar maps. *Bull. Amer. Math. Soc.*, 74:64–74, 1968.